University of Strathclyde, Glasgow

Department of Naval Architecture, Ocean and Marine Engineering

The Assessment of Mooring Line Damping for Offshore Structures

By

Minglu Chen

A thesis presented in fulfilment of the requirement for the degree of Doctor of Philosophy

2019

Declaration

This thesis is the result of the author's original research. It has been composed by the author and has not been previously submitted for examination which had led to the award of a degree.

Minglu Chen

Signature: Date:

Acknowledgement

I would like to express my sincere gratitude to my supervisor Professor Nigel Barltrop for his inspiration, encouragement, and guidance during my research. I would also like to give my thankful words to Professor Sandy Day, and Mr. Charles Keay for their help and advice in the model test process.

I cannot help expressing my special gratitude to Professor Shan Huang, who gave me constant support and valuable suggestions in project research and report writing before he moved to work in BP. He is not only a supervisor that exchanged ideas and proposed valuable advice to further research work, but also a friend that shared experience of enjoying the life abroad with me.

I would like to thank the faculty and staffs in the department, especially Thelma Will and Susan Pawson, who always offer responsive and friendly help and support. Also, I am grateful to Dr Zhengqiang Xu and other PhD students in the research area, who exchanged ideas with me and gave me help.

I would like to express my appreciation to my parents, Rui Chen and Xiaojuan Zhang, for their unconditional support, love and understanding. Lastly, I would like to express heartfelt thanks to my husband, Zhiming, and to my lovely daughter, Evelyn, who made my life complete.

Table of Contents

List of Figures

List of Figures

List of Figures

List of Tables

List of Tables

Nomenclature

General Symbols

$\vec{a}_i$ Acceleration vector of node i

$\vec{a}_w$ Fluid acceleration

a_0 Motion amplitude

B Buoyancy

B_{drift} Wave drift damping

$B_{current}$ Current damping

$B_{mooring}$ Mooring system damping

B_{wind} Wind damping

C_D Drag coefficient

C_{DT} Tangential drag coefficient

C_{DN} Normal drag coefficient

Note: In this study, the related Normal drag diameter is used with nominal diameter D, which equals to bar diameter. For tangential drag force calculation, a corresponding Tangential drag diameter of D/π is used.

C_m Inertia coefficient

D Nominal diameter of chain

d_i Cable element diameter

E Dissipated energy

E_i Young's modulus

F_H Horizontal force

$F(t)$ Hydrodynamic force in the unit length of the slender structure

$\vec{f}_D$, $\vec{f}_A$ Drag force and inertial force

$\vec{F}_{Di}$, $\vec{F}_{Ai}$ Drag and inertial force assigned on node i

$\vec{f}_{Di}$, $\vec{f}_{Ai}$ Drag force and inertial force acting on the element i

f_{DT}, f_{DN} Tangential and normal components for drag force $\vec{f}_{Di}$

dF_{DN} Normal drag force of the line element ds

H Vertical distance

$\vec{i}$, $\vec{j}$, $\vec{k}$ Unit vectors of the global coordinates

l_i Element length

L Total length of the cable

m_{ai} Added mass matrix of the cable element

M_i Mass of node i

M_{Ai} Added mass matrix of the cable element

P Tangency point of the cable on the seabed

p Length of the section of the cable on the seabed

q Suspended length

R Conversion matrix transforming the vector in global coordinate system to the local coordinate system

s Curves coordinate along the mooring line

T_h , T_v Horizontal and vertical force at any cross section

$\vec{T}_i$ Tension vectors in element i

T_x Horizontal component of the fairlead point tension

u Flow velocity

$\dot{u}$ Flow acceleration

$\vec{V}_i$ Flow velocity at the centre of element i

$\vec{V}_i'$ Velocity of the centre of element i

w Submerged weight per unit length (N/m)

W Gravity

X Horizontal distance

$\vec{X}_i$ Global coordinates for node i

x Horizontal component of transient displacement

ΔX , ΔZ Maximum values of horizontal and vertical displacement

Greek Characters

$\eta_0(s)$ Normal displacement amplitude

$\eta_1(s), \eta_2(s)$ are Farthest and closest displacement amplitude for the element

$\vec{\xi}$ Unit vector of the tangential direction

$\vec{\xi}$, $\vec{\eta}$, $\vec{\zeta}$ Unit vectors of the local coordinates

ρ Fluid density

ρ_w Water density

φ Angle between the cable tangent and the horizontal at the static equilibrium position

ω Motion frequency

σ_i Cross-section area for the element

τ Period

Abstract

With increasing water depth of oil and gas exploration, greater importance has been attached to the damping force from mooring systems. The effect is significantly important to slow drift motion of the floating structure, and it is also coupled with its motions. Coupled analysis is thus preferred to be applied to estimate the floating structure motions and to calculate the mooring system response, especially for offshore structures in deep-water.

In this study, the aim is to achieve a better understanding of mooring line induced damping estimation. Drag forces normal to the mooring line due to the motion of the mooring line through the water, are the main source of hydrodynamic damping of the mooring line. A method of energy dissipation based on the mooring line dynamic response obtained by Orcaflex is developed. The validation is established through two types of mooring lines in shallow water and deep water. The present approach shows a good agreement with the published results, but with two exceptions. One is for the mooring line oscillated by a very slow LF motion in shallow water, when the hydrodynamic damping is very small. Another one is for the wire mooring line oscillated by WF motion in deep water, the result shows significant discrepancy with that from the quasi-static method.

Then a non-dimensional analysis is completed, due to the strong complexity of the mooring line induced damping. The effects of the factors can be divided into three groups: first, the effects from pretension and scope are related to the geometry changes of the mooring line; second, the oscillation, current velocity and drag coefficient make contributions to the drag forces of mooring line directly; and the last, the effects of stiffness and seabed friction which, it was found, can be neglected.

In order to experimentally investigate the chain behaviour moving in water, a series model tests for the damping characteristics of a single chain line is implemented

through oscillation tests of various parameters. The drag coefficient (C_D) variations with different Reynold (R_n) and KC numbers are investigated. The drag coefficients in this study range from 1.5 to 4.0, which is case-dependent, because both Reynold (R_n) and KC number affect them. With the increase of KC number, the drag coefficient shows a decrease with exceptions occurring in low KC cases. In addition, it is shown that the chain segments near the fairlead and touch down area are most sensitive to the drag coefficient, which is consistent with the velocity distribution along the mooring line.

Finally, the validation is established by comparing the results of experimental tests and numerical simulations. Based on the assessment of drag coefficient from the scaled experimental investigation, numerical simulations of estimated drag coefficient are carried out within Orcaflex. A good agreement is achieved between the numerical calculations and experimental measurements, which illustrates that the present method can be applied for mooring line damping estimation. Meanwhile, the effects of the amplitude and frequency of the oscillation are studied.

1 Introduction

1.1 Background

1.1.1 Deepwater exploring

The ocean area covers up to 2/3 of the earth surface, it is said to be ‘the sixth continent’, e.g. here are huge resources that can be exploited and utilized. With the increasing development of the world economy, deep-water exploring has become a trend. The gas and oil industry is now cumulatively concentrating their efforts and activities in developing fields in deeper waters since first discovery of deep-water oil reserves by shell in 1975, the first deep-water platforms were implemented in the ‘80s.

Koch reported that there were 63 of 83 working rigs in 2014 operated in the deep water of the Gulf of Mexico region, as opposed to 14 five years previously. Deepwater drilling permits have been increasingly issued all over the world, from 14 in 2010, 274 in 2011, and 603 in 2014. Meanwhile, the drilling depths for these are increasing: from 2005 to 2010, the average depth of drilled wells increased by 40%. The exploitation of deep water region has been stepped forward and the record for the world’s deepest floating facility reached 9,500 feet (2900m) (Koch, 2015).

Even though shallow water has been relatively less expensive and less technically challenging for operators to explore and drill, changing economics and the exhaustion of some shallow offshore resources has helped to push producers to deep-water or, in some areas, ultra-deep water resources. It is reported that global offshore oil production from deep-water reached 9.3 million barrels per day in 2015, which has increased 25% from nearly 7 million barrels per day a decade ago. On the contrary, the share of offshore production from shallow water in 2015 was 64%, the lowest on record.

Chakhmakhchev and Rushworth (2010) presented that more than half of new global oil and gas reserves were discovered offshore in the last 10 years, according to the IHS data, as shown in Figure 1-1. They also indicated that deep and ultra-deep water discoveries are the dominant source of new reserve additions accounting for 41 percent of total new reserves based on a statistical evaluation of discoveries between 2005 and 2009. It was predicted that this trend will continue into the future, making deep-water a key contributor to a new reserve and supply growth (Chakhmakhchev and Rushworth, 2010), as presented in Figure 1-2. Five years later, Total (2015) estimated that the number would climb up to nine million barrels per day by 2035. Deepwater activity will continue to be a driving force behind the growth of the global oil industry for decades to come. Although, the production of oil and gas in deep-water experienced a nadir in 2014 due to the steep decline in oil and gas prices, deep-water production still provides challenges and opportunities.

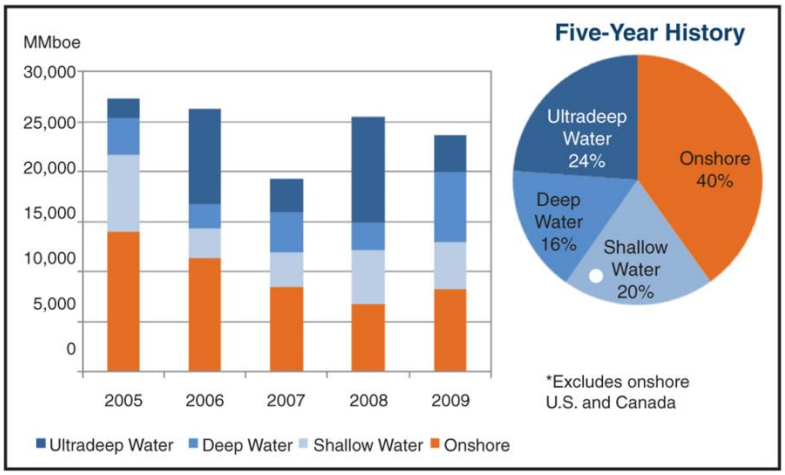

Figure 1-1 The new discovered global reserves during 2005-2009

According to the US Mineral Management Service (MMS), deep-water production slightly rebounded in 2016. As expected, the major growth during 2016 in floating production system was in FPSOs (Dupre, 2015), as the picture shown in Figure 1-3.

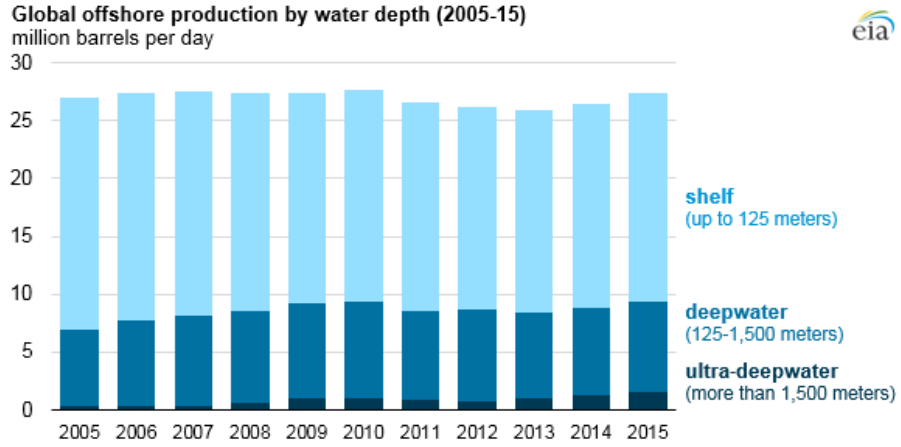

Source: U.S. Energy Information Administration, based on Rystad Energy
Note: Includes lease condensate and hydrocarbon gas liquids.

Figure 1-2 Global offshore production in 2005-2015

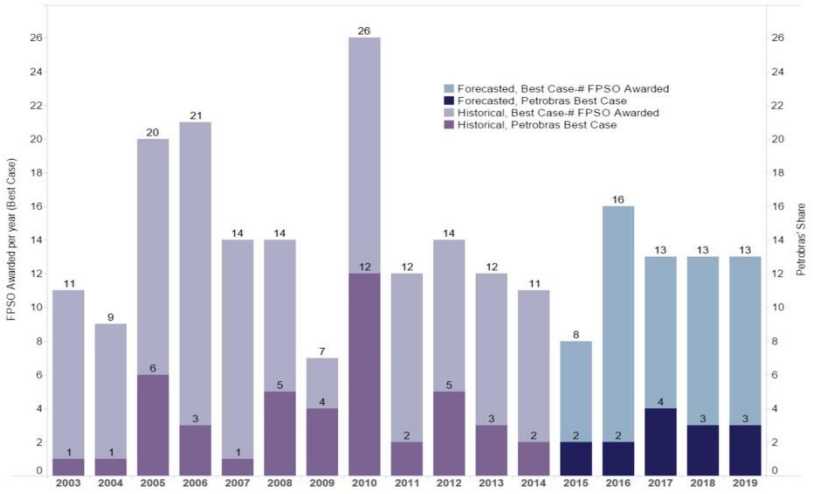

Figure 1-3 FPSO awards 2003-2019 with Petrobras' proportion (Data courtesy Energy Maritime Associates)

1.1.2 FPSO (Floating Production, Storage and Offloading vessel)

The FPSO is one of the most popular categories; others are TLP, Spar, Semi-submersible for exploitation in deep-water open area shown in Figure 1-4. FPSO has advantages including operating flexibility, range of water depth, conversion possibilities, and storage capacity range. Even though they cannot support heavy workover, due to these inherent advantages, this vessel type has more options to see active service than

other floating production system types in the downturn market since 2014 (Dupre, 2015).

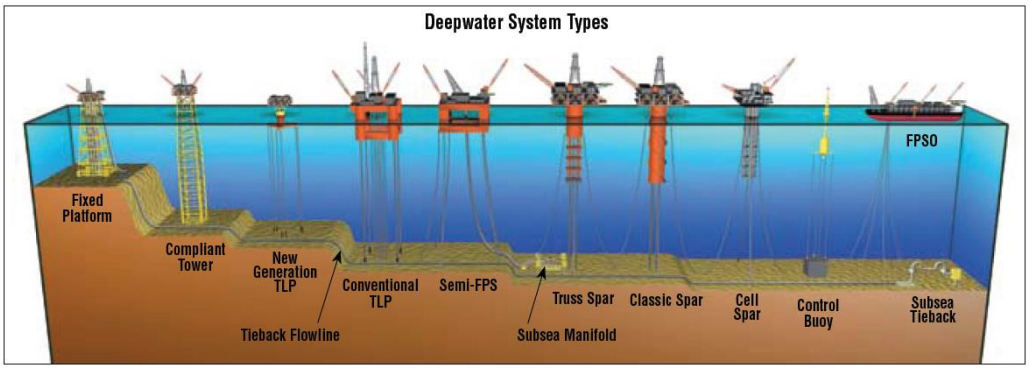

Figure 1-4 Deepwater System types

According to statistics by World Energy Reports, FPSO has shown a remarkable growth since 1997, as displayed in Figure 1-5. Although the production, market price and variable demand for oil and gas have remained in flux since 2014, the data of worldwide FPSO available have also continued to rise. Oil and Gas price fluctuation are not only difficult to project, but they often require short-term decisions for increasing or curtailing production(Barton, 2017). FPSOs generally offer a cost-effective solution especially for marginal fields and changing price conditions. As noted, FPSOs can be converted from previously used storage vessels tankers. It is estimated that single-hull conversions can be accomplished at a cost of 10% of new-builds and, depending on the extent of the required conversion, can be available for service within a two-year timeframe – normally 20% less time than for construction of a new-build FPSO (Barton, 2017).

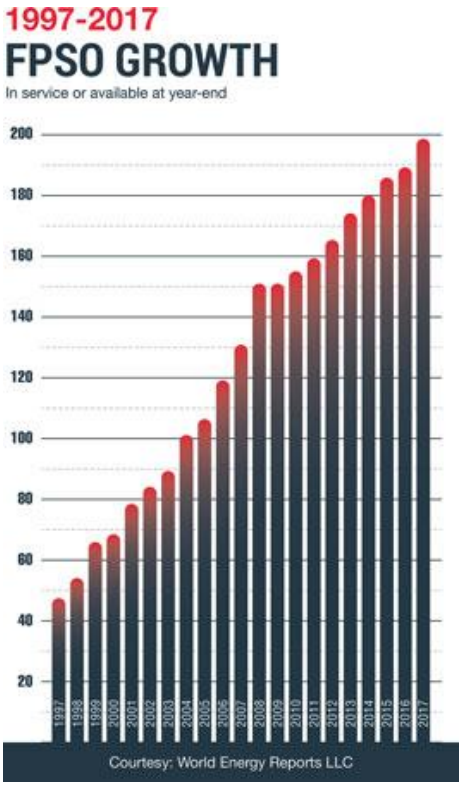

Figure 1-5 FPSO growth in last two decades (Offshore-Mag, 2017)

1.1.3 Mooring system

An offshore mooring system consists basically of three parts: an anchor system, a mooring line and a specific mooring layout. The mooring system layout depends on the local environmental conditions and the purpose of the offshore unit. Spars and Semi-submersibles use spread moorings to be positioned in a fixed heading. The turret mooring system is usually used on ship-shape offshore unit, such as FPSO. This vessel is able to weathervane, rotating about the turret. Tension leg is a specific type mooring used on TLPs.

A catenary mooring system is the most common mooring system in shallow water. To keep station for a floating structure, the catenary configuration provides a restoring force on ship motions mostly through the weight of the mooring lines. The catenary lengths have to be much larger than the water depth to make sure that the anchor points

are subjected to horizontal force. That is to say, it is not practical and economic to apply catenary mooring because the chain becomes very long and heavy with the water depth getting deeper. The taut mooring system is appropriate in deep water due to its lighter weight, shorter mooring line and smaller mooring radius. The restoring forces are generated by the elasticity of the mooring line. The anchor points in the taut mooring system have to be capable of withstanding horizontal and vertical forces. The sketch of catenary mooring system and taut mooring system is shown in Figure 1-6 (Yuan et al., 2011).

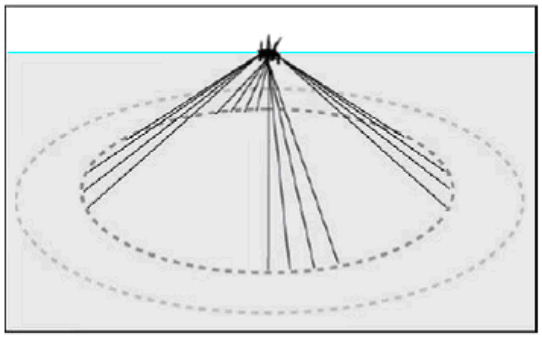

(a) Catenary mooring system **(b) Taut mooring system**

Figure 1-6 Mooring line configuration

1.2 Motivation

1.2.1 Mooring system integrity

The mooring system is one of the critical components for safe station keeping of floating structures; it is recognised as one of the foundations of safe production operation. However, frequent accidents occurred with the increased use of moored floating structures, many of which were related to the failure of a mooring line. Some accidents caused huge loss, not only the loss of money, but also the loss of life (Drori, 2015). The main cause of the accidents can be divided into these types: chain breaks at fairlead and link; break of the chain in ground mud; seabed trench near the suction piles and the failure of the synthetic ropes.

The offshore industry has experienced numerous unexpected mooring line failures in recent years. There were more than two mooring system failures per year on average between 2001 and 2011 (K. Ma, 2013). 'JIP FPS mooring integrity report'(Denton, 2006, NOBELDENTON, 2005) reported the failure statistics for North Sea operations for different floating units during the period 1980 to 2001, the number of operation years per failure for drilling semi-submersible is 4.7, 9.0 for production semi-submersible and 8.8 for FPSO. According to the statistics from (Drori, 2015), there were 107 mooring incidents from 73 facilities across the industry during 1997 to 2012. The probability of a single mooring line failure on floating production could be, on average, around 2E-2 per year, which is to say, there is a high chance, of about 50%, of a mooring failure for a moored structure through a 25-years design life cycle, as shown in Figure 1-7.

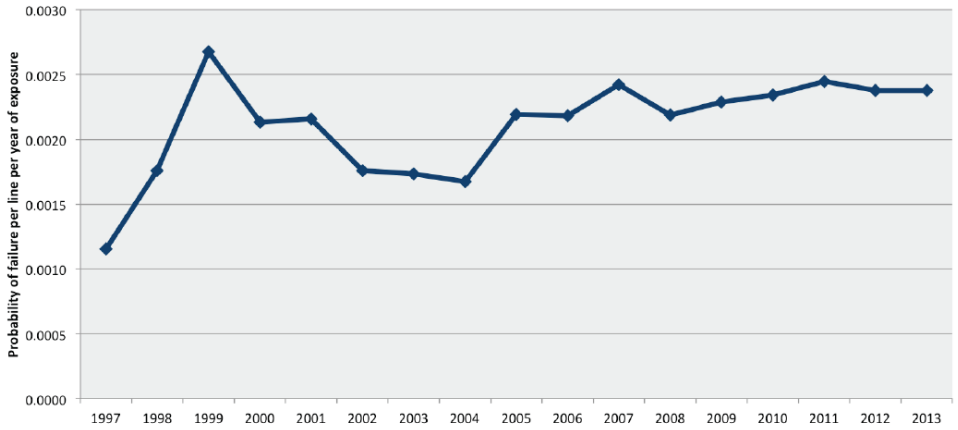

Figure 1-7 The probability of a single mooring line failure (statistics during 1997-2012)

There was an incident with the Gryphon FPSO offshore Aberdeen, which occurred in February 2011. During a severe storm (about 111.1km/h maximum wind speed with a significant wave height of 10m to 15m), it lost position and drifted 180 meters off-station after four mooring lines failed, leading to a significant damage to the subsea infrastructure (Smith, 2011).

Regarding the failure modes of mooring system, most of the cases are because of the failure of a single mooring line. Although in the design criteria for mooring system, the

single mooring line failure is normal and should not threaten the safety and integrity of the system, its failure can lead to multiple failures in mooring system if undetected. Multiple failures in mooring system are classified as the highest safety critical risk category: category 1. When multiple failures occur in mooring system, there is a significant chance of the failure for the whole system, especially for the station keeping dependent systems, such as risers. The integrity of the mooring line is thus of most importance to the moored floating structures.

Many class documents relating to mooring system are published: In-Service Inspection of Mooring Hardware for Floating Structures (API-RP2RD, 1998), Rules for Classification of mooring system design for offshore floating structures (DNV-OS-E301, 2010), Guide for Building and Classing Floating Production Installation (ABS, 1993), Rules and Regulations for the Classification of a Floating Offshore Installation at a Fixed Location (2013) etc.

Large ship-shaped FPSOs are dominated by low frequency (LF) motions. From (API-RP2SK, 2005), the broad range in the frequency of the LF force usually includes the natural frequency of moored FPSO systems, which means resonant motion are triggered. Once it occurs, large LF motion can yield high mooring forces, which can be more severe than that due to the extreme sea-state (such as 100-year waves).

1.2.2 Global analysis of moored floating system (coupled and de-coupled analysis)

Traditionally, the motions of moored offshore structures and the loads in the moorings and risers are calculated separately, which is uncoupled (or decoupled) analysis, as shown in Figure 1-8. In step 1, the motions of the floater are calculated with environmental forces, but simplifying and modelling moorings and risers as non-linear position-dependent forces, known as stiffness. The restoring forces of the mooring and riser system are included quasi-statically using non-linear springs; however, the velocity-dependent forces (damping contribution) from the mooring and riser system

are either neglected or roughly applied with linear damping force acting on the floater structure. The influence of current forces on the mooring and riser system stiffness is either neglected or included with an additional current force on the floater. Both the effects are substituted by additional 'floater coefficients'. Followed by step 2, dynamic responses of moorings and risers are analysed based on the floater motion responses calculated in the step 1, and, if necessary, the original damping estimates revised. Due to the simplification and linearization, the horizontal turret forces and line tensions might be estimated inaccurately (Ormberg and Larsen, 1998).

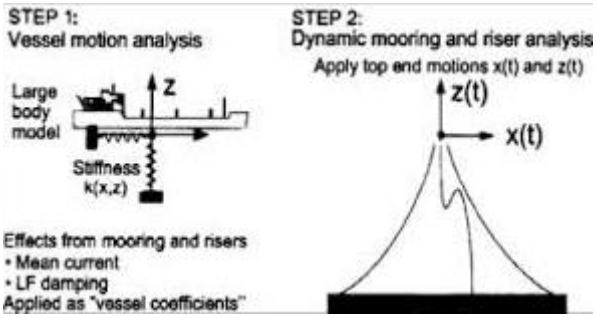

Figure 1-8 De-coupled analysis

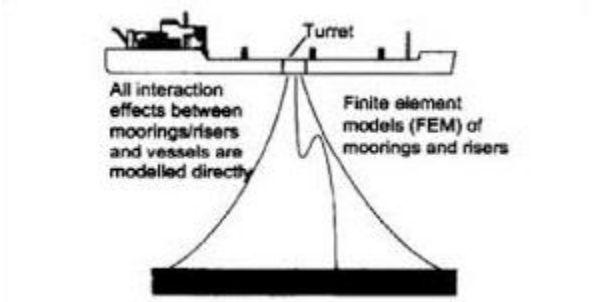

Figure 1-9 Coupled analysis

In coupled analysis, as shown in Figure 1-9, the floater and the mooring/riser system are integrated in the model, and they are analysed simultaneously. Coupling effects refer to the influence on the floating structure mean position and the dynamic response from the slender structure causing restoring, damping and inertia forces.

In shallow water, the floater motions are mainly excited and damped by fluid forces on the floater itself. Thus, employing the uncoupled analysis, the motions of the floater can be predicted with satisfactory accuracy. In this traditional separated approach, the current loads and the low frequency damping contribution from the mooring system are neglected or simplified.

With increasing water depth and in areas where the environmental conditions are severe, the offshore floating structures are often moored permanently with mooring systems that inevitably have soft elasticity characteristics as this reduces the wave-frequency mooring forces. The low-frequency horizontal motions induced by low-frequency second order wave drift forces also become larger. The horizontal motions of the moored structures are dominated by the low-frequency resonant motion components, and the mooring forces. Coupled analysis is thus considered to be an ideal method for mooring analysis due to its fewer simplifications. Ormberg and Larsen (1998) compared and illustrated the differences between the coupled analysis and uncoupled analysis with model tests and simulations for a turret-moored ship. They also recommended applying coupled analysis for deep water structures design. But because of the large number of time-consuming analysis required, some coupling effects are partly or fully ignored, which means simplifying approximations are widely applied in mooring system analysis.

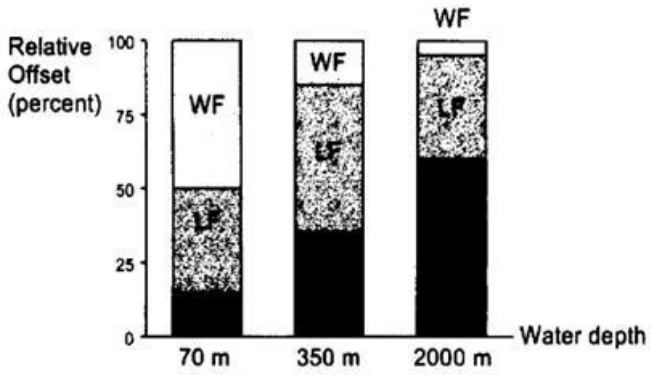

Figure 1-10 Motion response components for a catenary moored ship at different depth (Ormberg and Larsen, 1998)

So generally, in order to obtain a more accurate calculation of moored structures mean offset and LF motion, the magnitude of the second order wave drift forces and the

values of the low-frequency hydrodynamic damping must be known. The LF damping of a mooring line is commonly simply applied as a linear damping coefficient in dynamic analysis; accurately estimating the LF damping induced by mooring line is thus of most importance to predict the motions of a moored offshore structure in deep water.

1.2.3 Moored offshore structures' motions

Offshore platforms are subject to environmental loads, mainly created by waves, wind and ocean currents. These environmental loads induce motion responses on the platform the platform - mooring systems. Typically, motions of floating structures can be divided into wave-frequency, high frequency, and slow drift motions.

The wave frequency motion is mainly produced by first order interactions between waves and the floating body. The amplitude and frequency of these motions are, in general, similar to those of the waves that induce them.

High frequency motions are generated by non-linear wave excitation. Their natural periods are in the order of two to four seconds and they are frequently significant for TLP structures. They are out of the scope of this thesis, since they do not appear in catenary-type moored platforms.

Similar non-linear interactions between the floating body and the waves cause slow and mean drift motions. This kind of motion appears in every type of floating platform. They arise from resonant slow-drift oscillations. The typical period of these oscillations are in the range of 50 to 150 seconds for conventional moored platforms. This type of motion for a moored floating body typically occurs in surge, sway and yaw. Slow drift motions are characterized by large horizontal excursions of the platforms that drive, as a result, enormous forces on the mooring lines.

These types of oscillations are critical in catenary type moored platforms and are being studied in this thesis.

1.2.4 Mooring line induced damping

The contribution of the damping of the moored structures mainly comes from the wave drift damping; the wind damping; the current and viscous flow damping and the mooring line damping. Initially, the research in this damping area concentrated on the potential wave drift damping and on viscous damping. The system damping was supposed to be significantly dominated by the wave damping from the hull (Huijsmans, 1984), and the mooring line induced damping was thought to be of little importance and neglected. Since (Huse, 1986a) first published his study about the effect of the mooring line damping theoretically and experimentally, the significant effect of mooring lines damping is increasingly of concern in predicting offshore structure motions. Huse et al. (1988) developed a simple procedure with a non-dimensional method to estimate the mooring line damping, and verified it using a ship model.

Barltrop (1998) summarised the studies of the contributions from mooring line damping, which are present in Table 1-1. Huse (1989) concluded that 80% of the total low frequency damping is due to mooring line damping for a 120000 DWT tanker with a 10-leg wire/chain mooring system. Matsumoto (1991b) did research on a tanker in 108m of water and turret moored with an 8-leg chain mooring system, it was shown that the mooring line damping contributes about 65% of the total when the tanker oscillates about 10% of water depth in low frequency. Dercksen (1992) based upon the study for a 200000 DWT tanker turret moored using six chains in 82.5m water depth, conclude that the mooring line damping can contribute up to 60% of the total at shorter wave peak periods. Triantafyllou (1994) indicate that the contribution from mooring line damping is 25-30% of total for a semi-submersible.

Table 1-1 Contribution of line damping (Barltrop, 1998)

Reference	Vessel	Water depth	No. of lines	Line type	Line damping/ Total damping
Huse and Matsumoto (1989)	120000 DWT tanker	200m	10	96mm wire+ 90mm chain	80-85%
Matsumoto(1991)	180m×30m tanker	108m	8	76mm chain	50-65%
Dercksen et al. (1992)	200000 DWT tanker	82.5m	6	140mm chain	30-60%
Triantafyllou et al. (1994)	Jack Bates Semi-sub	300-900m	8	127mm chain+wire	25-30%

It was considered that the mooring lines provide not only restoring forces to the whole system, but also have great effects on the LF damping (Nakamura et al., 1991). Such damping will contribute largely to reduce the resonant horizontal motions induced by the LF drift forces. The damping effect from mooring system is the most important factor influencing the amplitude of motions of moored structures. Accurate prediction of damping is thus essential for the prediction of motions of the moored structures.

In the recent years, many researchers have done some study to design mooring line system. With the offshore floating structures are widely used in deep and ultra-deep water, studies on design truncated mooring systems are investigated for model tests. In the process of truncation mooring system design, mooring damping equivalence is one of the most important that to be considered (Xu and Huang, 2014, Xu et al., 2018, Fan et al., 2014). An improved quasi-static method is developed for mooring induced damping estimation, and the physical model experiments are conducted based on both statics and mooring induced damping equivalence(Fan et al., 2017b, Fan et al., 2017a, Fan et al., 2018). Xiong et al. (2016) also proposed an improved numerical approach for the estimation of the mooring induced damping for truncated mooring system.

With the development of floating wind turbine and wave energy converter, the researches on mooring line systems have been done since they provide position function and affect the motion performances for offshore floating structures(Karimirad, 2013, Qiao and Ou, 2014, He et al., 2018).

According to the previous studies, it is shown that the mooring line induced damping has significant influence on the LF motions of offshore floating structures. Therefore, in order to obtain a good prediction of LF motion through coupled dynamic analysis, one key point is to accurately estimate the mooring line induced damping.

The mooring line damping for a catenary mooring is mainly due to three mechanisms: firstly, the catenary mooring line shape changes in response to the excitation from the top end, the mooring line elements move in the direction perpendicular to their axes and this leads to energy dissipated because of the hydrodynamic drag force along the line; Secondly, the motion of the line at wave frequency introduces low frequency damping due to the quadratic nature of the drag force; finally, the vortex induced vibration can increase the drag force contribution significantly and therefore the effective drag coefficient used to calculated the low frequency damping increased.

A lot of investigations have been done to predict the magnitude of the mooring line damping. The numerical calculation results are in good agreement with the experimental results when only LF oscillations are taken into consideration, while a considerable discrepancy still exists for WF oscillations superimposed. For instance, according to the study of Huse (1989), it is found that compared to the experimental results, the numerical calculation over-predict the mooring line damping by a factor of 1.2 to 2.0, with a WF motion superimposed. It is also shown that the superimposed WF motion increase the LF damping by a factor in the range of 2 to 4.

Another issue about the mooring line damping estimation is that, only a single- or bi-harmonic WF motion is taken into account when considering the effect of superimposed WF oscillations on the mooring line damping. Rarely researches have been done on the

effect of random WF motions to the mooring line damping, including the physical model tests. However, the moored offshore floating structures are under the random WF motions in reality. Therefore, the influence of random WF motions on the mooring line damping needs to be assessed precisely.

In de-coupled analysis, the mooring line damping is predicted and treated as an input in the calculation of the moored structure motions. In coupled analysis, the mooring line damping is presented by the drag force, which is related to the drag coefficient. Drag coefficient is an empirical value; its selection can be the potential reason for the discrepancy between the numerical calculation and the experimental results. A proper drag coefficient is hence crucial to precisely estimate damping contributions and calculate the current/wave loads of mooring lines.

1.2.5 Mooring line dynamic response

The catenary equation is a solution considering the statics of a mooring line under its own weight, applied tension at one end, and with or without elasticity. Although that treatment completely covers all quasi-static analyses of mooring lines, the effect of dynamic response of the mooring and the direct environmental loads on the mooring lines have been neglected.

Usually, the restoring forces acting on a floating body caused by mooring systems are calculated based on simplified quasi-static formulations. These formulations assume that mooring lines and risers respond statically to the moored floating offshore structure. The mooring systems are regarded as mass-less non-linear springs, therefore only the stiffness of mooring systems is considered in order to calculate the hull motions. With this assumption, the inertia effects and hydrodynamic loading on mooring lines are neglected. After the floater motions are computed, the mooring systems dynamics can be evaluated independently by inputting the fairlead responses. As mooring systems operate in increasing water depth, the damping caused by the surrounding fluid affects the overall motion of the mooring line as well as the tension forces in it considerably;

thus the reliability and accuracy of this approach is expected to diminish. Therefore, the real mooring force might exceed the predicted forces obtained from simplified quasi-static formulations (Kreuzer and Wilke, 2003).

The quasi-static analysis is regarded as the preliminary requirement to study the performance of mooring lines. At each instance in time, wave-induced motions statically offset the mooring system; the dynamic effects associated with mass, damping, and fluid acceleration on the mooring line are neglected. The entire line profile can be determined based on the static equilibrium of the mooring line at each instance in time. The quasi-static approach assumes that the mooring line takes up the successive 'static' positions, thus higher safety factors are required when static rather than dynamic analysis is used. Meanwhile an arbitrary 450m water depth limitation has been imposed when quasi-static analysis is used (Barltrop, 1998).

According to the research of Kwan and Bruen (1991), quasi-static analysis gives a very poor representation of wave frequency tension. The assumption that the mooring line will take up the successive static position during the course of the wave frequency oscillation is obviously inaccurate, especially in deep water. Thus a thorough assessment of mooring line behaviour under waves requires the solution of the equations of the motion rather than solutions of static equilibrium.

In a dynamic analysis, the line's inertia and drag are included together with both horizontal and vertical motions. As a result the mooring line is generally unable to instantaneously follow the floater motion which is then accommodated through a combination of catenary and axial deflection. The difference in mooring line behaviour predicted with quasi-static and dynamic approaches, as shown in Figure 1-11.

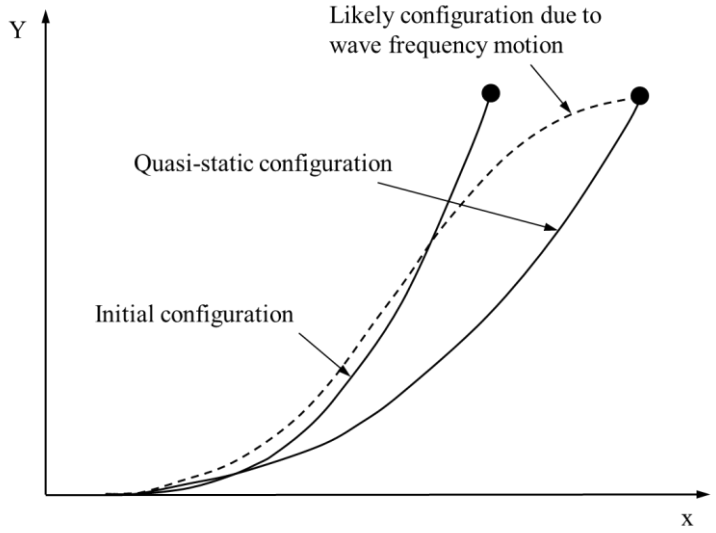

Figure 1-11 Quasi-static and dynamic behaviour of mooring line (Barltrop, 1998)

1.3 Research outline

The integrity of a mooring system is of prime importance for the operation of these floating structures, especially for the permanently moored vessels, such as FPSOs. The prediction of magnitude of mooring line damping is usually used in uncoupled analysis, where the damping induced from mooring is treated as an input to compute the floater motions. To more precisely and effectively estimate the responses for a moored offshore structure in deeper water, the mooring induced damping is calculated implicitly but simplifying approximations are still used in coupled analysis. In this thesis, combining the methods of numerical simulation and model test, the sensitivity of the damping to the fairlead excitation; the effect of different types of superimposed WF oscillation, pretension, drag coefficient, current velocity, scope, stiffness, and seabed friction, on the damping of mooring line are investigated.

1.3.1 Objectives

Based on the introductory remarks, a number of studies associated with the mooring line induced damping were mainly in respect to numerical methodology. However, it

can be noticed that none of these studies seem to be applicable to the calculation and experimental tests on a chain mooring line with random WF motion superimposed with LF oscillation. Accordingly, in order to estimate the mooring line damping applied with Orcaflex, there is a need for an appropriate approach of drag coefficient estimation. The proper determination of drag coefficient based on the consideration of R_n number and KC number, is the premise of simulating the numerical model.

The objectives of this thesis are to build an efficient, low cost and stable process for the assessment of the mooring line induced damping, in which the WF motion is investigated on its contribution to the damping force. In the meantime, the method to estimate drag coefficient for mooring line at model scale over the typical range of R_n number and KC number for cases that include LF oscillation and combined with WF motions is to be developed.

1.3.2 Study scope

To estimate the damping induced by the mooring line system, a single mooring line is investigated for an example FPSO which is located in 200m water depth; the thesis will include:

1) Different amplitudes and frequencies of the LF oscillations, used to assess the damping of mooring;

The method to calculate the damping induced from mooring line is studied. Based on the parametric studies, the effect of the LF motion on the mooring line damping is studied, with different amplitudes and frequencies. The LF sinusoidal motion is applied on the top end of the single mooring line, evaluating the energy dissipation within the mooring line movement.

2) WF motions are superimposed with LF oscillation to estimate its impact upon mooring induced damping; environmental loads are considered to assess its effect on the drag force acting on the mooring line;

The impact of superimposed WF motion is investigated on mooring line damping, using different amplitudes and frequencies. Meanwhile, harmonic and random WF motions are considered to evaluate its effects on mooring line damping.

3) Model tests for a single mooring line are arranged to verify the method for calculating the mooring line induced damping;

A single 1:80 scaled model of mooring line is selected; it is excited by an oscillator on its fairlead point. The oscillator provides LF motion with and without WF motion superimposed. The results are validated with those of numerical simulations.

4) Non-dimensional studies of the effects of different parameters upon the mooring induced damping are presented.

In order to get rid of the effect of model scale dimensions, the effects from excitation motions, pretension, drag coefficient, current velocity, scope, stiffness, and seabed friction are investigated based on numerical simulations using Orcaflex.

1.3.3 Approaches for research

The contribution of the mooring lines to the total system damping is the sum of the contribution to the energy dissipation due to the hydrodynamic forces on the lines, friction between the lines and the seabed and material damping of the lines. Here, drag forces normal to the mooring line due to the motion of the mooring line through the water, are the main source of hydrodynamic damping of the mooring line. A method of energy dissipation based on the mooring line dynamic response obtained by Orcaflex is developed. In order to validate the sufficiency of the numerical calculation, a series of model tests will be carried out.

Due to the motion of the floating structure, the mooring lines are forced to move through the water, resulting in drag and lift forces on the line. These forces are taken up primarily by the fairlead and to a smaller degree by the anchor. The hydrodynamic drag forces result in an energy dissipation, and thus in a damping of the LF motion of the structure.

Being proportional to velocity squared, the drag force is non-linear. To use it in a simple manner, the force must be linearized to obtain the equivalent viscous damping ratio. The linearization is carried out in order that the energy dissipated during one oscillation cycle by the non-linear drag force is equal to that induced by the equivalent linear damping force.

The linear damping coefficient in the motion equation comprises the contributions of several damping mechanisms. Since we are dealing with a linear problem, this damping coefficient can be written as follows:

$$B_{total} = B_{drift} + B_{current} + B_{mooring} + B_{wind} \qquad \textbf{1-1}$$

Bases on the research of (C. Webster, 1995), the calculations of the mooring line damping in the surge direction are completed by the ‘indicator diagram’ method. The indicator diagrams were first developed in the Steam Age as tools for understanding the efficiency of steam engines. The ‘indicator diagram’ can be derived by plotting the time history of the top-end surge motion against the time history of the horizontal force. The area under the resulting closed loop is then related to the energy dissipation E

$$E = \int_{t}^{t+\tau} F_H \cdot \frac{dx}{dt} dt \qquad \textbf{1-2}$$

Where x is the surge motion associated with the period τ , F_H is the corresponding horizontal force.

The damping of the mooring is mainly due to the fluid viscous drag force acting on the mooring lines. For such slender structures, the hydrodynamic loads are usually calculated by using the semi-empirical Morison's equation, which is formulated as the sum of a drag force and an inertia force:

$$F(t) = \frac{1}{2}\rho C_D D v|v| + \frac{1}{4}\rho \pi D^2 C_m \dot{v} \quad \textbf{1-3}$$

Where C_D is the drag coefficient; C_m is the inertia coefficient; ρ is the fluid density; v is the flow velocity; $\dot{v}$ is the flow acceleration; D is the effective diameter of the slender cylinder structure; $F(t)$ is the hydrodynamic force in the unit length of the slender structure.

For a chain mooring line moves with velocity $u(t)$, a relative velocity approach considering the interaction between the cylinder and the fluid is improved in the actual problem of an offshore structure. Considering the added mass effect due to the flow entrained by the cylinder, the inertia force per unit length acts in phase with the acceleration and is expressed as:

$$dF_A = \rho \dot{v} dV + C_a \rho (\dot{v} - \dot{u}) dV \quad \textbf{1-4}$$

Defining $C_m = 1 + C_a$, where C_a is added mass coefficient. The wave load normal to an element section of a chain mooring line is represented by the sum of a drag force and an inertia force:

$$dF = \frac{1}{2}\rho C_D (v-u)|(v-u)|dA + C_a \rho (\dot{v} - \dot{u}) dV + \rho \dot{v} dV \quad \textbf{1-5}$$

Where u is the velocity of the cylinder, $\dot{u}$ is the acceleration of the cylinder, and coefficients C_D and C_m are now evaluated with the relative velocity 'definitions' of the Reynolds number and Keulegan-Carpenter numbers:

$$R_n = \frac{(v-u)D}{\nu} \quad , \quad KC = \frac{(v-u)T^*}{D} \qquad \textbf{1-6}$$

T^* represents the period of the function $(v-u)$.

1.3.4 Structure of the thesis

The thesis is composed of 7 parts. Chapter 1 presents a brief introduction, the background, the motivation for the current research, following with the objective and scopes of the study. Chapter 2 reviews the previous works related to mathematical and numerical modelling for mooring line response, the method of mooring line damping and researches on model tests of mooring line system. The theoretical models to assess the mooring induced damping are explained in Chapter 3, and the method is verified with results from previous publication in Chapter 4. Meanwhile, the non-dimensional analysis for mooring line damping induced by surge motion is following investigated. The results include variations in amplitude, frequency, heave motion, pretension, scope, drag coefficient, stiffness and current. In Chapter 5, model tests for a single mooring line response are arranged and introduced. A parametrical study of the effect of oscillation upon the mooring line damping is investigated, including LF motions and WF motions, based on the results from experimental tests. In Chapter 6, the results of model tests are compared with that of numerical simulation. According to the relationship between drag coefficient and Reynolds and KC number, some recommendations for calculating the values of the hydrodynamic coefficient are provided. Finally, discussion, conclusion and recommended future work are provided in Chapter 7.

2 Literature review

The methods to research mooring system are mainly divided into model tests and numerical simulations. Experimental methods include model tests and full scale tests, which are performed in the ocean laboratory and outdoors respectively. Model tests based on a reasonable scale ratio and scaling criteria usually provide more reliable results. Model tests however have disadvantages of being time-consuming and costly, numerical simulations are commonly applied to research. Most of the contributions in the literature addressing mooring system fall in one of the following categories: 1) analysis for moored structures; 2) simple analytical models; and 3) model test investigations.

2.1 Interaction between mooring system and moored structures

In shallow water, the traditional de-coupled approach is quite desirable to estimate the offshore structure motions because of its high efficiency and sufficient accuracy. However, with the water depth increasing, the coupling effects between the floater and the mooring line system becomes larger. In this case, the validity of de-coupled method which neglects the coupling effects becomes questionable. Many researchers made contributions on the analytical method for global responses of moored structures (Garrett, 2005, Jing et al., 2012, Chen et al., 2006, Ormberg and Larsen, 1998, Tahar and Kim, 2003, Vendhan, 2019).

The necessity of coupled analysis for deep-water applications was recognised by Paulling (1986). The coupled method was applied when the importance of the mooring line damping became widely accepted in the industry. In order to assess the effects of geometric and hydrodynamic nonlinearities and dynamic coupling between the platform, moorings and risers, a fully coupled time-domain analysis is preferred. The coupled analysis can be conducted in frequency or time domain (Garrett, 2005). Karimirad (2013) presented the numerical modelling of a catenary moored spar-type floating wind

turbine (FWT) using the coupled method. It was indicated that the damping and inertia forces of the mooring are important for the tension response. Jonkman et al. (2009) established a fully coupled time domain aero-hydro-servo-elastic model to analyse the dynamics of FWT, including linear hydrostatic restoring, nonlinear viscous drag, and the added mass and damping contributions from linear wave radiation, with a quasi-static mooring line module. The mooring lines in these models are treated as static or quasi-static module, which ignores the dynamic characteristics of a mooring line. However, the dynamics of a mooring line should not be ignored when the water depth increases, and the reason is that the mooring line damping could significantly affect the motion response of platform.

Ormberg and Larsen (1998) did case studies for a turret moored ship operating in different water depth. It was concluded that when the current loads and LF damping from moorings and risers are neglected, the de-coupled method would severely under-predict the mean offset and over-predict LF motion. Both line tension and turret forces are under-predicted by a de-coupled approach compared to the coupled analysis. With the water depth increasing, the trend of the under-prediction for vertical turret forces becomes more severe. A coupled analysis is therefore recommended for design checks, especially for deep-water applications.

The coupled analysis can be conducted in frequency or time domain. Due to the geometric and hydrodynamic nonlinearities and dynamic coupling between the platform, moorings and risers, a fully coupled time-domain analysis is preferred for an accurate prediction. However, due to the disadvantage of high-demanding in computer hardware exists in the fully coupled analysis in time-domain, different efficient methods have been proposed for practical needs. For instance, Low and Langley (2006) developed an improved frequency domain coupled analysis which can provide high accuracy for the analysis of ultra-deepwater floating systems. Different from the floating system moored in shallow water, geometry nonlineaity is not significant for deepwater systems. The frequency domain analysis would thus suffer considerable loss of accuracy. (Low and Langley, 2008) proposed a hydrid frequency/time domain approach, and it was shown a

good agreement with a fully coupled analysis for a floating system moored in 200m water depth.

2.2 Mooring analytical method

Model test facilities are not always available and suitable (owing to scale effects, ultra-deep water, etc.). Many analyses on the mooring line contribution to the low-frequency damping rely alternatively on the rigorous nonlinear finite element approach. The numerical solutions to solve the dynamic behaviour of mooring system fall into two main categories: the finite difference approach and the finite element method (FEM).

Lumped Mass Method (LMM)

This approach involves the lumping of all effects of mass, external forces and internal reactions at a finite number of points (‘nodes’) along the line. By applying the equations of dynamic equilibrium and continuity (stress/ strain) to each mass a set of discrete equations of motion is derived. These equations may be solved in the time domain directly using finite difference techniques. At first, materials damping, bending and torsional moments are normally neglected. This procedure implies that the behaviour of a continuous line is modelled as a set of concentrated masses connected by massless springs. Some researchers also developed new lumped mass approaches, such as seabed contact and a clump weight was considered by Khan and Ansari (1986); an improvement of the numerical scheme was investigated by Huang (1994); snap loading was modelled by applying the Galerkin method (Palm et al., 2013).

Walton and Polachek (1959) were some of the earliest investigators using this approach to solve mooring problems caused by transient motions of a moored vessel. Their space wise discretization neglected material elasticity. Moreover no data on hydrodynamic drag forces and seabed interaction were available and no validation of the algorithm was given. The explicit central difference method was proven to provide conditionally stable solutions for the given schematization.

The lumped mass model was validated with a forced harmonic oscillation test by Nakajima et al. (1982). The computational models were in good agreement with experimental tests, although a limited set of tests were carried out that did not cover slack conditions. The LMM model was also verified with the dynamic responses of oscillation tests for chains, steel wires and chain-wire combi-lines by Boom (1985). A moored semi-submersible was modelled in irregular waves simultaneously. It is found that the LLM method is an effective means that efficiently and accurately predict dynamic line motions and tensions for engineering application.

Khan and Ansari (1986) developed a lumped mass model in three-dimensions. The cable segments are assumed rigid and massless and subject to hydrodynamic drag forces, and the segments masses are discretized into point masses at the node. Huang (1994) developed a three-dimensional finite-difference model that incorporated axial elasticity of the cable, and the improved model was applied to a subsea unit being towed by a manoeuvring vessel. More recently, the LMM has been developed further in order to solve offshore mooring problems by (Azcona et al., 2017b, Hall and Goupee, 2015), who extended the model of Walton and Polachek (1959) with material elasticity and seabed contact. Using hydrodynamic force coefficients derived from forced oscillation tests on model chains; they found a good agreement between numerical results and model tests for harmonic oscillation.

Finite Element Method (FEM)

The Finite Element Method utilizes interpolation functions to describe the behaviour of a given variable internal to the element in terms of the displacements of the nodes defining the element (or other generalized co-ordinates). The equations of motion for a single element are obtained by applying the interpolation function to kinematic relations (stress/ strain) and the equations of dynamic equilibrium.

Various models based on the FEM have been presented either using linear or higher order shape functions. The FEM models for mooring line analysis were developed by

(Garrett, 1982, Aamo and Fossen, 2000, Tahar and Kim, 2008). Computer codes based on the FEM have proven to be less computer time efficient when compared with the LMM algorithms. Buckham (2003) developed an improved FEM model using a cubic spline fit through the node points, a better approximation to the bending terms and a new presentation of torsional effects are then achieved. The model of sufficient fidelity could predict the dynamics of low-tension cables undergoing intricate deformation. The high-order feature make FEM good at accurately estimating mooring line behaviour over a wide range of conditions.

Experimental investigation was carried out to obtain the dynamic tension and the nonlinear characters for a mooring line transfers from taut to taut-slack(Zhang et al., 2012). It is presented that a skip tension of 5 times the former steady tension and twice the latter steady tension is accompanied with the transform. The skip tension may result in the platform breakage. From the study of (Thomsen, 2017), a number of relevant commercial software packages for mooring dynamic analysis are assessed, and their capabilities of fulfilling the requirements of modelling the mooring system. It is concluded that two software packages DeepC and OrcaFlex are found to be best suit the standard requirements.

Antonutti et al. (2018) presented a new workflow based on EDF R&D's open-source, finite element analysis tool Code_ Aster, enabling the dynamic analysis of catenary mooring systems for a floating wind turbine. It is indicated that the mooring tension predicted is in good agreement with the results provided by the classic quasi-static approach, and also observed satisfactorily in the experiments.

2.3 Mooring line damping

The mooring line damping for a traditional catenary mooring system results from the line hydrodynamic drag with possible vortex-induced vibration, line internal forces, and line friction on the seabed. Hydrodynamic drag and friction damping are significantly affected by the motion of a floating platform aside from the internal damping cause by

material properties. Many studies investigated the contribution of mooring line damping to the global responses of a deep-water floating platform, such as the quasi-static model series of mooring damping calculation (Huse, 1986b, Huse, 1991, Bauduin and Naciri, 1999) .

The contribution of LF damping of mooring line to the low frequency behaviour of the moored structure was investigated by (Boom, 1985), since dynamic behaviour of a mooring line can increase both the mooring stiffness and low frequency damping. In 1986, there was the first publication to present the effect of the drag forces on the mooring lines, discussed with theoretical and experimental methods (Huse, 1986a). Its importance was further regarded as the main source (as much as 80%) of surge damping for a vessel in (Huse et al., 1988), and a simple procedure of energy dissipation was presented. He described simplified ways to account for low and wave frequency motions in damping calculation, and found that the wave frequency motion superimposed with low frequency oscillation could enlarge the mooring line damping by 2-4 times (Huse, 1989). It is also emphasized that the mooring line damping cannot be neglected for the prediction of low-frequency surge motion of moored vessel in (Matsumoto, 1991a).

Triantafyllou and et al. assessed the various components of the damping coefficient of a moored structure (Triantafyllou, 1994). The mooring line drag amplification due to VIV and wave-induced motions is predicted based on a comprehensive data base, it was emphasized that mooring line damping coefficient would be 50% under estimated if neglecting the drag amplification for mooring line. The authors also summarized that there are four sources for the damping of the moored floating structures: wave drift damping, wind damping, current and viscous flow damping, and mooring line damping. Among all of the above sources, the mooring line damping is one of the largest components for accurate prediction of the performances of the floating platforms.

C. Webster (1995) applied the indicator diagram method to calculate the mooring-induced damping, he proposed non-dimensional investigation of mooring line damping

and identified its dimensionless parameters. The damping of the mooring system was determined with energy dissipation due to the motion of moored offshore structure. Based on non-linear dynamic analysis of mooring lines, simulations for parametric studies of mooring-induced damping are carried out in non-dimensional way. The results demonstrate the trends of the mooring-induced damping with variations in pretension, amplitude, period, scope, stiffness, drag coefficient and current. This method was also used to calculate the mooring line damping in the time domain by Qiao and Ou (2010). The seabed friction of the chain line was taken into account, and different oscillation amplitude and frequency were applied to assess the maximum tension and damping of the mooring line.

Johanning et al. (2007) compared experimental results for tension and damping of a 7m catenary chain with results from a numerical time domain model in Orcaflex. The results give confidence that non-linear numerical solutions can appropriately predict these quantities, even when non-linear phenomena dominate. Bauduin and Naciri (1999) developed a new quasi-static method, which can estimate the normal velocity of the mooring line in a more accurate way, and further accurately predict the contribution for mooring ling damping. The results show its advantages when compared with finite element method and existing quasi-static method, and are validated with the results from model tests.

Fan et al. (2017b) proposed an improved quasi-static methods for estimating mooring line damping of truncated mooring system, and in the method normal drag forces, tangential drag forces and seabed friction are considered. The improved quasi-static method is verified by scaled model tests results to be effective. Thus, based on the damping equivalence, the approach can be applied in designing truncated mooring system (Fan et al., 2017a, Fan et al., 2018).

Qiao and Ou (2014) investigated the estimation of mooring line damping on the basis of a 5 MW offshore wind turbine model. A numerical estimation method of the mooring line energy absorption was validated by performing scale model tests. Different

parameters include excitation amplitude, period, and drag coefficient were analysed for mooring line damping induced by the horizontal and vertical excitation.

Xiong et al. (2016) proposed an improved numerical approach for the estimation of the mooring induced damping, and is validated by both the experimental and the published results. Meanwhile, the mooring line induced damping of the truncated mooring lines applied in the physical experiment is compensated by comparing with those in full length. It was also indicated that the dissipated energy increased with the wave-frequency motion superimposed to the low-frequency motion.

In the studies of (Xu and Ji, 2014, Xu et al., 2018), free decay method was applied to obtain system critical damping, and the system damping can be gained by multiplying the damping ratio to the critical damping. Model tests of a semi-submersible moored with different mooring systems were carried out to study mooring line damping. It is indicated that the mooring tensions and induced damping were closed related, and the hybrid mooring system with buoys could lead to positive role in increasing the mooring induced damping. In the process of truncated mooring system design, it is important to accurately simulate the mooring line induced damping and dynamic response.

Karimirad (2013) investigated a floating wind turbine in deep water depth supporting a 5 MW turbine system. The results show that the mooring line damping can help to damping-out the high-frequency elastic-deformations of the mooring system. However, the mooring damping-effects did not significantly affect the motion responses. It is found that the damping and inertia forces of the mooring lines are important for the tension response.

The mooring induced damping was determined with combined first- and second-order motion by statistical linearization (Sarkar and Eatock Taylor, 2000). A dynamic stiffness approach was applied to calculate the dynamic responses of the mooring cable. The application of the statistical method saved time, when compared to the traditional finite element method. The responses of the mooring line were calculated by enforcing a

sinusoidal motion at the attachment point, the equivalent linear reactive contribution of the mooring line can be estimated with frequency dependent impedance properties (Fitzgerald and Bergdahl, 2008). The linearized properties can present the contribution of mooring cable in frequency domain analysis.

Thomas and Hearn (1994) indicated that the out-of-plane seabed friction can be negligible and that in-plane effects can influence the peak dynamic tension. Liu and Bergdahl (1997) did research on the effect of seabed friction to mooring line damping. They carried out dynamic analysis of mooring lines in frequency domain, using a finite element model of the cable. By comparing the results of frequency domain analysis with those of time domain analysis, it was found that the linearized frequency domain solution could predict acceptable results for most of the cases studied. They also proposed an improvement on Huse's quasi-static model for mooring line-induced damping. The authors pointed out that, in shallow to intermediate water depth, the transverse motion amplitude of an element of the line due to a periodic low-frequency surge motion was quite different if the two half-cycles were considered to start at the mid-position, as shown in Figure 2-1. This led to the definition of two different amplitudes for each half-cycle. In so doing, the dissipated energy increases notably and thus the mooring line damping. It is found that their method yielded estimates of the mooring line damping generally closer to the fully dynamic results than Huse's model(Liu and Bergdahl, 1998).

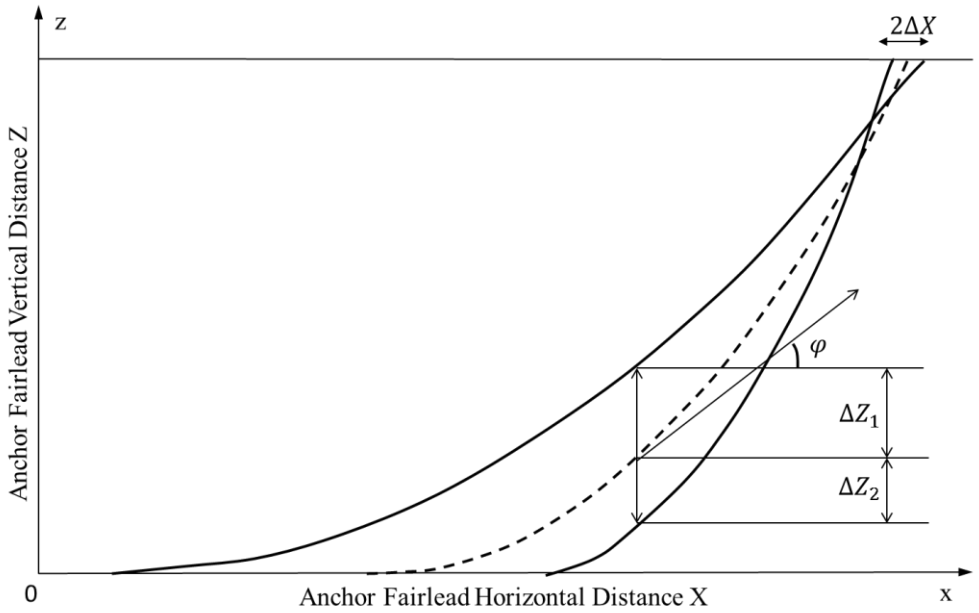

Figure 2-1 Near, mid and far mooring line profile

A new method was applied on two selected mooring line configuration by Brown and Mavrakos (1999). The results calculated with first- and second-order motions were compared with Huse's model and with predictions by fully dynamic numerical analyses and some experiments. It was recommended that both frequency- and time-domain calculations need further validation against experimental measurement.

2.4 Experimental validation

Mooring line analytical methods have been studied by many researchers (Brown and Mavrakos, 1999, Mavrakos et al., 1996, Johanning et al., 2007, Huang, 1994). It is common that both frequency- and time-domain calculations need further validation against experimental measurements (Azcona et al., 2017a, Bergdahl et al., 2016, Dessi and Minna, 2014, Karimirad, 2013, Sethuraman and Venugopal, 2013). Model tests have often been used to investigate the mooring line dynamic responses, and also estimate the relative importance of the various sources of damping affecting the slow-drift motion of a moored structure, i.e., wave drift damping, viscous hull damping, and mooring line damping.

Experimental studies were set-up to estimate the extreme loads for the mooring system. Model tests for an internal turret-moored and an external turret-moored FPSO were set-up by O'Donoghue and Linfoot (1992), the LF and HF components of the mooring tension were separated to investigate the relation to extreme mooring tension and turret response. Liu and Bergdahl (1999) also did some research on the combination between the LF and the WF components of mooring line tension based on the model test results, and proposed to estimate a formula considering the correlation effects.

Raaijmakers (1997) presented an experimental verification of the simple quasi-static model which was presented by Huse. Model tests are widely used in hybrid model testing for deep-sea moored offshore systems. Fan et al. (2014) developed an innovative approach to design an equivalent truncated mooring system for hybrid model testing. The damping of the system was regarded as one of the most important characteristics that needed to be considered in order to design scaled model effectively.

To identify the mooring line damping experimentally, two methods are usually applied: decay tests and forcing the top end of a chain with an oscillation motion. Decay tests can be applied as in the early works (Huse, 1989), the damping ratios are calculated using analytical methods, it was found that the mooring lines caused an increase in damping from 0.23 to 0.3. Decay tests of a moored hull were conducted by (Bauduin and Naciri, 1999, Schellin and Kirsch, 1989, A.M.A. Hassan, 2010). The mooring line damping is obtained approximately by subtracting the hull contribution from the average damping over the entire decay test. Low-frequency damping was obtained by simulations in still water and in regular waves.

The second method, as discussed by C. Webster (1995) and applied by Raaijmakers (1997) is performed with a horizontal sinusoidal oscillation motion driving the top end of a chain (Nielsen and Bindingbø, 2000). The damping from the region of the inter-connecting columns of an innovative floating production system theoretically is estimated and compared to the results of the experimental data from a scale model in regular waves (Brown and Fang, 1996, Raaijmakers, 1997). Model tests were also

performed by (Wichers and Huijsmans, 1990, Wichers and Huijsmans, 1984) to analyse the effect on the overall mooring line damping of combining the low-frequency surge motion of the fairlead to its wave frequency heave motion. They concluded that wave frequency motions induce a considerable increase in the mooring damping. Model tests were carried out to estimate the effects of damping from the mooring line on the slow drift oscillation by Nakamura et al. (1991). In these tests, the top end of chains with various pretensions was subjected to harmonic surge oscillations.

Some scholars concern is to determine correct scaling to perform perfect dynamic similitude between full-scale prototypes and small-scale model tests. The experiments in restricted water depth require appropriate scaling of both cable elastic stiffness and its free-falling velocity, as shown by Papazoglou et al. (1990). It is emphasized that properly scaling the line's static configuration through the imposed limited water depth is of key importance to obtain effective results for full-scale designs. Bergdahl et al. (2016) indicated that correct propagation celerity in scaled chain model of longitudinal elastic waves, is very important to present perfect geometrical and dynamic scaling in vacuum. It is indicated that the scaling error due to an incorrect Reynolds number is of minor importance.

A number of contributions outline simple analytical models with a view to obtaining a mooring line damping linear coefficient without resorting to model tests or fully numerical finite element calculations which are both time-consuming and expensive.

2.5 Drag coefficient for chains

Due to the limitation of the force model for slender structures, the force transfer coefficients are mainly determined from laboratory experiments or field tests. Whereas field measurement of hydrodynamic coefficients is complicated owing to the uncertainty of the ocean environment and the high cost of the experiment set up. Many experiments have been conducted in the laboratory to determine hydrodynamic coefficients (C_D and C_M) in one way or another and often for very special situations.

In many cases, the objective and/or experiment set-up limited the range of test conditions so that the results are quite restricted. Once the experimental data of time series have been measured, an appropriate method of data processing is another problem to determine the hydrodynamic coefficients. Several methods of data processing are available, as shown in Appendix B.

Empirical data on hydrodynamic coefficients for chain-shaped structures in oscillatory flow is limited. Most of the data of drag coefficient for chain is from simple towing tests, which are occasionally conducted by the chain manufacturers. These drag coefficients of chains are usually defined with respect to their nominal diameters. The experiments for chain are very complicated because of its complexity of shape. Another problem is the positioning of the force gauge due to the interconnected chain links. Due to these reasons, it is quite challenging to determine the hydrodynamic loading on the chain in a tank.

Lyons et al. (1997) carried out some model tests by using chain samples with a large geometric scale and considering different oscillatory motions. In their model tests, the mooring segments were mounted on an oscillator which provided synchronised inline and transverse motions by using two different motion carriages. In order to ensure the chain did not significantly deform laterally or rotationally due to fluid loading, a square section steel rod was passed through the chain to form a stiff stick of chain elements. The tri-axial forces were obtained by force cells fixed at both ends of the mooring segment. The velocities of the carriage and oscillator were taken from their velocity controllers, and accelerations could be derived consequently. The drag coefficients were then calculated from measurements of hydrodynamic forces on vertically oriented sections of chain, using a Fourier series approach. A series of fixed amplitude oscillations were tested respectively with different frequencies and the drag coefficient with KC numbers ranging from 70 to 580 were plotted against angular frequency in the publication (Lyons et al., 1997). Herein, the chain is stud type with nominal diameter of 25mm.

An investigation applying with an optical tracking system, for hydrodynamic force acting on chains was implemented by Yang (2007). The tests involve free and forced oscillations of long chain segments under conditions representative of mooring systems in still water. The fluid force is obtained from the solution of the slender structure dynamic equations of motion using the measured displacement and force, since there is no available technique for direct measurement of the hydrodynamic force on an oscillated chain. The instantaneous values of drag coefficients then were derived for a series of free oscillation tests, and a considerable range of scatter was exhibited.

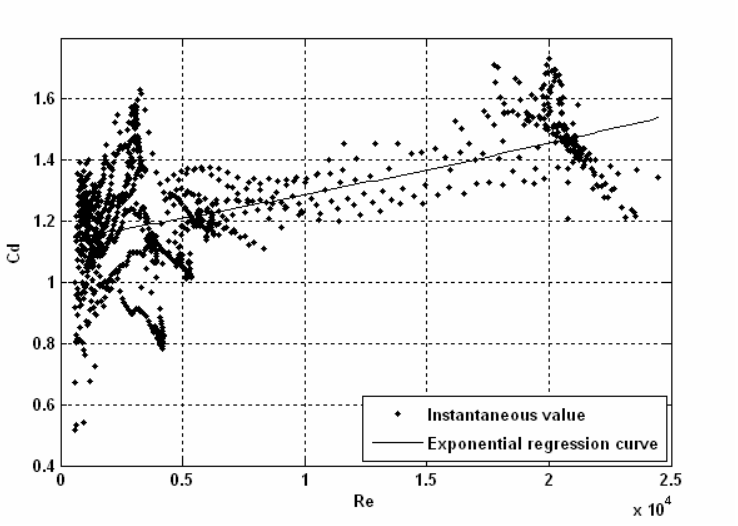

Figure 2-2 Drag coefficients for chains in large scale tests (Yang, 2007)

For the forced oscillation tests, the derived added mass coefficients in general showed more scatter than the drag coefficients, and they did not have a consistent KC - dependence (Yang, 2007). In the thesis, the measured drag coefficients for two sets of different shape of chains are presented in Figure 2-2, which provide data for a wide range of Reynolds number. Here, the drag coefficient is calculated based on the equivalent diameter which is equal to 1.8 times nominal diameter of stud-less chain. It was indicated the Fourier-averaged hydrodynamic coefficients as function of the KC number of a single chain in Figure 2-3.

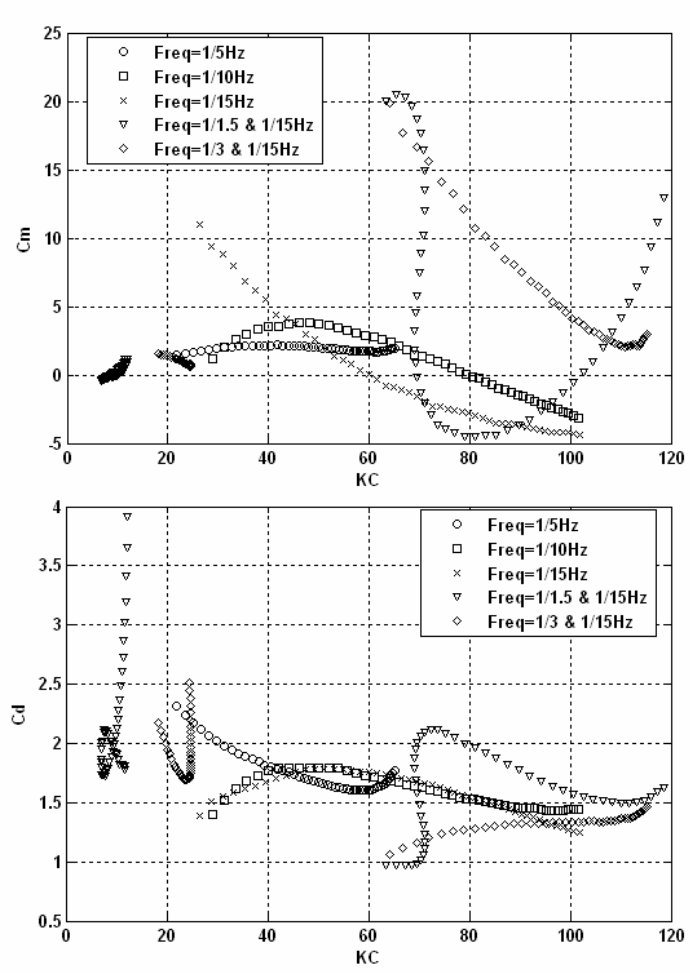

Figure 2-3 Fourier-averages drag and added mass coefficient of chain (diameter:1.954 cm)

with semi-taut catenary (Yang, 2007)

According to the review of previous experiments for chains, it is shown that there are big discrepancies in the drag coefficients for chains under oscillation tests. DNV recommended the values of drag coefficients only related to the Reynolds number (R_n), which are obtained by towing test for smooth chain under steady flows (DNV-RP-C205, 2010). In general, the measurement of hydrodynamic coefficients for the chain is more difficult than for other slender structures. More future effort on the hydrodynamic coefficients of chains is necessary, to generate a reliable database.

Table 2-1 Drag coefficients for chains (DNV-RP-C205, 2010)

Chain Type	***Normal drag coefficient*** C_D ***(*** $R_n = 10^4 - 10^7$ ***)***
Stud Chain	2.2-2.6
Stud-less Chain	2.0-2.4

3 Theoretical calculation of the mooring line damping

Offshore floating structures are maintained on station by a variety of mooring systems, and operate with severe environmental loads. The moored structure experiences complicated first- and second-order motions in the sea, such that the coupling effects between platform and mooring lines is of importance to accurately predict the motions of the platform and the tension of the mooring system. Recently, numerical calculation to simulate the offshore moored structure operated in the environmental loads has significantly improved, with the progress of the computing technology and development of fluid mechanics.

With regard to the theoretical approaches for a hull, the hydrodynamic coefficient matrices, such as the inertia and damping matrices; and wave load transfer function are calculated based on potential flow theory; the wind and wave load are computed with empirical equations. For a mooring line system, in order to estimate its initial behaviour in still water, static analysis is firstly considered under its own weight in the water, applied pretension force at one end, with and without elasticity. The catenary equation is usually used at the initial stage; it will be presented later in Appendix A. Following the static analysis, the numerical solution of mooring line response can be estimated by quasi-static and dynamic analysis.

3.1 Mathematical model

The response of mooring line is accomplished in two steps: the first step is static analysis, which determines the equilibrium configuration of the system under weight, buoyancy, and hydrodynamic current drag and provides a start configuration for the dynamic simulation later on; the second step is dynamic analysis, with which the response of the mooring line is calculated by solving the dynamic equation.

3.1.1 Mooring line statics

The catenary equation is a classic method to analyse the cable static response. The method is widely applied due to its simplicity and it can meet the requirement to provide the configuration for the cable line.

An element dl of a mooring line is selected as an objective, the static equilibrium equation for this element in its own plane can be written as follows by resolving forces tangentially and normally to the element:

$$(T + dT)\, d\varphi = w\, dl \cos\varphi \tag{3-1}$$

$$T + dT = T + w\, dl \sin\varphi \tag{3-2}$$

Rearranging and neglecting the small terms, the equilibrium can be rewritten as:

$$T d\varphi = w\, dl \cos\varphi \tag{3-3}$$

$$dT = w\, dl \sin\varphi$$

Finally, the catenary equation is derived as follows:

$$z = \frac{T_h}{w}\left(\cosh\left(\frac{w x}{T_h}\right) - 1\right) \tag{3-4}$$

Where T_h represents the horizontal force at any cross section; w is the submerged weight per unit length (N/m). The catenary equation is based on an assumption that the mooring line moves in two dimensions, namely, every node in the mooring line is always located in the plane determined by the vector of fairlead pointing to the touch down point and the vertical axis vector.

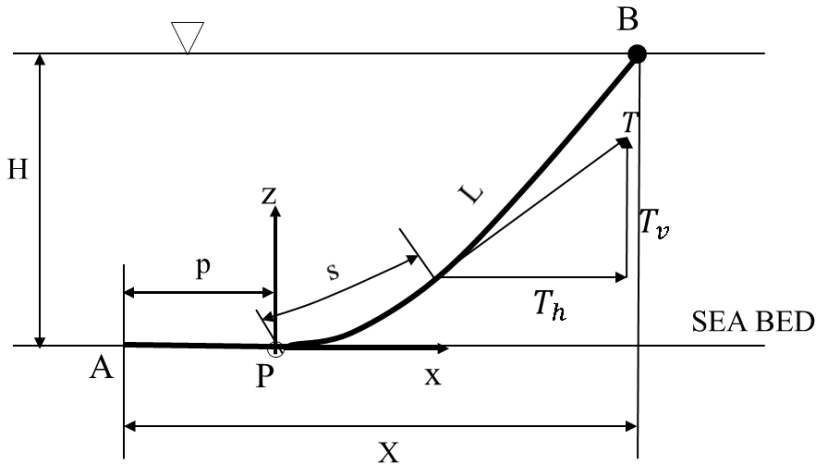

Figure 3-1 Catenary Mooring Line

Considering the bottom section laying on the seabed of catenary mooring line, as shown in Figure 3-1, point A and B are the anchor and fairlead point for the catenary mooring line, the vertical distance H and horizontal distance X are then determined. L is the total length of the cable. Point P is the tangency point of the cable on the sea bed, and also the origin point of coordinates $P-xy$. p is the length of the section of the cable on the seabed. The catenary equation is then rewritten,

$$z=\begin{cases}\dfrac{T_h}{w}\left(\cosh\dfrac{wx}{T_h}-1\right), & 0\le x\le X-p\\ 0, & -p\le x\le 0\end{cases} \tag{3-5}$$

Defining $a=\dfrac{T_h}{w}$,

$$\begin{cases} z(X-p)=H \\ z'(X-p)=\tan\varphi_w=\dfrac{T_v}{T_h}=\dfrac{w(L-p)}{wa}=\dfrac{L-p}{a}\end{cases} \tag{3-6}$$

Substituting Equation (3-6) into Equation (3-5) results in:

$$a = \frac{(L-p)^2 - H^2}{2H} \qquad (a)$$

$$e^{(X-p)/a} = \frac{H}{a} + 1 + \frac{L-p}{a} \qquad (b) \qquad \textbf{3-7}$$

The transcendental equation of the suspended length ($q = L - p$) is obtained by:

$$F(q) = \exp\left[(X - L + q)\cdot\frac{2H}{q^2 - H^2}\right] - \frac{2H}{q-H} - 1 = 0 \qquad \textbf{3-8}$$

Applying Newton iteration, q can be calculated from the equation above, then the value of a is obtained from equation (3-7), the horizontal and vertical component of fairlead tension are obtained from:

$$\begin{cases} T_h = w\,a \\ T_v = w\,q \end{cases} \qquad \textbf{3-9}$$

3.1.2 Mooring line dynamics

In the dynamic approach, the equation of motion of line dynamics is formulated and numerically solved to develop tension-displacement characteristics, which are then used as non-linear restoring forces in the motion response analysis of the moored platform (Khan and Ansari, 1986). The advantage of the dynamic analysis is that the line's inertia and drag are included (together with both horizontal and vertical motions). Including the nonlinearity of the mooring line makes this kind of analysis; which is usually performed in the time domain, time-consuming.

As summarized by Kwan and Bruen (1991), among different nonlinear effects of the mooring line there are four primary nonlinear effects which can have important influence on mooring line behaviour.

(1) Nonlinear Stretching Behaviour of the Line – The effect of this nonlinear behaviour typically occurs in synthetic materials such as nylon. Chain and wire rope are commonly regarded as linear. In many cases the nonlinearity can be neglected, and a linearized behaviour assumed using a representative tangent or secant modulus.
(2) Changes in Geometry – The geometry nonlinearity is associated with changes in shape of the mooring line.
(3) Fluid Loading – The Morison equation is most frequently used to represent fluid loading effects on mooring lines. The drag force on the line is proportional to the square of the relative velocity between the fluid and the line, and hence is nonlinear.
(4) Bottom Effects – In most mooring designs, a considerable portion of the line is in contact with the seafloor. The interaction between the line and the seafloor is usually considered to be a frictional process, and hence is nonlinear. In addition, the length of the grounded line constantly changes, causing an interaction between this nonlinearity and the geometric nonlinearity.

The dynamic equation can be solved with the finite element or the finite difference method. Although the former has a more rigorous mathematical derivation, the latter method is simple, and this advantage becomes more obvious, especially during conditions of large elastic deformation.

3.1.2.1 Lumped Mass method

The mooring line is discretized with several mass-less spring elements, and every element is between to two nodes. The weight of each element is evenly assigned to the two nodes, while the stiffness of the spring is determined by the characteristics of cable material. As described in (Hall and Goupee, 2015), the cable is broken up into N even-length line segments connecting $N+1$ node points. The index starts at the anchor, with the anchor node given a value of 0 and the cable segment between nodes 0 and 1 given element 1, illustrated in Figure 3-2.

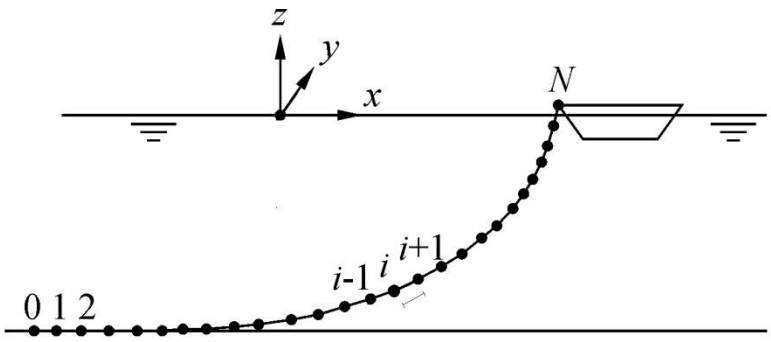

Figure 3-2 Mooring line discretization

The right-handed inertial reference frame is defined with the z -axis being measured positive up from the water plane. In addition, local coordinates are established for each node on the cable. The element i is selected as an example, as illuminated in Figure 3-3, the origin of the local coordinates is node i , the tangential direction of node i pointing to node $i+1$ is represented by ξ , two normal directions are η and ζ .

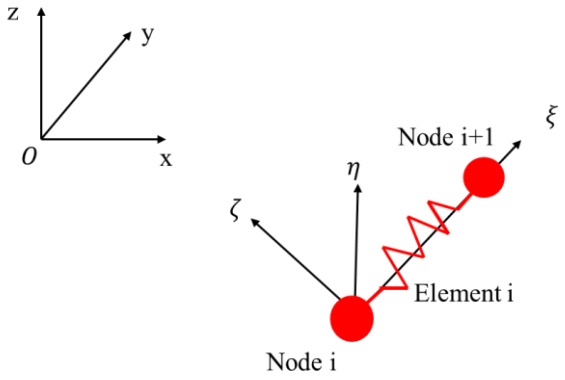

Figure 3-3 Local coordinate system of element #i

The relationship between the global coordinates and the local coordinates can be represented by a transformation matrix. Defining the unit vectors of the local coordinates are $\vec{\xi}$, $\vec{\eta}$ and $\vec{\zeta}$, meanwhile the unit vectors of the global coordinates are $\vec{i}$, $\vec{j}$ and $\vec{k}$. The conversion matrix can be derived as follows:

Assuming a certain vector $\vec{F}$, is represented by $F_x\vec{i} + F_y\vec{j} + F_z\vec{k}$ in the global coordinate system, and also represented by $F_\xi\vec{\xi} + F_\eta\vec{\eta} + F_\zeta\vec{\zeta}$ in the local coordinate system. The relationships of the unit vectors of the global and local coordinate system are:

$$\begin{cases} \vec{\xi} = \xi_x\vec{i} + \xi_y\vec{j} + \xi_z\vec{k} \\ \vec{\eta} = \eta_x\vec{i} + \eta_y\vec{j} + \eta_z\vec{k} \\ \vec{\zeta} = \zeta_x\vec{i} + \zeta_y\vec{j} + \zeta_z\vec{k} \end{cases} \quad \textbf{3-10}$$

The vector $\vec{F}$ of the local coordinated system can be rewritten as:

$$\begin{aligned} & F_\xi\vec{\xi} + F_\eta\vec{\eta} + F_\zeta\vec{\zeta} \\ &= F_\xi\left(\xi_x\vec{i} + \xi_y\vec{j} + \xi_z\vec{k}\right) + F_\eta\left(\eta_x\vec{i} + \eta_y\vec{j} + \eta_z\vec{k}\right) \\ &\quad + F_\zeta\left(\zeta_x\vec{i} + \zeta_y\vec{j} + \zeta_z\vec{k}\right) \\ &= \left(F_\xi\xi_x + F_\eta\eta_x + F_\zeta\zeta_x\right)\vec{i} + \left(F_\xi\xi_y + F_\eta\eta_y + F_\zeta\zeta_y\right)\vec{j} \\ &\quad + \left(F_\xi\xi_z + F_\eta\eta_z + F_\zeta\zeta_z\right)\vec{k} \end{aligned} \quad \textbf{3-11}$$

The relationship among coordinate transformation is built as:

$$\begin{pmatrix} \xi_x & \eta_x & \zeta_x \\ \xi_y & \eta_y & \zeta_y \\ \xi_z & \eta_z & \zeta_z \end{pmatrix} \begin{pmatrix} F_\xi \\ F_\eta \\ F_\zeta \end{pmatrix} = \begin{pmatrix} F_x \\ F_y \\ F_z \end{pmatrix} \quad \textbf{3-12}$$

The conversion matrix R **,** transforming the vector in global coordinate system to the local coordinate system is determined:

$$R = \begin{pmatrix} \xi_x & \xi_y & \xi_z \\ \eta_x & \eta_y & \eta_z \\ \zeta_x & \zeta_y & \zeta_z \end{pmatrix} \quad \textbf{3-13}$$

In the local coordinate system for element i, the unit vector of the tangential direction $\vec{\xi}$, is obtained as:

$$\vec{\xi} = \left(\vec{X}_{i+1} - \vec{X}_i \right) \Big/ \left| \vec{X}_{i+1} - \vec{X}_i \right| \qquad \textbf{3-14}$$

While $\vec{X}$ is the node coordinates in the global coordinate system.

3.1.2.2 The equilibrium equation

As displayed in Figure 3-4, the equilibrium equation for node i can be expressed as:

$$M_i \vec{a}_i = \vec{T}_i - \vec{T}_{i-1} + \vec{F}_{Di} + \vec{F}_{Ai} - \vec{W}_i \qquad \textbf{3-15}$$

While M_i is the mass of node i, $\vec{a}_i$ is the acceleration vector of node i, $\vec{T}_i$ and $\vec{T}_{i-1}$ respectively represent the tension vectors in element i and $i-1$, which are located at opposite sides of node i. $\vec{F}_{Di}$ and $\vec{F}_{Ai}$ are the drag and inertial force assigned on node i, from fluid acting on element i and $i-1$. Finally, B and W, are buoyancy and gravity.

The drag and inertial forces are calculated using Morison's equation. The internal and external forces are included in the discretized formulation is described in the following section.

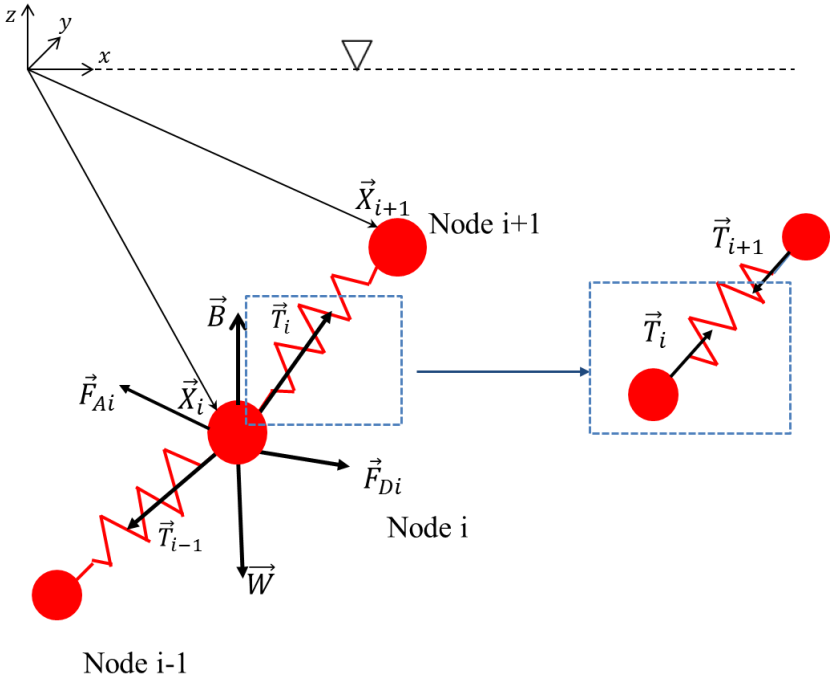

Figure 3-4 Forces acting on node #i

3.1.2.3 Submerged weight

Considering both the weight and the buoyancy, the node mass in the water, which is called submerged mass, is calculated with its buoyancy deducted. The mass for node i is calculated as:

$$M_i = \frac{1}{2}\left(m_{i-1} + m_i\right) \tag{3-16}$$

Subtract the buoyancy force as:

$$\vec{W}_i = \begin{pmatrix} 0 & 0 & M_i g - B \end{pmatrix}^T \tag{3-17}$$

3.1.2.4 Linear tension

As illustrated in Figure 3-4, the tension vectors $\vec{T}_i$ and $\vec{T}_{i-1}$ acting on node i, from element i and $i-1$, can be calculated by the cable strain as:

$$T_i = E_i \sigma_i \left(\left| \vec{X}_i - \vec{X}_{i-1} \right| / l_i - 1 \right) \quad \textbf{3-18}$$

Where l_i is unstretched length, E_i is Young's modulus, σ_i is cross-section area. $\vec{X}_i$ and $\vec{X}_{i-1}$ are the instantaneous coordinates for node i and $i-1$. With regard to chain, Figure 3-5 presents the nominal geometry of a stud link chain together with a stud-less link chain. Due to its complex configuration, chain is usually considered equivalent to a line with constant cross section along its length, the equivalent diameter can be expressed as (Orcaflex):

$$OD = \begin{cases} 1.80D\ m & (studless) \\ 1.89D\ m & (studlink) \end{cases} \quad \textbf{3-19}$$

Where D is named nominal diameter, as shown in the Figure 3-5.

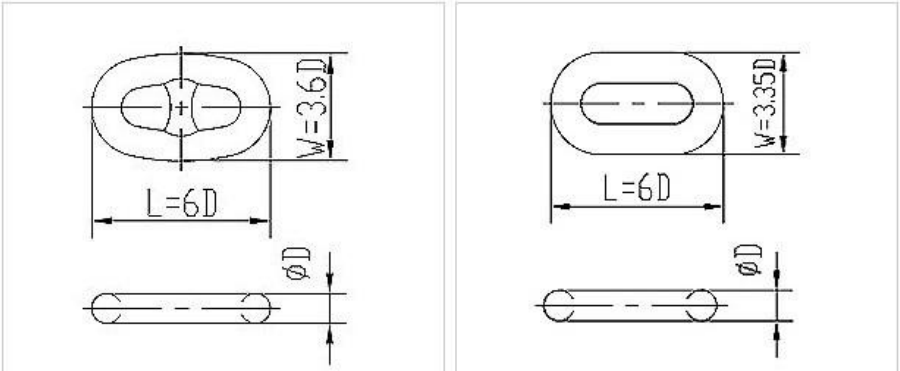

Figure 3-5 Studlink and studless chain

The tension acting on node i is always along tangential direction, its vector expression in the local coordinate system, $(T_i \quad 0 \quad 0)^T$ is converted to the global coordinate system as:

$$\vec{T}_i = R_i^{-1}\begin{pmatrix} T_i & 0 & 0 \end{pmatrix}^T = \begin{pmatrix} \xi_x & \eta_x & \zeta_x \\ \xi_y & \eta_y & \zeta_y \\ \xi_z & \eta_z & \zeta_z \end{pmatrix} T_i \begin{pmatrix} 1 \\ 0 \\ 0 \end{pmatrix} = T \begin{pmatrix} \xi_x \\ \xi_y \\ \xi_z \end{pmatrix} \quad \textbf{3-20}$$

$$= T_i r_i$$

3.1.2.5 Fluid viscosity

The fluid viscosity acting on an element of the mooring line is empirically computed using Morison equation, due to its shape of slender rod. The viscosity is usually divided into two parts: the drag force $\vec{f}_D$ and the inertia force $\vec{f}_A$.

Selecting element i as the objective, the drag force acting on the element $\vec{f}_{Di}$ is related to the relative velocity of its own speed and the fluid speed. The relative velocity vector in the local coordinate system is transformed applying the conversion matrix:

$$\vec{u}_i = R_i\left(\vec{V}_i - \vec{V}_i'\right) \quad \textbf{3-21}$$

Where $\vec{V}_i$ is the flow velocity at the centre of element i; $\vec{V}_i'$ is the velocity of the centre of element i, which represents the element velocity; the relative velocity is then $\vec{V}_i - \vec{V}_i'$.

The drag force $\vec{f}_{Di}$ is divided into two parts: the tangential f_{DT} and the normal f_{DN} The drag vectors in the local coordinate system is obtained: the tangential component, $f_{D\xi} = f_{DT}$; the normal vectors are resulted with resolution of f_{DN}:

$$\begin{cases} \left(\vec{f}_{Di}\right)_\xi = \dfrac{1}{2}\rho_w C_{DT}\pi d_i \left|\left(\vec{u}_i\right)_\xi\right|\left(\vec{u}_i\right)_\xi \\ \left(\vec{f}_{Di}\right)_\eta = \dfrac{1}{2}\rho_w C_{DN} d_i \sqrt{\left(\vec{u}_i\right)_\eta^2 + \left(\vec{u}_i\right)_\zeta^2}\left(\vec{u}_i\right)_\eta \\ \left(\vec{f}_{Di}\right)_\zeta = \dfrac{1}{2}\rho_w C_{DN} d_i \sqrt{\left(\vec{u}_i\right)_\eta^2 + \left(\vec{u}_i\right)_\zeta^2}\left(\vec{u}_i\right)_\zeta \end{cases} \quad \textbf{3-22}$$

While ρ_w is the water density; C_{DT} and C_{DN} are the tangential and the normal drag coefficient for mooring cable, separately; d_i is the cable element diameter.

The inertial force $\vec{f}_{Ai}$ is related to the relative acceleration of the element acceleration and that of the fluid. The inertial force $\vec{f}_{Ai}$ is calculated by added mass matrix multiplying the relative acceleration:

$$\vec{f}_{Ai} = M_{ai} R_i (\vec{a}_w - \vec{a}_i) \tag{3-23}$$

While M_{Ai} represents the added mass matrix of the cable element; $\vec{a}_i$ represents the node acceleration for the element; $\vec{a}_w$ represents the fluid acceleration.

In addition, the added mass of the cable element has no contribution in tangential direction, result in:

$$M_{ai} = \begin{bmatrix} 0 & 0 & 0 \\ 0 & m_{ai} & 0 \\ 0 & 0 & m_{ai} \end{bmatrix} \tag{3-24}$$

$$m_{ai} = \rho_w C_m l_i \sigma_i \tag{3-25}$$

While m_{ai} is the added mass matrix of the cable element; C_m is the inertial coefficient; l_i is the element length; σ_i is the cross-section area for the element.

The drag and inertial force are converted in the global coordinate system:

$$\begin{aligned} \vec{F}_{Di} &= \frac{1}{2}\left[R_{i-1}^{-1} \vec{f}_{Di-1} + R_i^{-1} \vec{f}_{Di} \right] \\ \vec{F}_{Ai} &= \frac{1}{2}\left[R_{i-1}^{-1} \vec{f}_{Ai-1} + R_i^{-1} \vec{f}_{Ai} \right] \\ &= -\frac{1}{2}\left(R_{i-1}^{-1} M_{ai-1} R_{i-1} + R_i^{-1} M_{ai} R_i \right) \vec{a}_i \end{aligned} \tag{3-26}$$

Finally, substituting equation (3-20), equation (3-26) into equation (3-15), combining the acceleration terms, result as:

$$M_{ti}\vec{a}_i = T_i r_i - T_{i-1} r_{i-1} + \frac{1}{2}\left(R_{i-1}^{-1}\vec{f}_{Di-1} + R_i^{-1}\vec{f}_{Di}\right) - \vec{W}_i \qquad \textbf{3-27}$$

3.2 The energy dissipation approach

The mooring induced damping for a catenary mooring results from the contributions from the line friction on the seabed, the internal friction within the chain and the hydrodynamic drag force along the line for its motion through the water. The hydrodynamic drag is of most importance among these effects.

The energy dissipation approach was introduced by Huse (1986b) as a theoretical method to calculate the energy dissipated by the drag force on the mooring line. The method calculated the energy dissipated by the mooring lines during one surge cycle (one period T) of the fairlead point using the positions of the fairlead and lift-off points of each mooring line at extreme points of the motion. Afterwards, the method was applied in conjunction with the energy dissipated by the velocity term in the equation of motion to calculate the mooring line damping (Huse et al., 1988).

3.2.1 The Huse's model

In Huse's model (1986b), some assumptions are made in the energy dissipation method as follows:

(1) Inertial forces acting on the mooring line are negligible;
(2) Motions are slow enough that the catenary shape is retained all the time;
(3) The friction between the seabed and the mooring bottom component is not taken into consideration;
(4) Calculations include drag forces that are normal to the line at all points;

(5) The drag coefficient is regarded as a constant, which is not related to Reynolds number and *KC* number;

(6) Motion components of the line are within the vertical plane of the line.

It is assumed that the fairlead point of the mooring line moves with a low frequency oscillation $X = a_0 \sin(\omega t)$, while a_0 is the motion amplitude of the moored offshore structure, and ω is the motion frequency.

According to the analysis of section 3.2.2.5, the normal drag force dF_{DN} by an element of the line ds is defined as:

$$dF_{DN} = \frac{1}{2}\rho_w D C_D V |V| ds \quad \textbf{3-28}$$

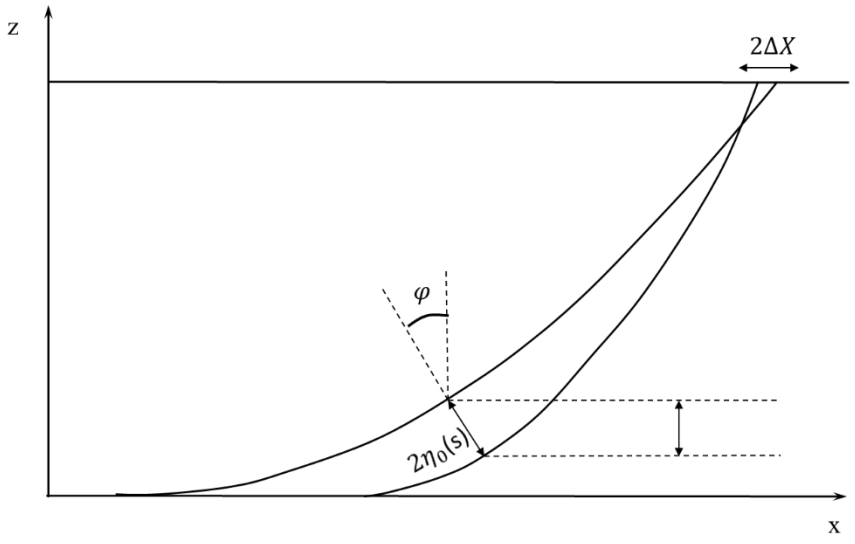

Figure 3-6 Extreme mooring line configuration during one surge cycle (Huse's model)

In Huse's energy dissipation model, the normal displacement for an element that is caused by the oscillation on fairlead point of mooring line, is defined as:

$$\eta(s,t) = \eta_0(s)\sin(\omega t) \quad \textbf{3-29}$$

In the equation, s is the curve coordinate along the mooring line; $s = 0$ locates at anchor point, and $s = L$ locates at fairlead point, L is the total length of mooring line. $\eta_0(s)$ is the normal displacement amplitude.

The relative velocity between the mooring line element and the fluid velocity is obtained by the derivation of equation (3-29):

$$V = \frac{d\eta(s,t)}{dt} = \omega \eta_0(s)\cos(\omega t) \tag{3-30}$$

Substituting equation (3-30) into equation (3-28), the dissipated energy during a cycle for an element ds is expressed by:

$$dE = \frac{4}{3}\rho_w D C_D \omega^2 \eta_0^3(s)\, ds \tag{3-31}$$

As displayed in Figure 3-6,

$$2\eta_0 = \Delta Z \cos\varphi + \Delta X \sin\varphi \tag{3-32}$$

Where φ is the angle between the cable tangent and the horizontal at the static equilibrium position. ΔZ and ΔX are the maximum values of vertical and horizontal displacement for the element during a cycle.

The horizontal displacement is assumed negligible by Huse, and it results in:

$$\eta_0 = \frac{1}{2}\Delta Z \cos\varphi \tag{3-33}$$

Substituting equation (3-33) into equation (3-31), the integration along the total length of the mooring line is defined as the energy dissipation during one cycle:

$$E = \frac{1}{6}\rho_w D C_D \int_0^L \Delta Z^3 \cos^3\varphi \, ds \qquad \textbf{3-34}$$

3.2.2 Liu's model

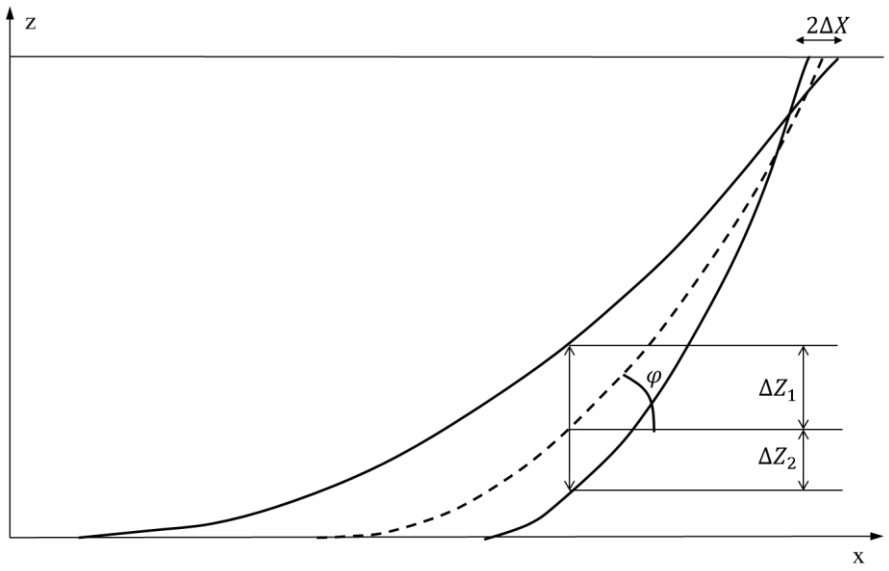

Figure 3-7 Extreme mooring line configuration during one surge cycle (Liu's model)

Liu proposed an improvement on Huse's quasi-static model for mooring line induced damping. The farthest and the closest vertical displacement for the element ds show asymmetry due to the geometric nonlinearity of the mooring line, a correction for the dissipated energy of equation (3-31) is thus expressed as:

$$dE = \frac{4}{3}\rho_w D C_D \omega_0^3 \left(\eta_1^2(s) + \eta_2^3(s)\right) ds \qquad \textbf{3-35}$$

Where $\eta_1(s)$ and $\eta_2(s)$ are the farthest and closest displacement amplitude for the element, respectively.

Neglecting the effect of the horizontal displacement, and integrating equation (3-35) along the total length of the mooring line, the energy dissipation during one cycle is obtained:

$$E = \frac{1}{6}\rho_w D C_D \int_0^L \left(\Delta Z_1^3 \cos^3\varphi + \Delta Z_2^3 \cos^3\varphi\right) ds \quad \textbf{3-36}$$

3.2.3 The 'indicator diagram' method

Quasi-static methods are not as rigorous as dynamic methods; therefore, dynamic approaches are more widely used to estimate the mooring line damping. Based on the nonlinear time-domain dynamic analysis, the 'indicator diagram' method was developed by (C. Webster, 1995), which is applied to estimate the mooring line damping in this thesis. The fairlead point of the mooring line is excited with a sinusoidal oscillation, of which the amplitude is a_0 , and the period is τ . The energy dissipation during one cycle of the mooring line is computed by the integration of the product of the horizontal tension and the velocity:

$$E = \int_t^{t+\tau} T_x \frac{dx}{dt} dt \quad \textbf{3-37}$$

Where E is the dissipated energy; T_x represents the horizontal component of the fairlead point tension; x is the horizontal component of transient displacement.

In order to linearize the mooring line damping, an equivalent linear damping coefficient is defined, thus the transient horizontal tension of the mooring line is:

$$T_x \approx T_x' = \zeta \frac{dx}{dt} \quad \textbf{3-38}$$

By the assumption of linearization, the dissipated energy in a cycle is computed:

$$E' = \int_t^{t+\tau} T_x \frac{dx}{dt} dt = \zeta \int_t^{t+\tau} \left[\frac{dx}{dt}\right]^2 dt = \frac{2\pi^2 a^2 \zeta}{\tau} \quad \textbf{3-39}$$

The time histories of the simulations are plotted in a special way on the indicator diagram. The motion of the fairlead point is plotted on the horizontal axis; the

component of the tension in the same direction as the motion is plotted on the vertical axis. The dissipated energy absorbed by the mooring line during one period is simply the area contained within the trace on one of these plots. The 'indicator diagram' method to estimate the mooring line damping follows the procedure shown in Figure 3-8.

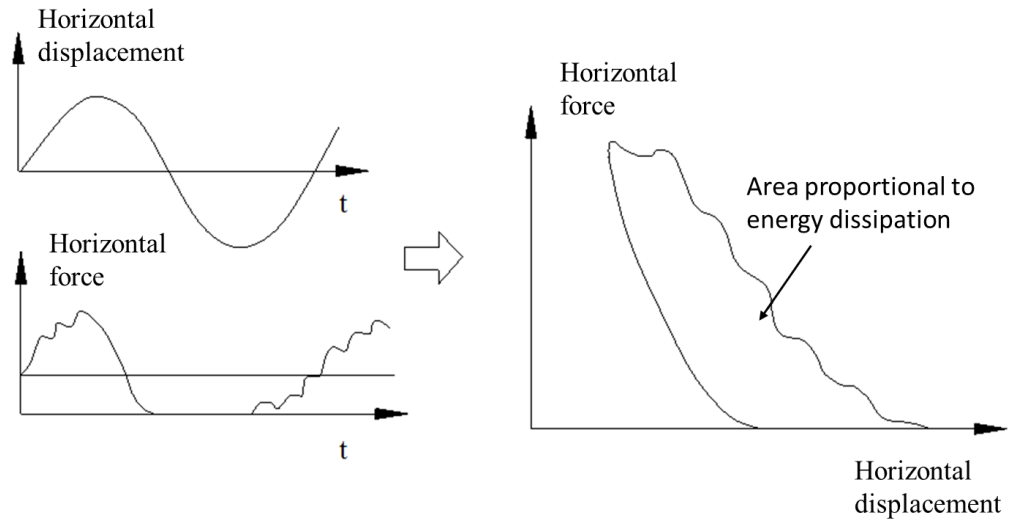

Figure 3-8 Indicator diagram for mooring induced damping (Webster, 1995)

3.3 Concluding remarks

In this chapter, the mathematical models of analytical calculation for the mooring line responses are studied, the details of mooring line static and dynamic responses are presented. At the start of the calculation, the static equilibrium configuration of the line is calculated, which is the starting point for dynamic simulation. Following the static analysis, mooring line dynamic analysis is conducted within six LF oscillation period cycles. In the process of dynamic analysis, the hydrodynamic loads on the line are computed using Morison's Equation. Due to the drag forces acting on the mooring line, energy dissipation of the mooring line could be calculated to estimate the mooring induced damping.

4 Dimensional study of mooring line damping

4.1 Introduction

In order to investigate the effects of the parameters that make contributions on mooring line damping, more calculations based on Orcaflex are carried out. Meanwhile, due to the advantages of non-dimensional approach in research on multivariate problems, this approach is applied to investigate the contributions of the variables on mooring line damping.

In prior to investigating the characteristics of mooring line damping using dimensional method, it is necessary to validate the accuracy and effectiveness of the assessment method for mooring line induced damping. In this case, the numerical calculation using 'indicator diagram' method based on the mooring line dynamic response in time domain, is verified with other numerical approaches used by some scholars (Xiong et al., 2016, Bauduin and Naciri, 1999).

4.2 Numerical validation

In this thesis, dynamic analysis based on the lumped mass method is applied using Orcaflex, and 'indicator diagram' is used to estimate the mooring induced damping. In order to validate the method, two types of mooring lines are selected as representatives in shallow water and deep water. The selected two mooring lines are used as the benchmark in (Bauduin and Naciri, 1999), where results from quasi-static and time domain dynamic method are presented. The properties for the mooring lines are listed as Table 4-1.

As is presented in Table 4-1, Line I is a chain mooring line, which is used in shallow water, while Line II represents the line made of wire, which is used in deep water. Compared to the chain line, the wire line has a lower wet weight, however with a still

considerable axial stiffness. Several cases are carried out with a defined oscillation excited at the fairlead point of the mooring line. The motion is applied as a surge motion in the vertical plane of the mooring lines. In this case, the environmental loads are not included that the mooring lines are performed in calm water.

Based on the nonlinear finite element dynamic analysis applied with Orcaflex, the mooring line damping effect is assessed by the dissipated energy. It can be obtained by integrating the work done by the upper tension during one surge oscillation period.

Table 4-1 Properties of the lines used for validation

	Line I	**Line II**
Water depth (m)	82.5	500
Unstretched total length (m)	711.3	4000
Line type	Chain	Wire
Diameter (mm)	140	130
Normal drag coefficient	3.2	1.8
Weight in air (N/m)	3586.5	800.5
Weight in water (N/m)	3202.0	664.4
Axial stiffness EA (N)	1.69E9	1.30E9
Horizontal pretension (kN)	427.7	1905.3
Pretension angle (°)	51.8	31.6
Anchor fairlead distance (m)	683.4	3910.1
Anchor lift-point distance	541.6	2239.1

The motion is assumed to be sinusoidal, the amplitudes and periods are listed in the first column of Table 4-2 and Table 4-3. The results are compared with those from the above references, where quasi-static method is used. The results based on the time-domain dynamic method are also listed and compared in (Bauduin and Naciri, 1999).

The last two columns of Table 4-2 and Table 4-3 show the error comparing the present method with the results given by Bauduin and Naciri (1999).

In Table 4-2, it is found that based on the method applied in this thesis, the results agree well with those using quasi-static methods. Meanwhile, it is worth mentioning that the results are more consistent with them using time-domain (TD) method. However, there is an exception for oscillation with amplitude of 10m and period of 200s. The reason for this error is probably because the energy dissipation is very small in this case, thus a small fluctuation of the results leads to a considerable discrepancy.

Table 4-2 Dissipated energy for Line I (unit: MJ)

Excitation	Liu	Bauduin and Naciri, Quasi-static	Xiong et al., Quasi-static	Bauduin and Naciri, Time Domain	Present Time Domain	Error Present/B&N Quasi-static	Error Present/B&N Time Domain
5.4m*10s	4.19	4.466	4.740	5.051	4.770	6.81%	-5.56%
10m*100s	0.36	0.365	0.386	0.395	0.428	15.07%	6.33%
20m*100s	6.73	8.100	7.983	8.637	8.415	3.83%	-2.63%
10m*200s	0.09	0.089	0.097	0.085	0.142	59.55%	67.06%
20m*200s	1.68	2.005	2.037	2.063	2.431	21.20%	17.79%

Table 4-3 Dissipated energy for Line II (unit: MJ)

Excitation	Liu	Bauduin and Naciri, Quasi-static	Xiong et al., Quasi-static	Bauduin and Naciri, Time Domain	Present Time Domain	Error Present/ B&N Quasi-static	Error Present/B&N Time Domain
5.4m*10s	151.12	143.900	175.46	8.220	7.581	-94.99%	-12.34%
30m*330s	20.840	24.240	29.547	24.420	20.74	3.56%	2.79%
50m*330s	85.190	123.500	141.77	119.010	102.17	-1.25%	2.48%

It is also shown that with higher oscillation amplitude, the dissipated energy is much bigger, which means higher amplitude of LF motion will lead to more significant increase of mooring line damping. The increase of the oscillation period however would make less effect on the dissipated energy.

Meanwhile, for line I, the indicator diagrams for case 5.4m*10s and 20m*200s are presented in Figure 4-1, and it is found that the area for the former one is much bigger although its smaller displacement range and horizontal force level. It is because the former case has a HF component with its horizontal velocity, thus leading to higher dissipated energy absorbed of the mooring line. It means HF oscillation will make significant contribution to mooring induced damping.

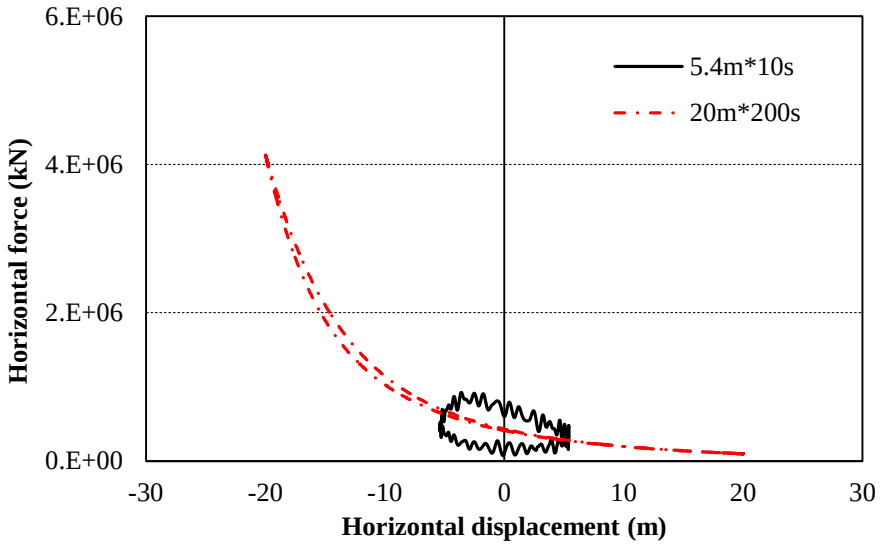

Figure 4-1 Indicator diagrams for case 5.4m*10s (blue) and 20m*200s (red)

From Table 4-3, it is found that the results of present study are in good agreement with those of previous studies, except the result of quasi-static method for case 5.4m*10s. It is because that the quasi-static calculation is based on the assumption of remaining quasi-static catenary profile all the time; but regarding to the high frequency oscillation of 10s, because of the light weight and large depth of Line II, it is more likely to break the quasi-static condition than Line I. It is thus lead to a considerable discrepancy between the quasi-static method and time-domain dynamic method for HF oscillation.

The results of remaining two LF excitations considered for Line II also indicate that the dissipated energy will have considerable increased with the increase of the oscillation amplitude. This trend is in good agreement with that of Line I in shallow water.

From the results of a typical chain mooring line in shallow water and a wire line in deep water; it can be found that the comparison with the results of the relevant references that: the present method give results of good agreement with the quasi-static method in shallow water; the higher amplitude of the LF oscillation will make significant increase on dissipated energy for mooring line, it is not only suitable for the chain mooring in shallow water but also the light weight mooring line in deep water; for Line I in shallow water, the increase of the oscillation period leads to a decrease of dissipated energy; in shallow water, the HF horizontal force components of the mooring line will significantly increase the mooring line damping; however, this HF component tends to be little difference for Line II in deep water.

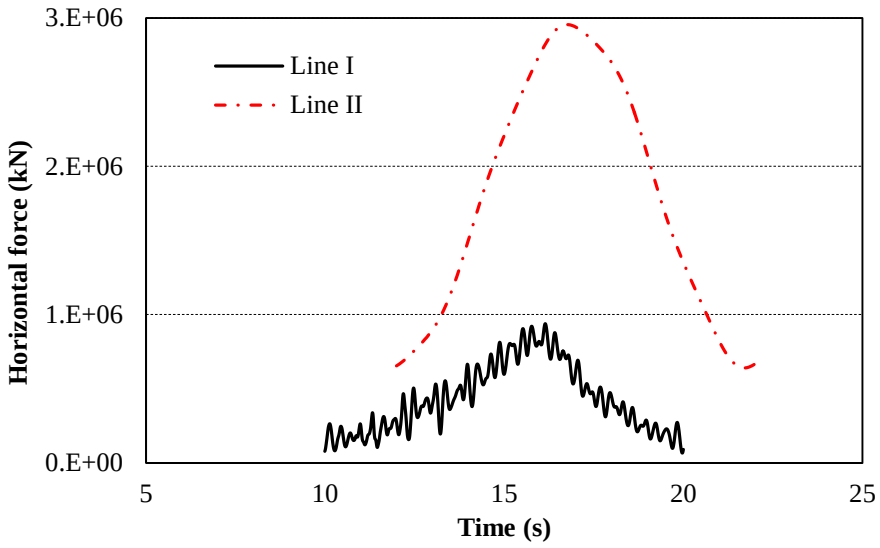

Figure 4-2 Horizontal force during a period

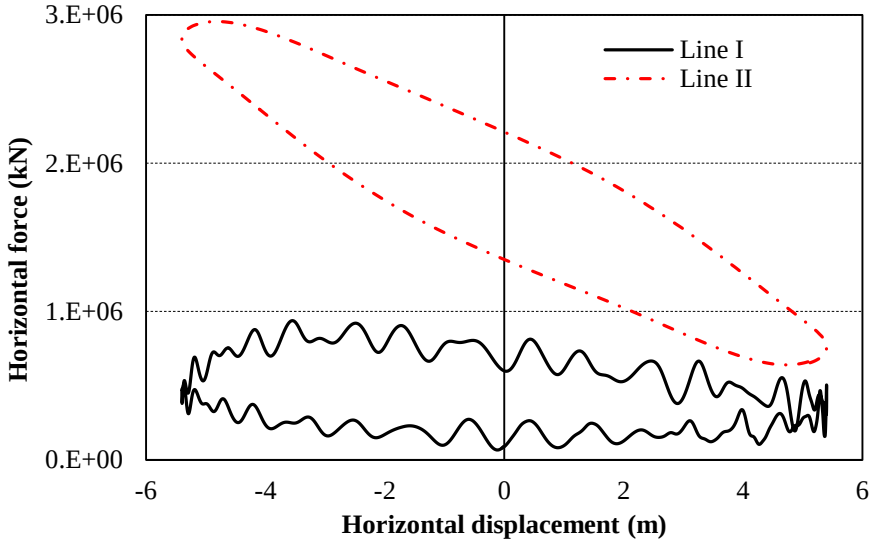

Figure 4-3 Indicator diagrams for case 5.4m*10s of Line I (blue) and Line II (red)

It can be seen from the results that

1) From the results for Line II in 500m, the mooring line damping increases significantly when compared to Line I in 82.5m;
2) For both Line I and Line II, the mooring line damping of cases with WF oscillations are bigger than those with LF oscillations;
3) It is known that the mooring line damping is mainly due to the drag force, and it is related to the square of relative velocity between line velocity and fluid velocity. That is why the mooring line oscillated by WF motion makes more damping contribution than that of LF oscillation.

However, as we can see, the mooring line induced damping is a complex variable. It is affected by the LF oscillation, HF oscillation, and its amplitude and frequency. Moreover, for the oscillation of 5.4m*10s, the mooring line responses of Line I and Line II show a distinct difference, as in Figure 4-2. Meanwhile, the mooring induced damping, which is represented by the indicator diagram in Figure 4-3, also varies considerably. It is deducted that the water depth, mooring line material, pretension and etc., these factors will make a difference to the mooring line damping. In order to

investigate the influence of those factors of significance to estimate the mooring line induced damping, the dimensional analyses are thus applied.

4.3 Parametrical study for a single mooring line

Take a single mooring line as a component of a complete mooring system for an offshore structure, Regarding to the mooring line, the instantaneous tension at the fairlead point, T, is simplistically dependent on 15 variables, as described in (C. Webster, 1995)

$$T = f\left[a, A_s, (C_D D_h), (C_m A_h), E_s, g, H, I_s, l, \rho_w, t, \tau, T_0, U_c, w\right] \quad \textbf{4-1}$$

In order to understand the behaviour and interpret complex interactions between these variables, a non-dimensional analysis is applied to this multivariate function, and the non-dimensional tension can be in terms of 12 non-dimensional groups.

$$\frac{T}{wH} = f_1\left[\frac{a}{H}, \frac{l}{H}, \frac{t}{\tau}, \frac{T_0}{wH}, C_D\frac{D_h}{D_s}, C_m\frac{A_h}{A_s}, \frac{I_s}{A_s^2}, \frac{\tau}{2\pi}\sqrt{\frac{g}{H}}, \frac{\rho_w g}{w}, \frac{wl}{E_s A_s}, \frac{\sqrt{A_s}}{H}, \frac{\rho_w}{2}\frac{U_c^2}{wD_s}\right] \quad \textbf{4-2}$$

The 12 non-dimensional parameters would reflect different aspects of physics of mooring line which will determine the dynamic response and they are described in the following:

$\frac{a}{H}$ is the ratio of the amplitude of motion to the water depth;

$\frac{l}{H}$ is the ratio of the mooring line length to the water depth and is commonly called the 'scope' of the mooring line;

$\frac{t}{\tau}$ is the time relative to the period of the sinusoidal excitation;

$\frac{T_0}{wH}$ is the ratio of the static pretension of the mooring line to the weight in water of a length of mooring line equal to the water depth. This parameter, together with the scope, governs the geometry of the mooring line when no motions are imposed;

$C_D \frac{D_h}{D_s}$ is the ratio of the hydrodynamic, cross-flow drag forces acting on the real mooring line to those which would act on the reference mooring line if exposed to the same flow situation;

$C_m \frac{A_h}{A_s}$ is the ratio of the added mass loads to those which would act on the reference mooring line exposed to the same flow situation;

$\frac{I_s}{A_s^2}$ is the ratio of the moment of inertia in bending of the mooring line to the square of the structural cross-sectional area;

$\frac{\tau}{2\pi}\sqrt{\frac{g}{H}}$ is the ratio of the period of the excitation to the period of a pendulum of length H;

$\frac{\rho_w g}{w}$ is the ratio of the water mass density to the mass density of the mooring line material. This parameter measures the relative importance of the hydrodynamic loads to the internal mechanical loads;

$\frac{w\,l}{E_s A_s}$ is the strain at the top of the cable resulting from suspending the mooring line vertically in water of unrestricted depth. This parameter measures the relative 'stiffness' of the mooring line;

$\frac{\sqrt{A_s}}{H}$ is the ratio of the diameter of the reference mooring line to the water depth. Since almost all mooring lines are exceptionally thin compared to the water depth, this parameter approaches zero;

$\frac{\rho_w}{2}\frac{U_c^2}{w D_s}$ is the ratio of the hydrodynamic drag force per unit length on the reference mooring line due to current to the weight of the mooring line in water per unit length. This parameter is the tangent of the static stream angle (measured from the vertical) of the reference mooring line suspended from the top in water of unrestricted depth and exposed to a current, U_c.

Since most mooring lines are steel, the parameter $\frac{\rho_w g}{w}$ does not vary much. The added mass term, $C_m \frac{A_h}{A_s}$ does not make much differences. The parameter of $\frac{\sqrt{A_s}}{H}$ approaches zero, because the cross-sectional area of mooring line are very small compared to the water depth. These three parameters are neglected, and the Equation (4-2) can be simplified as:

$$\frac{T}{w h} = f_1\left[\frac{a}{H}, \frac{l}{H}, \frac{t}{\tau}, \frac{T_0}{w H}, C_D \frac{D_h}{D_s}, \frac{\tau}{2\pi}\sqrt{\frac{g}{H}}, \frac{w\,l}{E_s A_s}, \frac{\rho_w}{2}\frac{U_c^2}{w D_s}\right] \quad \textbf{4-3}$$

When concerned with the contributions of the mooring line to the damping, the energy dissipation from the mooring is taken into consideration; it is calculated within a cycle

of motion, as expressed in Equation (3-39). If we chose ζ as damping coefficient so that $E' = E$, then

$$\zeta = \frac{E\tau}{2\pi^2 a^2} = \frac{E}{awH}\left(\frac{\tau wH}{2\pi^2 a}\right) \qquad \textbf{4-4}$$

The equivalent linear damping coefficient is therefore obtained from the non-dimensional energy dissipation, $E/(awH)$ and other known parameters. As a consequence of the integration over time, it is seen that the non-dimensional energy dissipation, $E/(awH)$, does not depend on time, and it can be obtained from Equation (4-5):

$$\frac{E}{awH} = f_1\left[\frac{a}{H}, \frac{l}{H}, \frac{T_0}{wH}, C_D\frac{D_h}{D_s}, \frac{\tau}{2\pi}\sqrt{\frac{g}{H}}, \frac{wl}{E_s A_s}, \frac{\rho_w}{2}\frac{U_c^2}{wD_s}\right] \qquad \textbf{4-5}$$

4.4 Parametric study

As expressed in Equation (4-5), the energy dissipation is function of seven variables, and it is complicated to interpret the combination systematically. The effects from the parametric variables of the mooring line characteristics of excitation amplitude, excitation period, scope, and drag coefficient, current are determined independently. Only one variable is changed at each time and all others are remained same as the baseline. Here, the baseline mooring was defined:

$$\frac{l}{H} = 6.4, \quad \frac{T_0}{wH} = 1.37, \qquad \textbf{4-6}$$
$$C_D\frac{D_h}{D_s} = 0.67, \quad \frac{E_s A_s}{wl} = 1500, \quad \frac{\rho_w}{2}\frac{U_c^2}{wD_s} = 0$$

The baseline represents the characteristics for a mooring line system in the form of chain.

4.4.1 The effect of excitation

To investigate the response of the baseline mooring line, simulations were performed for a harmonic LF excitation and a LF motion superimposed with a harmonic WF motion. For a pure LF excitation, the motions five amplitudes (*a/H=0.03, 0.05, 0.08, 0.1, 0.15*), and two different non-dimensional periods of 9.96 and 15.59 were investigated. For the simulations of LF motion with a harmonic WF motions superimposed, the WF motions were consisted with five amplitudes (*a/H=0.012, 0.02, 0.028, 0.04, 0.048*) and two different periods of 0.63 and 0.95. These motions were excited in the surge direction in the plane of the mooring line for the following parametric study, but with an exception. For the simulations of vertical forced motion, the different WF motions were superimposed in the heave direction of the mooring line.

4.4.1.1 The effect of horizontal forced motions

The non-dimensional mooring line induced damping, for the range of the amplitudes and periods of LF excitation, are shown in Figure 4-4. With the amplitude increase, the mooring line damping is getting higher. Meanwhile, the faster excitation (smaller period) will lead to a higher rise in mooring line damping. This character of the curves is similar to those for LF motion with WF motion superimposed, as shown in Figure 4-5. Here, it can be seen that the period has a very significant effect on the mooring line damping; it means the energy dissipation due to the drag force acting on the mooring line is getting bigger when excited with higher frequency movement.

At the same time, it is shown that the level of mooring line damping is small with the pure LF motion oscillation, ranging from 0 to 0.005. However, the mooring line damping is dramatically bigger with WF motion superimposed, ranging from 0 to 3(for the cases simulated here). It is because most of the motion is absorbed by the stiffness of the mooring line when the LF oscillation is excited. The LF tension within the mooring line is close to the amplitude of the motion times the stiffness of the mooring line, the character is similar to a spring and so the damping is small. However, the WF

motion superimposed will lead to a significant drag force on the mooring line, which will produce the damping component.

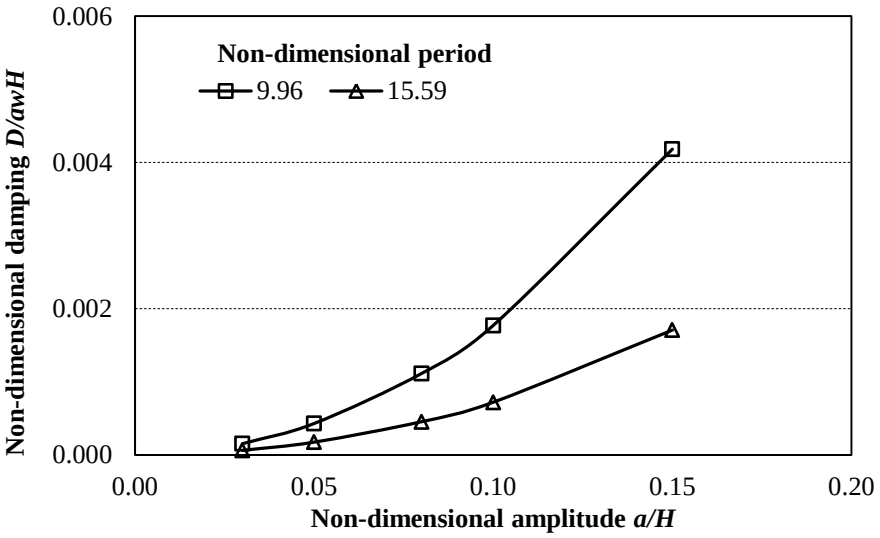

Figure 4-4 Variation of mooring line damping with various amplitudes and periods (LF motion)

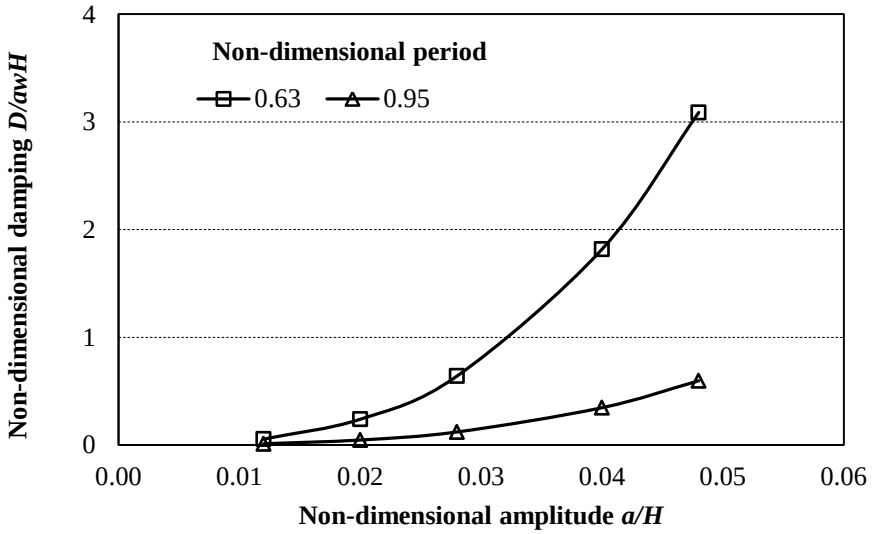

Figure 4-5 Variation of mooring line damping with various amplitudes and periods (WF motion)

4.4.1.2 The effect of vertical forced motions

As it is known, there are interactions between six degree-of-freedom movements for the floating offshore structures. In order to investigate the effect of heave motion on the mooring line damping, the WF motions of five amplitudes (*a/H=0.012, 0.02, 0.028, 0.04, 0.048*) are performed in surge, heave and both in surge and heave directions, respectively. The results of the mooring damping in horizontal and vertical directions are shown in Figure 4-6.

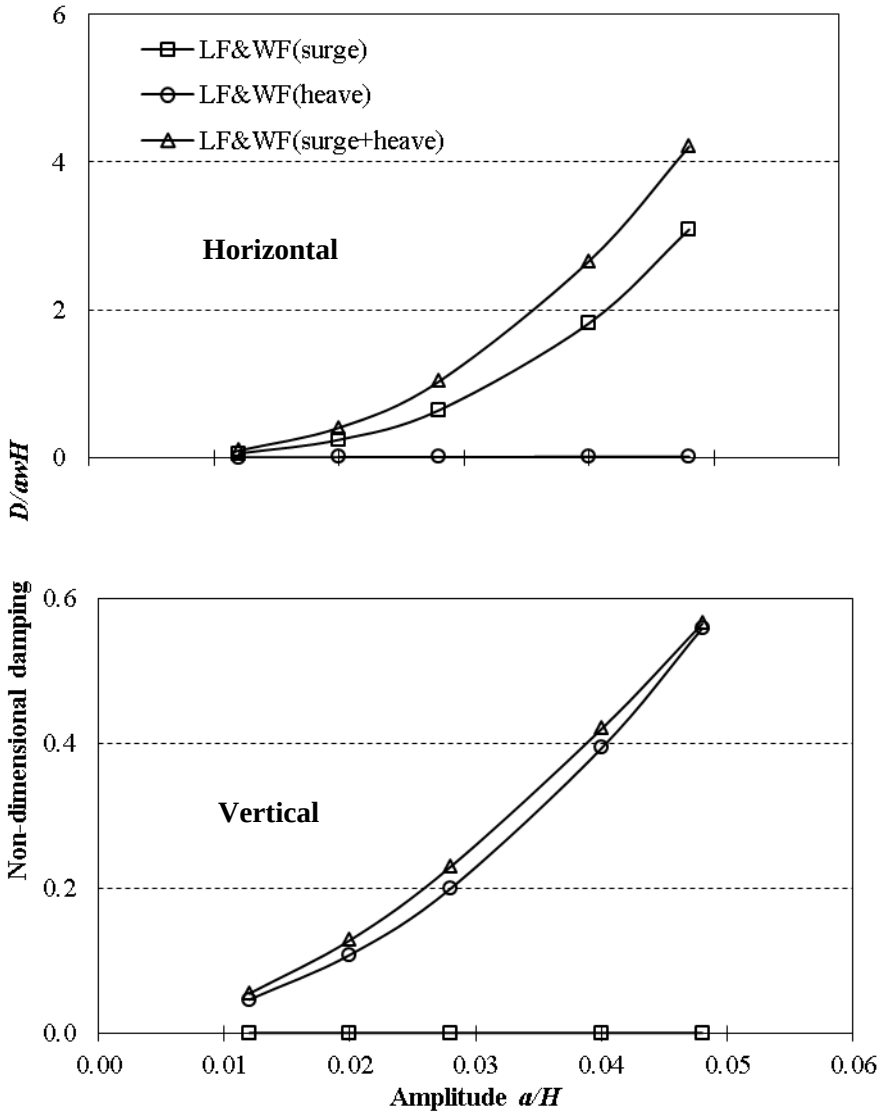

Figure 4-6 Variation of mooring line damping in horizontal and vertical directions

The horizontal component of the mooring damping shows that the WF heave motion would lead to a considerable drag forces in surge direction on the mooring line, and consequently, makes contributions on horizontal damping of the mooring line. However, the WF motions in surge direction would not make effect on the vertical component of the mooring line damping.

As the effect of the excitation was done, the other parameters in Equation (4-2) were then varied, one at a time, to estimate the contribution of each on the behaviour of the baseline mooring line. For the baseline, the oscillation with period of 15.59 and 0.63 are selected as the representatives of pure LF oscillation and the WF motion superimposed, respectively, which is performed in the simulations for the following investigations.

4.4.2 The effect of pretension

In order to estimate the effect of pretension on the mooring line damping, pretensions ranging from a typical catenary mooring line to nearly taut lines ($T_0/wH = 1.37$, 2.57, 5, 20, 60) were performed, desperately. Figure 4-7 shows a profile view of a mooring line of scope 6.4 for each of the selected non-dimensional pretensions.

The non-dimensional damping, with various pretensions, is shown along with the amplitude in Figure 4-8. The mooring line damping is increasing with the amplitude getting bigger, for the pretensions selected here. With the pretension increase from 1.37 to 20, the mooring line damping increase more dramatically. As we known, there is longer mooring length lifted for bigger pretension than that for smaller pretension, which means the drag force loaded line length is longer for the bigger pretension.

However, when the pretension becomes very large, the mooring line shows taut and the stretch of the mooring line becomes predominant. Most of the motion is absorbed by the stretching of the mooring line, and the mooring line behaves like a linear spring. In this case, the mooring line damping is lower (as seen the figures for $T_0/wH = 60$ in Figure 4-8).

When the mooring line is excited by LF motion and WF motion superimposed, the curves reflecting the damping levels versus the amplitudes are displayed in Figure 4-9. It is found that the amplitude has a slight effect on the mooring line damping for slack lines (as shown for $T_0/wH = 1.37$, 2.57). As the pretension becomes larger, the amplitude has more considerable effect on the mooring line damping. On the contrary to the case of LF oscillation, the mooring line damping for pretension 60 is almost same as those of pretension 20. It can be found that the superimposed WF motion dominates the energy dissipation of the mooring line, compared to the effect of the LF motion. When the mooring line becomes taut, the superimposed WF motion will make little contributions to mooring line damping because of movement limitation.

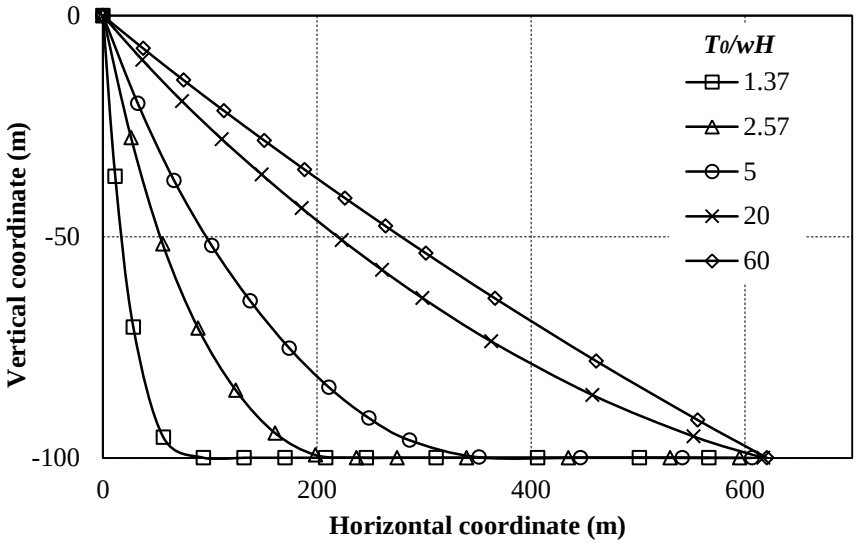

Figure 4-7 Mooring line geometry with pretensions

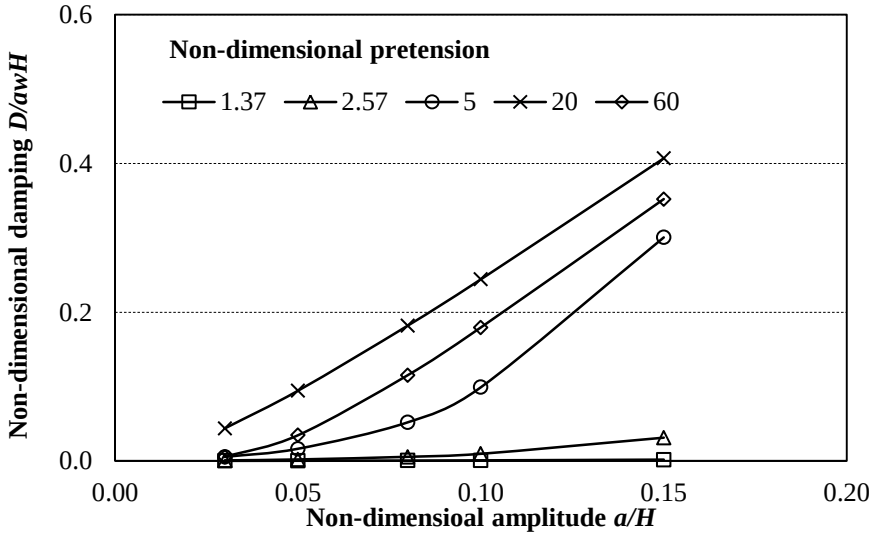

Figure 4-8 Variation of mooring line damping with varying amplitudes of LF oscillation (various pretension)

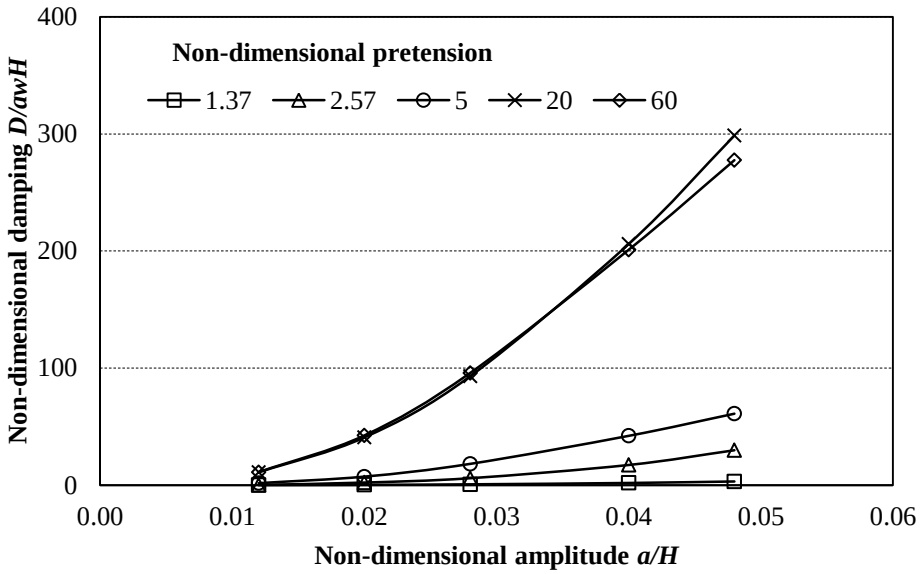

Figure 4-9 Variation of mooring line damping with varying amplitudes of WF oscillation (various pretension)

In order to estimate the effect of the pretension, the curves of mooring line damping levels versus the pretensions are presented in Figure 4-10 and Figure 4-11. It can be found that the features of the curves for combined oscillations are similar to those of LF oscillation. The damping reaches a peak at non-dimensional pretensions in the neighbourhood of 20. This character is in accordance with the study of Webster (C. Webster, 1995). For small pretension, the amplitude of the oscillation has a considerable

effect on the non-dimensional damping for both the LF oscillations and LF motion superimposed with WF motions. It is shown that the mooring line damping reaches a peak value for the moderate pretension. As the pretension becomes bigger, the mooring line damping appears to vary almost linearly with the amplitudes.

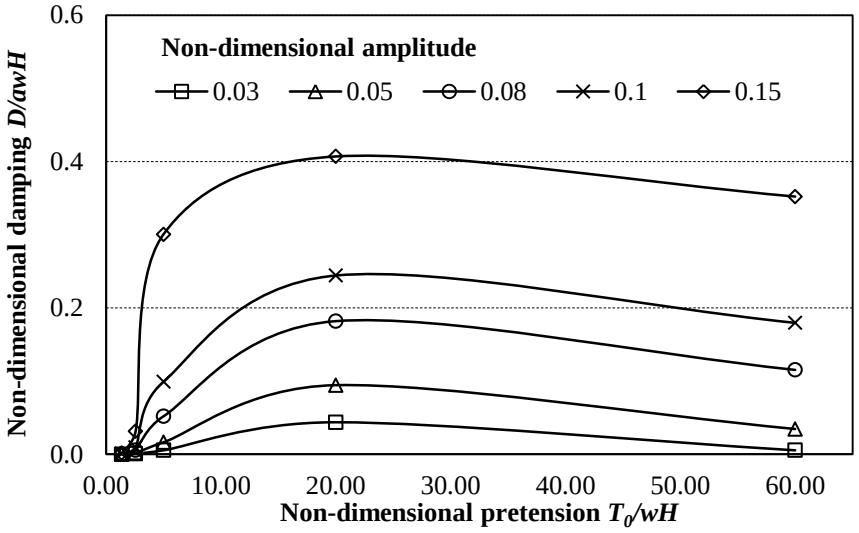

Figure 4-10 Variation of mooring line damping with pretension (various LF oscillation amplitudes)

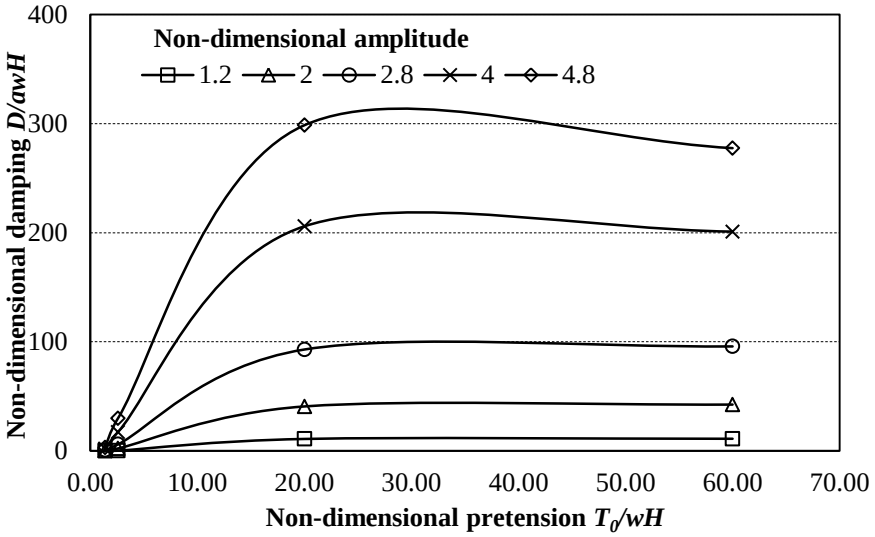

Figure 4-11 Variation of mooring line damping with pretension (various WF oscillation amplitudes)

4.4.3 The effect of scope

Different scopes of 3.2 and 6.4 were defined to estimate the effect on the mooring line damping, and the results are presented in Figure 4-12. When small amplitude motions are excited, a considerable component of the mooring line rests on the bottom and there is little difference of energy absorbed by changing the appearance of the mooring line profile. As a consequence, the mooring line damping for small amplitude is independent of scope. As the amplitude become bigger, the shorter scope mooring line is lifted up off the bottom all the way to the anchor, but the larger scope mooring still has some components resting on the bottom. The mooring line damping of the shorter scope increases dramatically with the amplitude.

The non-dimensional damping with scope of combined oscillations has similar character, as shown in Figure 4-13. It is seen that the shorter scope line makes more contribution to mooring line damping, compared to those of larger scope mooring line.

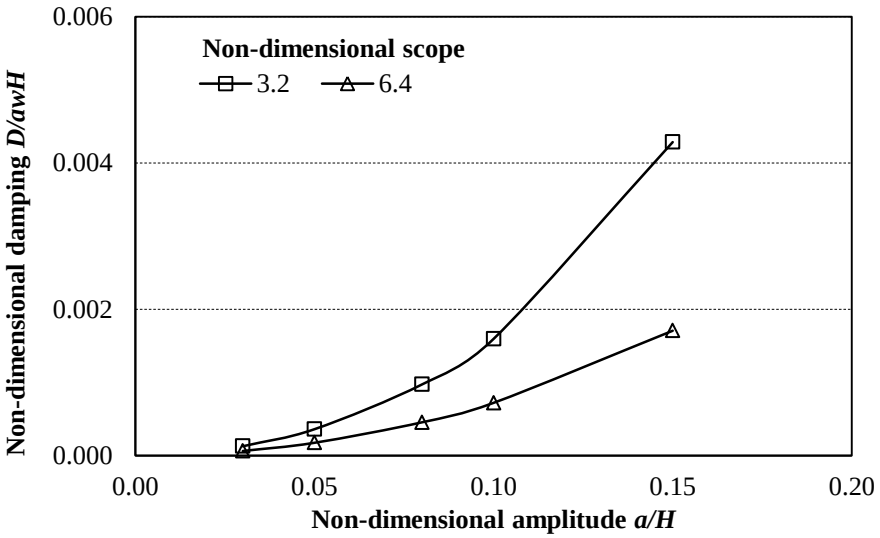

Figure 4-12 Variation of mooring line damping with scope (LF oscillation)

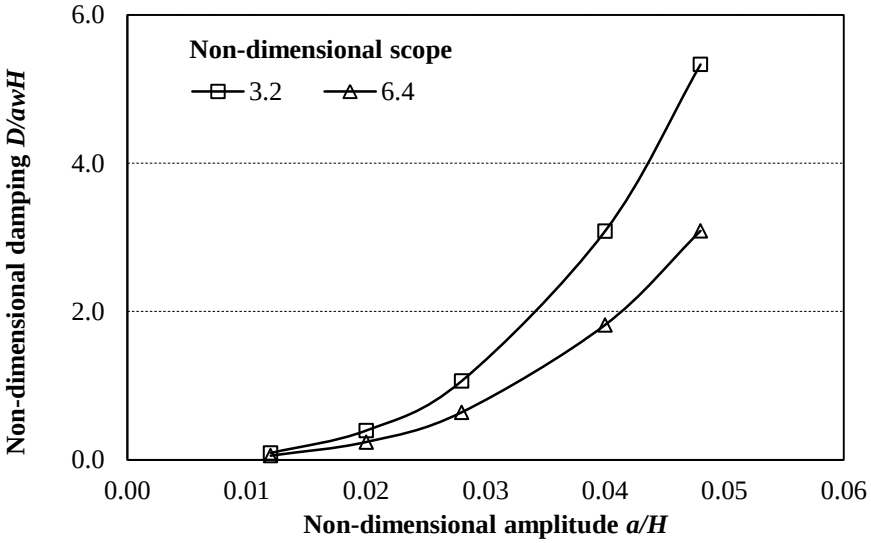

Figure 4-13 Variation of mooring line damping with scope (combined oscillations)

4.4.4 The effect of current velocity

Three different non-dimensional current values were investigated: 0, 0.36 and 9.3, and the results are presented in Figure 4-14. These values correspond to the current velocity of $0\,m/s$, $0.02\,m/s$ and $0.1\,m/s$. When the mooring line is undergoing LF oscillation only and subjected to a moderate current (see the figure for $\frac{\rho_w}{2}\frac{U_c^2}{wD_s}=0.36$), it makes almost no difference to the mooring line damping. As the current becomes severe (see the figure for $\frac{\rho_w}{2}\frac{U_c^2}{wD_s}=9.3$), it is seen that the current makes a significant contribution to the mooring line induced damping. On the contrary, when the three different currents are taken into account for mooring lines with combined LF and WF oscillations excited, the current has no effect on the mooring line damping even when the current becomes big, as displayed in Figure 4-15.

There are two reasons; firstly, we could find that the mooring line velocities of pure LF oscillation (*a/H*=0.08 shown in Figure 4-14) and combined LF and WF motions (*a/H*=0.028 shown in Figure 4-15) are of different orders of magnitude, as presented in

Table 4-4. For the cases of pure LF oscillations, the current would make considerable difference in relative velocity between the mooring line and the surrounded water, when its velocity is the same order of magnitude as the velocity of the mooring line movement. However, the WF component dominates the line movement for the combined oscillations; while the current velocity cannot make a large effect on the relative velocity, thus the energy dissipation of the mooring remains same. Secondly, the effect of current also makes contribution on the mooring line pretension. The pretensions for cases under different non-dimensional current of 0, 0.36 and 9.3, are 461.21kN, 461.2106kN and 461.2239kN, respectively. It can be found that the pretension increases by 0.0001% and 0.0030%, compared to that of no current load. The effect of pretension to the mooring line damping was discussed in section 4.4.2.

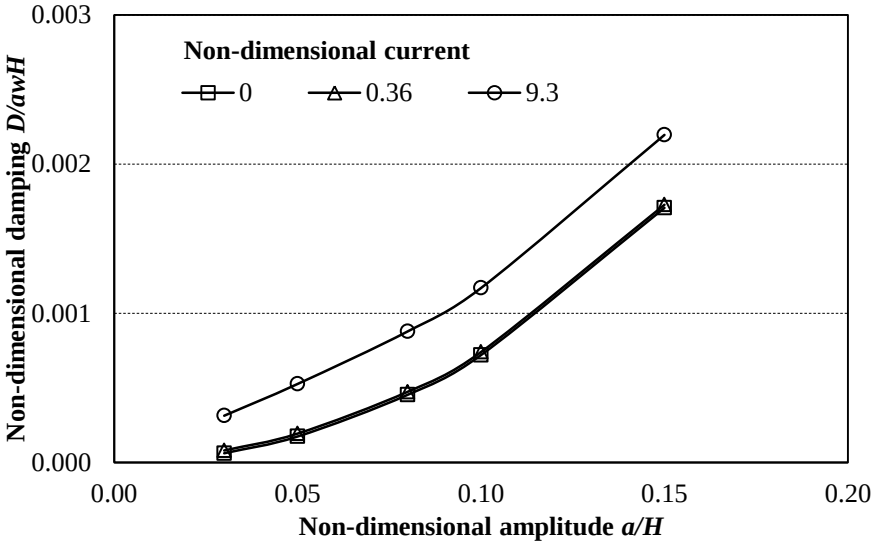

Figure 4-14 Variation of mooring line damping with current (LF oscillation)

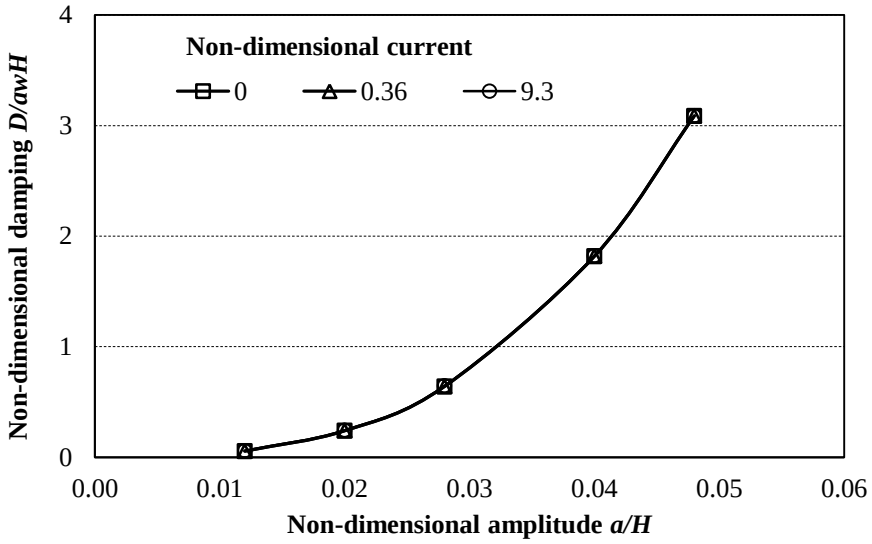

Figure 4-15 Variation of mooring line damping with current (combined oscillations)

Table 4-4 Velocity results of the mooring line excited by pure LF motion and combined motions

	Maximum velocity (m / s)	**Mean velocity** (m / s)
Pure LF motion	0.1514	0.0914
Combined motions	1.5719	0.8993

4.4.5 The effect of stiffness

A different stiffness parameter which is twice as stiff as the baseline was performed and the results are presented in Figure 4-16 and Figure 4-17. There is almost no difference in the damping for either the pure LF oscillation or combined oscillations. It is indicated that the effect of the line stiffness is negligible on the mooring line induced damping, at least for the mooring line pretensions investigated here.

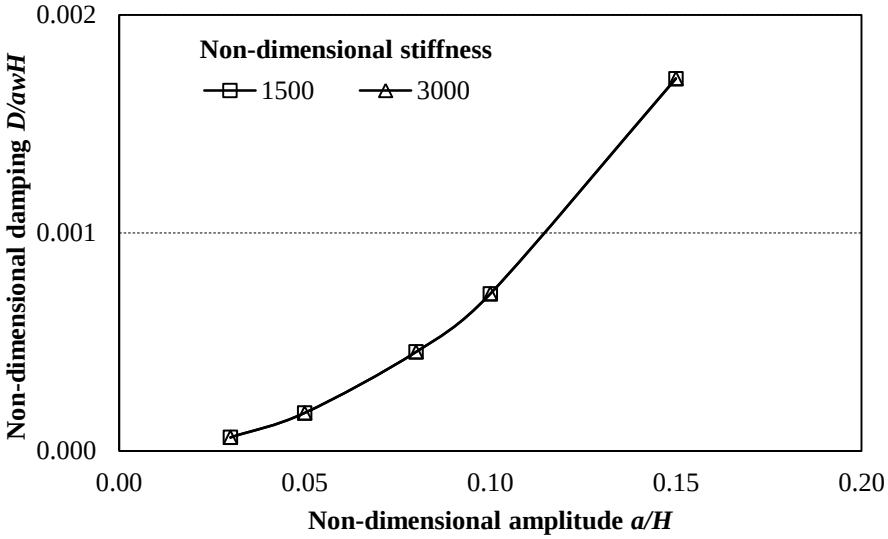

Figure 4-16 Variation of mooring line damping with line stiffness (LF oscillation)

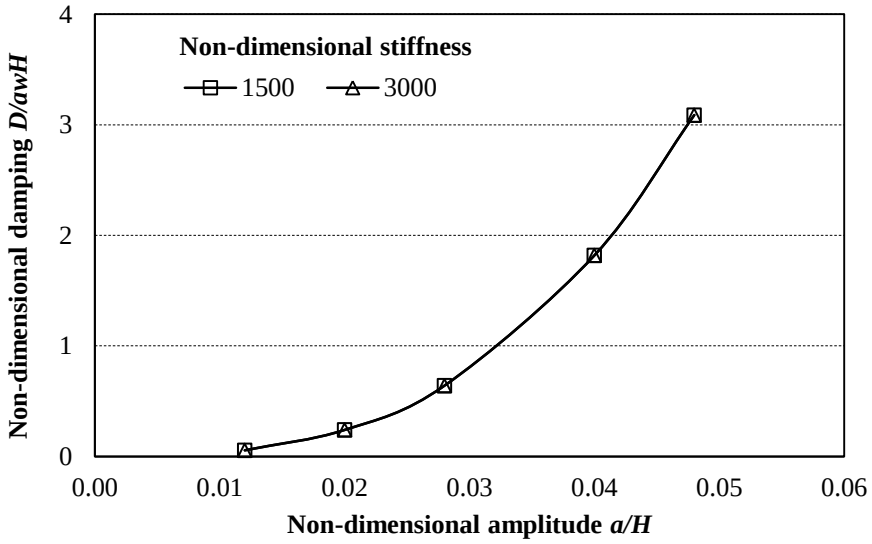

Figure 4-17 Variation of mooring line damping with line stiffness (combined oscillations)

4.4.6 The effect of drag coefficient

Three different values of the non-dimensional drag coefficient of 0.67, 1.2, and 3.6 were investigated, and the results for pure LF oscillations are shown in Figure 4-18. It is found that the damping grows with the increase of drag coefficient for pure LF

oscillation, and the character is in accordance with that for combined oscillations, as shown in Figure 4-19.

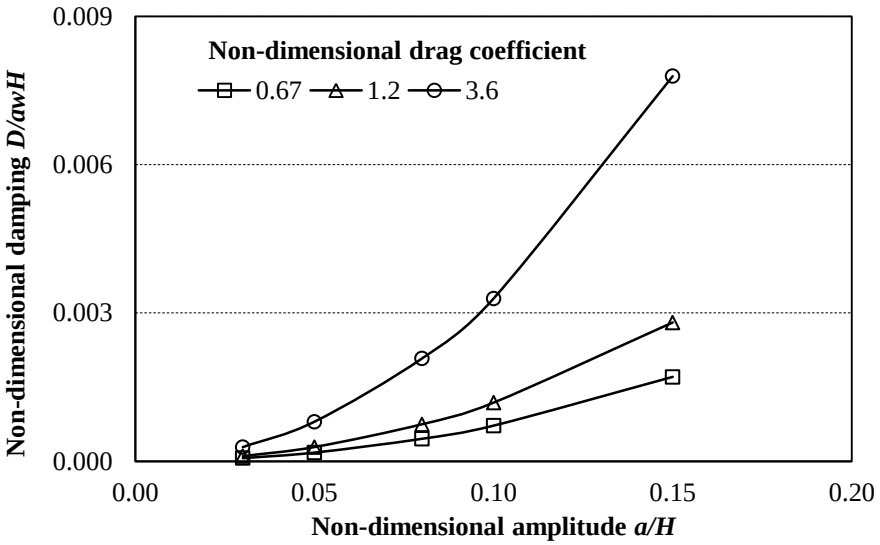

Figure 4-18 Variation of mooring line damping with drag coefficient (LF oscillation)

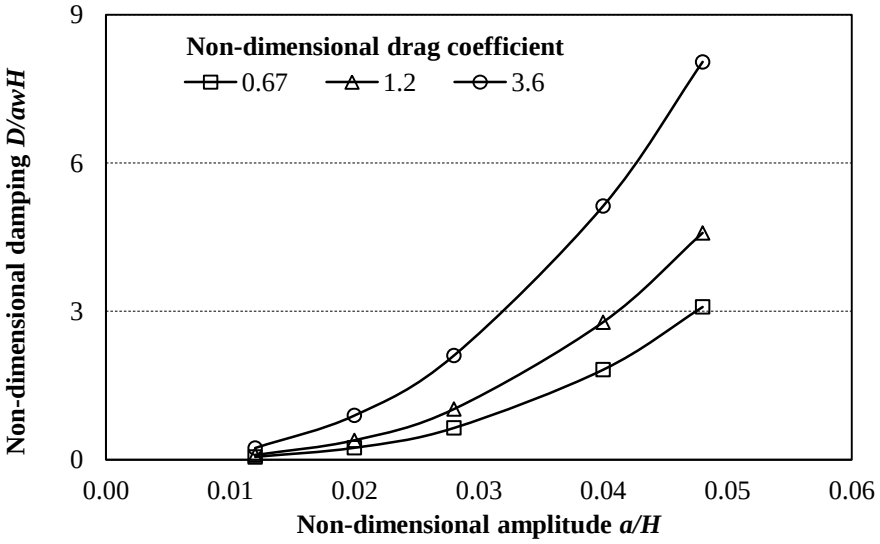

Figure 4-19 Variation of mooring line damping with drag coefficient (combined oscillations)

In order to check, quantitatively, the influence of the drag coefficient on the mooring line damping, computations for the growth proportion of the mooring line damping based on those of baseline were carried out, and the results were shown in Figure 4-20.

It is seen that there is no difference in growth ratio of the damping for different amplitude of LF oscillation. The growth ratio of damping because of the increase of drag coefficient (C_D) is defined as $\left(D_{C_{D2}} - D_{C_{D1}}\right) / D_{C_{D1}} \cdot 100\%$. For increase of the drag coefficient, the damping growth is independent of the amplitude of the LF oscillation. It is because the drag force acting on the mooring line is proportional to the drag coefficient and the square of velocity, while the velocities of these cases are very low. Thus the growth ratio of the mooring damping is only dependent on the value of drag coefficient. When further considering the change of growth ratio from the contributions of the drag coefficient, as shown in Figure 4-21, the curve presents a linear characteristic for cases of pure LF oscillation.

However, for the cases of combined oscillations, the computations for the growth proportion of the mooring line damping based on those of baseline were completed, and the results are presented in Figure 4-22. The growth ratio shows decrease with the amplitude of the oscillation. It is because the velocities for combined oscillations are big, then the drag force would increase quadratically with the velocity. This character is different from that for pure LF oscillation.

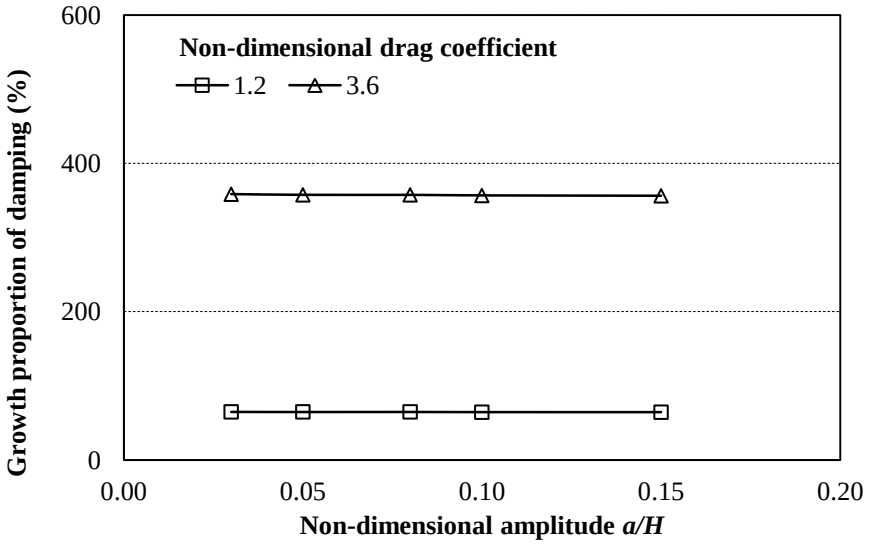

Figure 4-20Growth proportion of the mooring damping (LF oscillation)

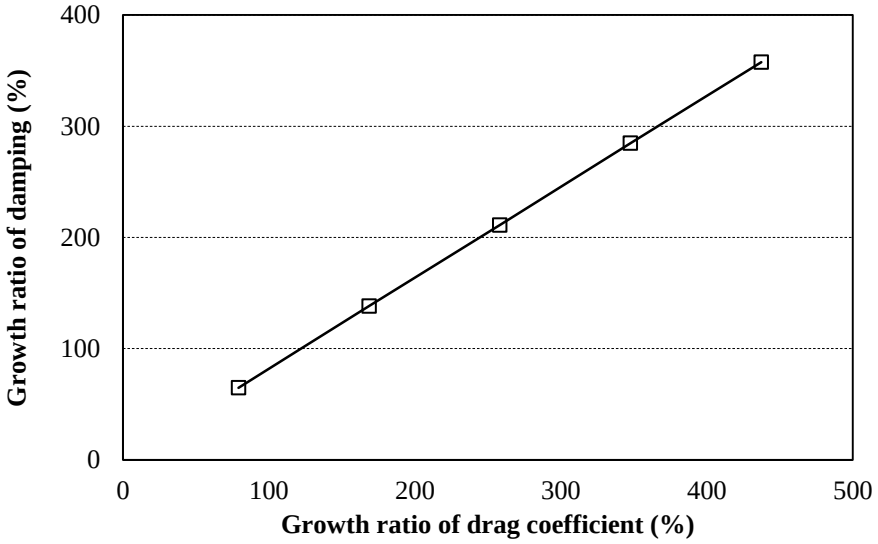

Figure 4-21 Growth ratio of the mooring damping with drag coefficient (LF oscillation)

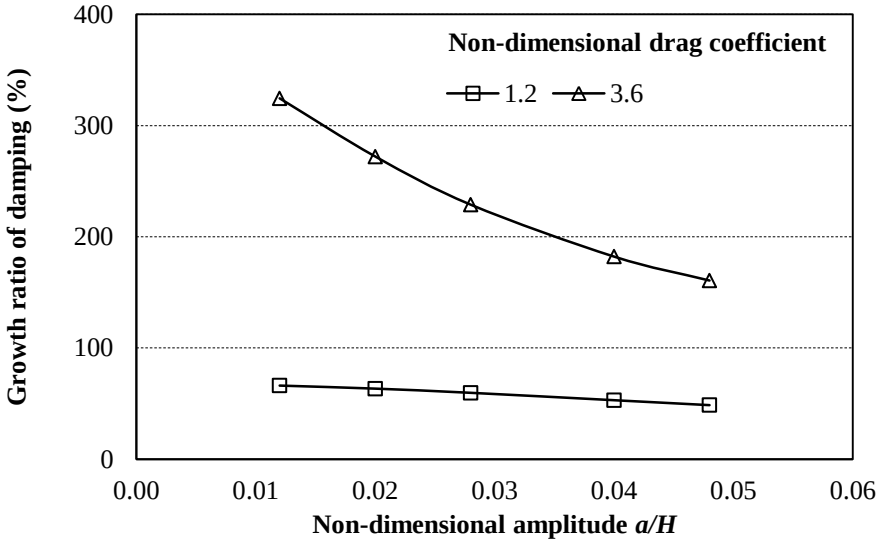

Figure 4-22 Growth proportion of the mooring damping (combined oscillations)

4.4.7 The effect of seabed friction

Other than the parameters discussed, the effect of seabed friction is investigated. The results of seabed friction coefficient of 0.4 are compared with those of baseline (friction coefficient=0), as shown in Figure 4-23 and Figure 4-24. It is seen that the seabed friction has a very small effect on the damping for either the pure LF oscillation or

combine oscillations. The effect of the seabed friction is negligible, at least for the in-line movement, no trenching of the line and moderate pretension investigated here.

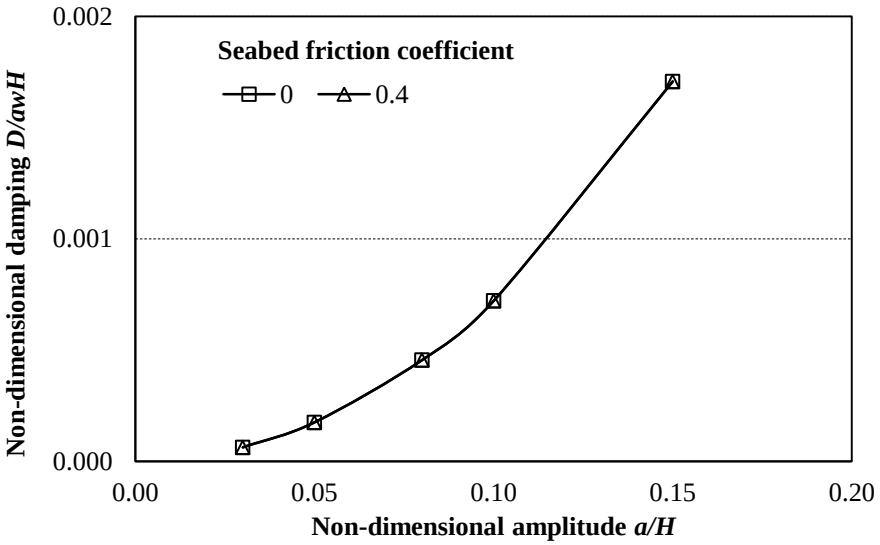

Figure 4-23 Variation of mooring line damping with seabed friction (pure LF oscillation)

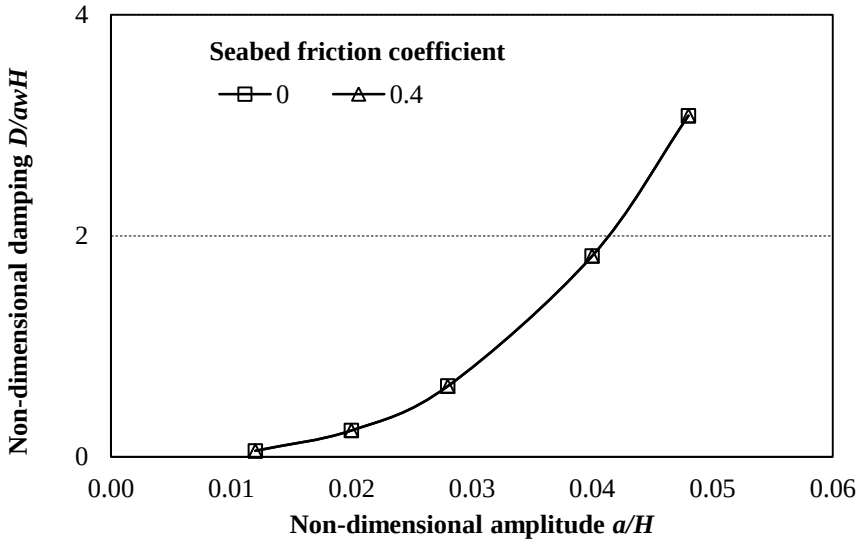

Figure 4-24 Variation of mooring line damping with seabed friction (combined oscillations)

4.5 Conclusion remarks

The calculation method for mooring line damping estimation applied in this study is verified with those methods by other researchers in this chapter. We can find that the results calculated by the present method agree well with those from references. It means the present method can be used to assess the mooring line damping effectively.

As concerning the factors that make effect on the mooring line damping, the dimensional analysis is studied in this chapter. The mooring induced damping is clearly a complex phenomenon and appears to be influenced by many variates.

The results of the mooring damping with surge motion and heave motion reveals the two motion system interact. When comparing with the excitation in both surge and heave direction, the WF heave motion would make significant contributions on horizontal damping; on the contrary, the WF motions in surge direction only make small impact on the vertical component of the mooring line damping. The variation in damping with pretension presents a peak at non-dimensional pretension around 20. The mooring line performs from catenary to taut when the pretension getting bigger. The stretch response of the taut mooring will decrease the mooring line damping. The influence from the current velocity depends on the relative velocity. When the current velocity is big enough to change the line movement, a considerable influence will occur in mooring line damping. As the drag coefficient is an issue on concerning the mooring-induced damping, it will be discussed in the experimental study.

The strong variation of mooring line damping with parameters studied may explain why it is difficult to find a simple and precise method to estimate the mooring line damping.

5 Experimental study on mooring line damping

5.1 Introduction

The numerical calculation methods for mooring line dynamic responses and its induced damping are introduced in chapter 3 and chapter 4. As presented in chapter 3, there are assumptions and some contributions neglected to simplify the numerical simulation. In addition, the hydrodynamic coefficients for the mooring line are defined based on empirical equations. Experimental approaches are thus of importance to verify the validity and certainty of numerical calculation.

Most of the theoretical calculation results are consistent with the experiment results when only the LF motion is taken into account, while a big discrepancy still exists between the theoretical calculation and the experimental results in the case pf LF superimposed with WF motions (Yang et al., 2016, Qiao and Ou, 2014, Johanning et al., 2007). (Huse, 1989) found that with the superimposed WF motions the calculations over-predict the mooring line damping by a factor in the range of 1.2 to 2. Similarly, Brown (Brown and Mavrakos, 1999) found that with only drift-induced oscillation the numerical values are in fair agreement with the experimental data, while for combined wave and drift motions, the agreement is not good with numerical mean values over-predicting the experimental values by 70%.

5.2 Experimental assessment methods of mooring induced damping

Regarding the physical model test investigations, two techniques can be applied to obtain mooring line damping, namely 1) the decay method and 2) the forced oscillation method. Both techniques are described as suitable methods in the literatures; however the decay tests method is an efficient method to obtain system critical damping. The damping ratio can be read from still water free decay curves. Then the system damping can be easily obtained by multiplying the damping ratio to the critical damping. It

should be noticed that the system damping obtained by free decay could be underestimated.

5.2.1 The decay test

The decay test method is based on displacing a structure and measuring the decaying motion once it is released. In order to obtain the mooring line damping, initially the system damping without mooring line should be determined. In this case, several defined springs are commonly applied on the offshore structure model; the decaying motion for the system of scaled offshore structure with prescribed springs is investigated. Then the objective mooring lines are used on the offshore structure model, its decaying motion is again recorded. The decaying motions for a FPSO without and with mooring/rise as an example are shown in Figure 5-1. Once the two decaying motions are known, the mooring line damping can then be evaluated by measuring the total damping and subtracting the 'system' damping that initially evaluated. The total damping can be calculated from the logarithmic decrement experienced by the moored structure during its decaying motion, by using the decreasing peak amplitude during a cycle $\hat{x}$.

$$B_m + B_s = \log\left(\frac{\hat{x}_i}{\hat{x}_{i+T}}\right) \qquad \textbf{5-1}$$

Where B_m is the mooring damping and B_s is the damping of structure model. The damping coefficient can then be found from average of N measured logarithm decrements from adjacent cycles in the decaying motion's time history:

$$b = \frac{2M_T\left(\sum_{j=1}^{N} B_{mj}/N\right)}{T} \qquad \textbf{5-2}$$

Where b is the damping coefficient; M_T is the total mass consisting of the mass of moored structure M_s and the mass of mooring lines M_m and their added mass respectively. T is the period of surge motion and N the number of cycles.

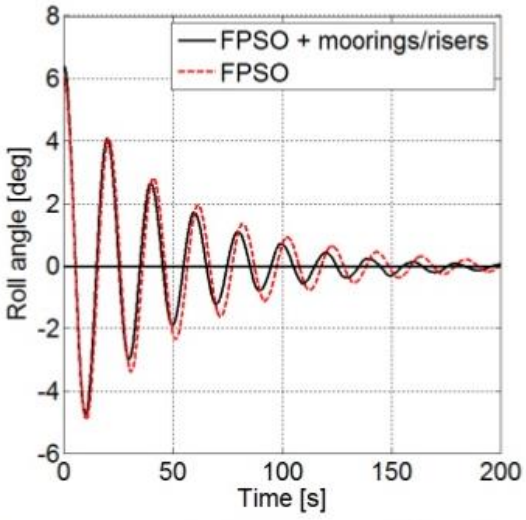

Figure 5-1 Diagram of decay motions for a FPSO model

5.2.2 The forced oscillation method

The force oscillation technique, used to evaluate the mooring line damping is carried out with the forced oscillation of the moored structure. In this case, the structure is excited with specific directional oscillation, e.g. surge, at sinusoidal displacements at specific amplitudes, and with varying frequency ratios and tensions. As the displacement and the mooring line tension are obtained, the indicator diagram will be derived by plotting the measured top-end motion against top end tension component, which is called the 'indicator diagram' method described in chapter 3.

In this chapter, the second technique is applied within physical model test to evaluate the mooring line damping. A single chain line is selected as the scale model, with varying defined oscillations exciting at the top-end of the mooring line. To assess the effects making contributions to mooring line damping, various amplitudes and

frequency ratios and tensions for the mooring line are investigated. Moreover, the comparison of results of numerical simulation and model test will be presented in this chapter.

5.3 Simulation laws

To ensure the model test efficiency and accuracy, model tests in naval architecture and marine engineering normally follow certain principals.

5.3.1 Froude law

Froude number are equal between prototype and model when gravity plays a major role, which means make two structures meet the gravity and inertia similarity.

$$F_r = \frac{v}{\sqrt{g\,l}} \tag{5-3}$$

According to the Froude law, the model velocity scale should meet $\lambda_v = \lambda_l^{1/2}$ and its force scale $\lambda_F = \lambda_P \cdot \lambda_l^3$.

5.3.2 Reynolds criteria

Reynolds number should be equal between prototype and model when the viscous load plays a major role, which means make two structures meet the inertia and viscous similarity.

$$R_e = \frac{v\,l}{v} \tag{5-4}$$

According to the criterion, the model velocity scale should meet $\lambda_v = \lambda_l^{-1}$, and force scale $\lambda_F = \lambda_P$.

Table 5-1 Froude scaling of various physical quantities

Parameter	Sign	Scale
Length	L_s / L_m	λ
Velocity	V_s / V_m	$\lambda^{1/2}$
Acceleration	a_s / a_m	1
Angle	ϕ_s / ϕ_m	1
Angular velocity	ϕ_s' / ϕ_m'	$\lambda^{-1/2}$
Period	T_s / T_m	$\lambda^{1/2}$
Area	A_s / A_m	λ^2
Volume	∇_s / ∇_m	λ^3
Inertia moment	I_s / I_m	λ^5
Force	F_s / F_m	$\gamma\lambda^3$

It is known that we cannot satisfy both Froude and Reynolds criteria in model scaling. In order to minimize the effect of different Reynolds number, appropriate and different drag coefficient values depend on Reynolds number are commonly applied in comparing the results of model tests with simulations and predicting the full scale model characteristics.

5.4 Experimental facilities and set-up

The experimental tests were carried out at Kelvin Hydrodynamics Laboratory of University of Strathclyde. This tank measures 76m by 4.6m with a variable water depth from 0 to 2.5m. According to the scaling criteria, the model of a single mooring line with scaling factor of 1:80 is selected as an objective. The mooring line selected is a

typical marine chain in the UK market. The bottom end of the mooring line is fixed on the bottom of the tank, and the top-end is hanging on an oscillator. The oscillator is a digital controlled sub-carriage, on which is located a computer-controlled digital drive. The mooring line dynamic simulation set-up is shown as in Figure 5-2. The configurations for the scaled mooring line are listed in Table 5-2, the photo of the catenary mooring line is shown in Figure 5-3.

Table 5-2 Configurations for mooring line model

	Diameter/ m	**Length/ m**	**Axial stiffness/N**	**Wet weight/N**	**Drag coefficient**	**Mooring radium/m**	**Pretension/ N**
Chain	0.004	8	50.3E3	2.6	1.6	7.25	9

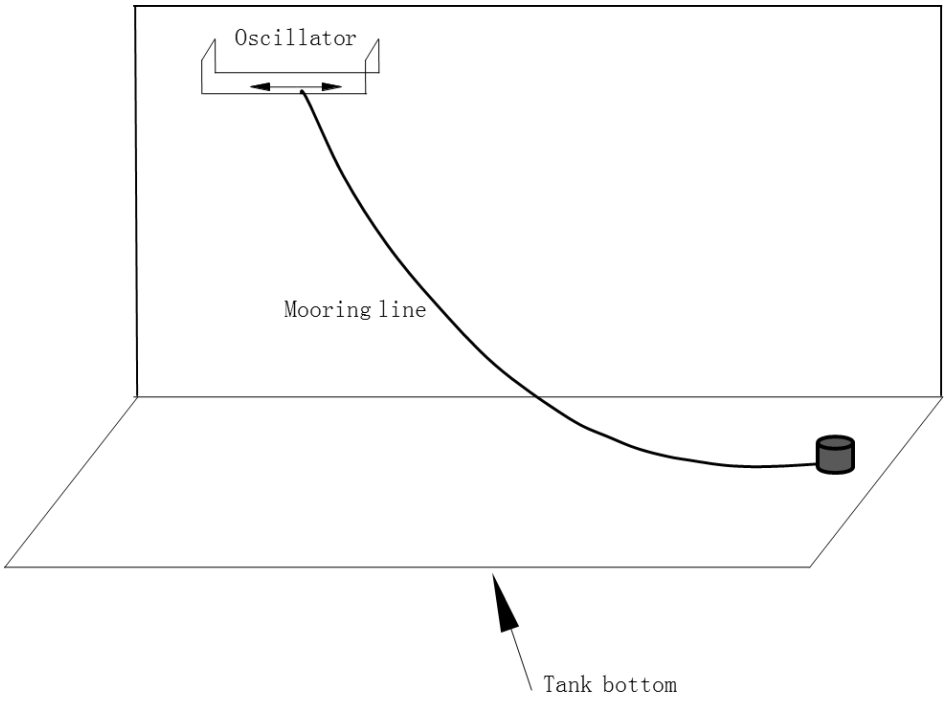

Figure 5-2 Model of mooring line dynamic simulation

Figure 5-3 The configuration of catenary mooring line

The instruments used in the experimental testing are listed in Table 5-3. The computer-controlled digital sub-carriage, located on the digital drive can excited the mooring line model with specific defined oscillations. The oscillation is generated in varying modes, LF motion, LF with superimposed harmonic WF motion and random WF motion. In this study, the oscillatory is excited at the suspension point in the surge direction and in the plane formed by the line static catenary suspension, as illustrated in Figure 5-2. The mooring line position and pretension is determined by adjusting the location of digital drive. In addition, a dynamometer together with an angle sensor is located at the top-end of the mooring line, where the tension in line and its angle at the top-end are measured.

From the recorded data of the time histories of the line tension and angle at the suspension point, the inertial first cycle is ignored for ramping process of the oscillation. In order to ensure the accuracy of the measured line response, the measured data is derived from the averaged analysis over six cycles of LF oscillation.

Table 5-3 The instruments used in experimental testing

Instrument	Purpose
Computer-controlled digital drive	Excited with defined oscillation
Digital-controlled sub-carriage	Mooring position adjustment
Force transducer	Force measurement
Angle cell	Angle measurement
PC based modular data acquisition/control system	Data acquisition and analysis
Underwater video system	Record mooring line movement

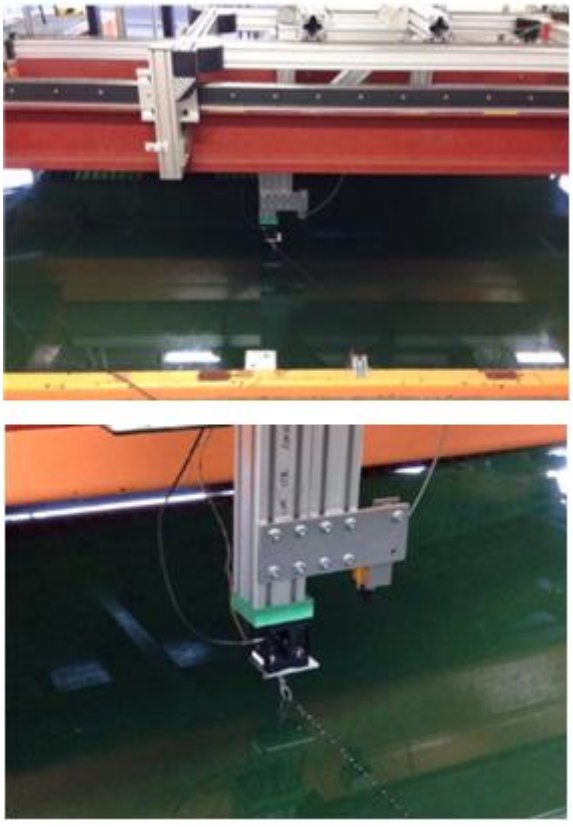

Figure 5-4 Photos of experimental tests

5.5 Experimental contents and results

5.5.1 Tension-offset characteristic of a mooring line

It is essential to simulate the mooring line in accurate way. To check and understand the mooring line system, the static characteristic of a mooring line should be tested to determine the top tension-offset characteristic. In this test, we applied the dynamic test system as shown in Figure 5-2, to determine the top tension-offset curve. As the bottom end of the mooring line is fixed on the tank bottom, its fairlead point link with oscillator would move along with the sub-carriage, thus various offsets are produced by adjusting the location of the carriage. Compared with the results of numerical calculations as shown with the line of target, the tension-offset characteristic of the mooring line model is presented in Figure 5-5.

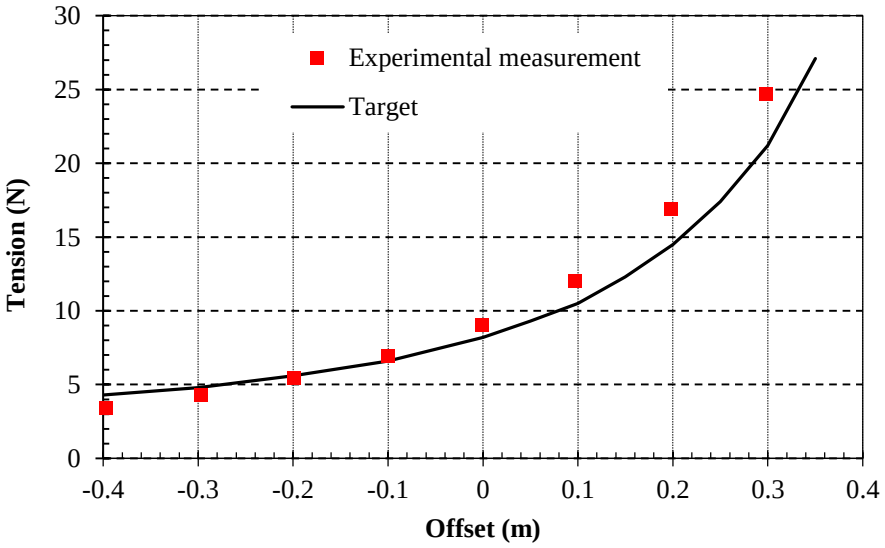

Figure 5-5 Tension-offset characteristics for the mooring line

The static offset-tension graph shows the restoring force reaction to horizontal displacement out of the platform equilibrium position for the initial configurations of synthetic mooring that were tested. Note that while the static response of the synthetic configurations is, in general, linear with respect to the displacement, that is not the case

of the cable-type mooring. The cable mooring seems to have a linear behaviour for small offsets from the origin, but as the offset ranges larger than 0.4 meters, the restoring force ramps up dramatically. For small displacement of the platform from the origin, the mooring will still have a loose pattern. However, as soon as the distance of the platform from its equilibrium position begins to increase, the cable lines become very taut. The restoring force they create in that case increase substantially since they will then behave as a spring with very large Young's modulus.

5.5.2 Effect of LF oscillation on mooring line damping

To determine the effect of LF oscillation on mooring induced damping, varying frequency ratios with specific different amplitudes of LF oscillations are applied on the fairlead point of the mooring line. In order to check, qualitatively, the influence of the LF motion on the results of mooring line damping, experimental tests were repeated with different value of the frequencies and varying amplitudes for LF oscillations. To simplify the calculation, the oscillations are defined as sinusoidal motion, which is expressed as $X = A\sin\left(\frac{2\pi}{T}t\right)$. The experimental tests and its results are listed in Table 5-4.

Table 5-4 Experimental results of mooring line damping (LF oscillation)

	LF Oscillation		**Experimental Results**	
	A_{lf} **(m)**	ω_{lf} **(rad/s)**	**Energy dissipation (N·m)**	**Damping coefficient (N·s/m)**
Case1001	0.25	0.1269	0.0117	0.4594
Case1002	0.25	0.1381	0.0137	0.5149
Case1003	0.25	0.1591	0.0172	0.5393
Case1004	0.25	0.1770	0.0205	0.6076

Case1005	0.25	0.1933	0.0248	0.6590
Case1006	0.25	0.2205	0.0336	0.7894
Case1007	0.1	0.1269	0.0004	0.0778
Case1008	0.15	0.1269	0.0023	0.2426
Case1009	0.2	0.1269	0.0042	0.2756
Case1010	0.3	0.1269	0.0220	0.6207
Case1011	0.35	0.1269	0.0410	0.8433

The results of the experimental cases on the mooring line damping in Table 5-4 and Figure 5-6 indicate that as the frequency of the LF motion increase, the mooring line damping also has a gradual increase. The reason of this trend is because the lower of the frequency of the LF oscillation causes the slower of the velocity of the mooring line. Although the values of maximum mooring line tension for different frequencies are almost the same as shown in Figure 5-8, the bigger velocities at higher frequency result in more dissipated energy from the mooring line.

As shown in Figure 5-7, it is found that the mooring line damping goes up with the increase of the amplitude of the LF oscillation, and it appears non-linear characteristics. It is because as the amplitude of the LF oscillation gets bigger, the mooring line would move farther away from its pre-tension position. As the mooring line was excited with a fixed frequency, the bigger oscillation amplitude means the faster velocity of it. As a result, the energy dissipation due to the mooring line damping will thus be increasing with the amplitude increase. Meanwhile, we can also find that the mooring line tension obtaining a dramatic increase because the increase of the amplitude, as displayed in Figure 5-9. With the amplitude increase, the drag force of the mooring line is getting bigger, because it is related to the velocity.

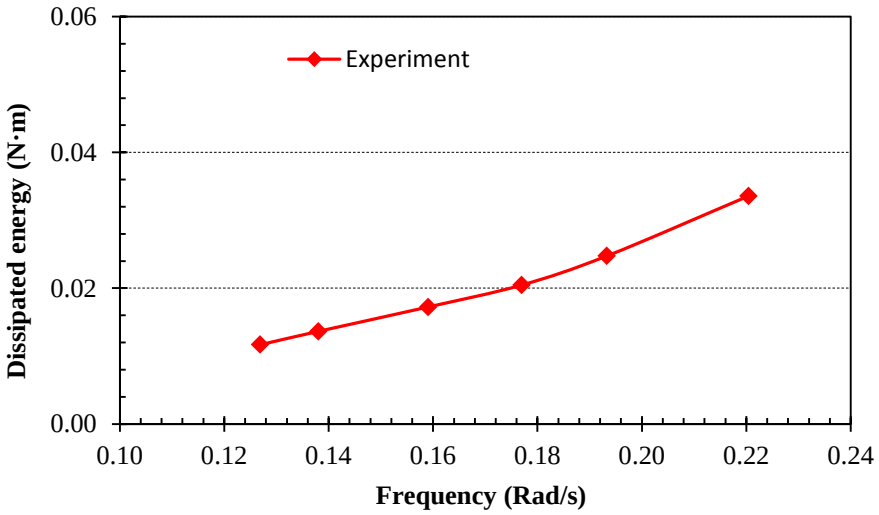

Figure 5-6 Dissipated energy of the mooring line with LF oscillation (varying frequencies)

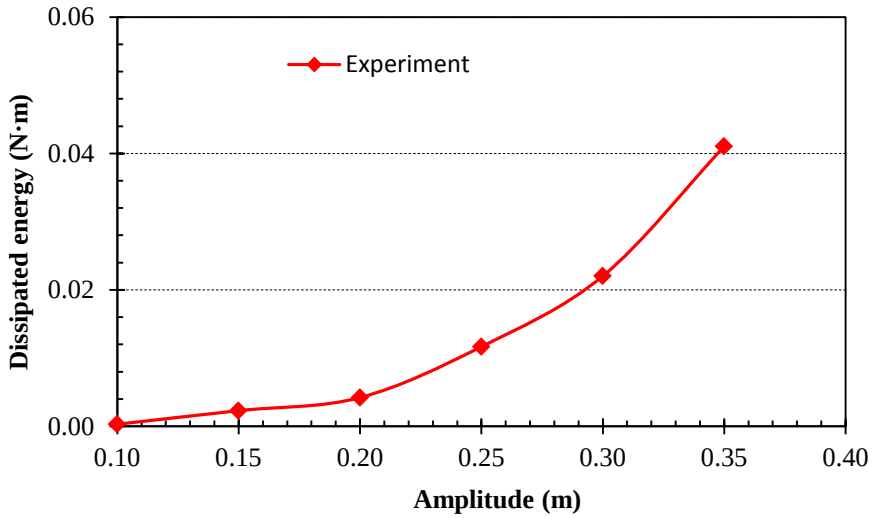

Figure 5-7 Dissipated energy of the mooring line with LF oscillation (varying amplitudes)

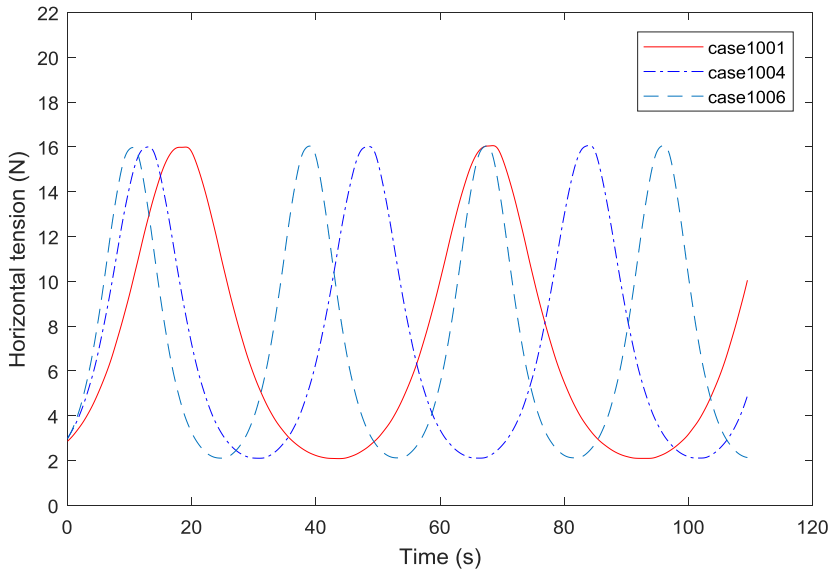

Figure 5-8 Mooring line tension with varying frequencies of LF oscillation

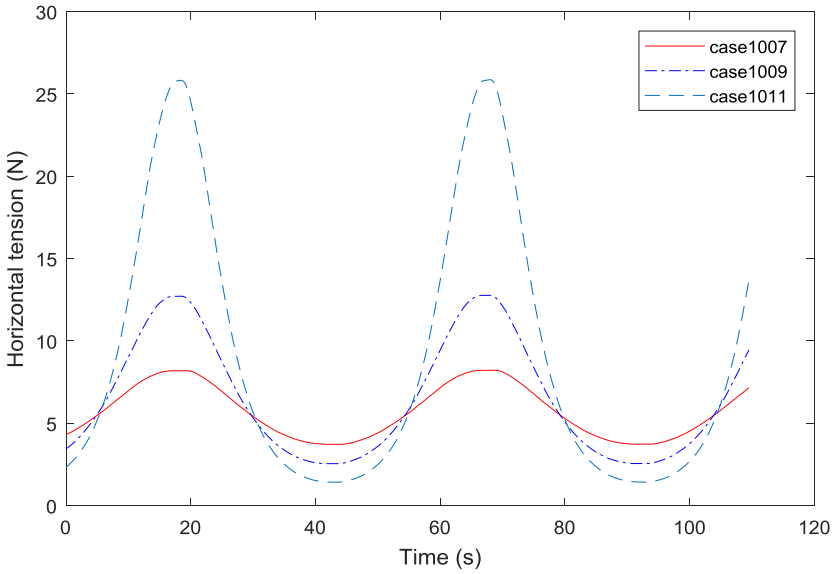

Figure 5-9 Mooring line tension with varying amplitudes LF oscillation

5.5.3 Effect of superimposed WF oscillation on mooring line damping

For fixed offshore structures, WF forces are the most important. For moored floating systems, wave frequency, slowly varying and steading forces can all be important. The effect of WF oscillation superimposed on mooring line induced damping was investigated by (Huse, 1989, Xu and Huang, 2014), it is indicated that it will lead to a significant contribution on the mooring line damping. In this thesis, varying amplitudes and frequencies of WF motions are selected to superimpose on a LF motion, and the effects of the WF motion are determined. In order to progressively assess its impact, the influences of a harmonic WF motion, two harmonic WF motions, and a random WF motion are studied.

5.5.3.1 Effect of a harmonic WF motion

According to the previous studies, drag coefficient is an important factor to the dissipated energy of mooring line. The importance was also discussed in (Huse, 1989). Here, it is supposed that it is more reasonable to define a higher drag coefficient than that applied in pure LF motion cases. Several frequencies and amplitudes of WF motion are considered and superimposed with a LF motion (case1009), where with the frequency of 0.1269 rad/s and amplitude of 0.2m. The results of measured mooring line damping under different cases of WF superimposed on LF motion are listed in Table 5-5 .

Table 5-5 Experimental results of mooring line damping (a harmonic WF motion)

	LF oscillation		**WF oscillation**		**Experimental Results**	
	A_{lf} **(m)**	ω_{lf} **(rad/s)**	A_{wf} **(m)**	ω_{wf} **(rad/s)**	**Energy dissipation (N·m)**	**Damping coefficient (N·s/m)**
Case2001	0.2	0.1269	0.1	2.5133	9.1470	573.71
Case2002	0.2	0.1269	0.1	3.1416	16.7148	1047.74

Case2003	0.2	0.1269	0.1	4.1888	40.6818	2550.22
Case2004	0.2	0.1269	0.1	6.2832	118.28	8212.80
Case2005	0.2	0.1269	0.01	3.1416	0.0394	2.48
Case2006	0.2	0.1269	0.03	3.1416	0.4522	28.31
Case2007	0.2	0.1269	0.05	3.1416	2.2609	141.69
Case2008	0.2	0.1269	0.07	3.1416	5.8702	368.15
Case2009	0.2	0.1269	0.12	3.1416	28.9475	1814.74

It can be found from the results of Table 5-5 that:

The superimposed WF motion will make significant contributions to mooring line damping, when compared to the base case of pure LF oscillation (Case1009);

With the increase of superimposed WF motion frequency, the dissipated energy of the mooring line presents a rising tendency, as shown in Figure 5-10. In Figure 5-12, it is presented that there are more WF oscillations included within a cycle of LF motion with bigger frequency of WF motion. Meanwhile, comparing the velocity of the fairlead point for Case2002 and Case2003 as shown in Figure 5-14, it is found that the higher frequency WF motion superimposed (Case2003) leads to the bigger velocity of the mooring line. It also can be found from the statistics results in Table 5-6, the value of maximum and standard deviation of Case2003 are both higher than those of Case2002. The bigger velocity would then cause bigger drag force acting on the mooring line during a LF cycle. As a result, a growth of dissipated energy for mooring line with the superimposed WF motion frequency increasing.

Comparing the horizontal tension for the cases presented in Figure 5-12, we can find that the maximum mooring line tension is getting bigger as the WF motion frequency increases. It is because the drag force acting on the mooring line is increasing with the frequency of the superimposed WF motion increases. And also, we can find that the

superimposed WF motion (Case2002 and Case2003) will lead to a considerable increase of mooring line tension, compared to that of pure LF oscillation (Case1009).

As shown in Figure 5-11, when varying amplitude of WF motions are superimposed with the selected LF oscillation, it is found that the mooring line dissipated energy is growing as the amplitude of WF motion increasing. Moreover, as the amplitude of the WF motion gets bigger, the energy dissipation is rising with a faster rate. It is because the velocity of the mooring line are increasing with the amplitude of the superimposed WF motion increasing, as presented in Figure 5-15 and Table 5-6. It would lead to an increasing of the drag force acting on the mooring line. This is also the reason of the increase of the mooring line tension with the amplitude of WF motion increases, as presented in Figure 5-13.

Here, the method of least squares is used to fitting the results of all the cases of WF motion superimposed, including varying frequencies and amplitudes. The fitted equations can be used to estimate the mooring line energy dissipation of LF oscillation superimposed with harmonic WF motion for initial checking. The non-linear fitting methods for the cases in Figure 5-10 and Figure 5-11 are executed and expressed separately as:

$$E = -0.5206\omega_{wf}^{3} + 11.596\omega_{wf}^{2} - 40.99\omega_{wf} + 47.187 \quad \textbf{5-5}$$

$$E = 17195A_{wf}^{3} - 124.2A_{wf}^{2} + 9.0404A_{wf} - 0.0857 \quad \textbf{5-6}$$

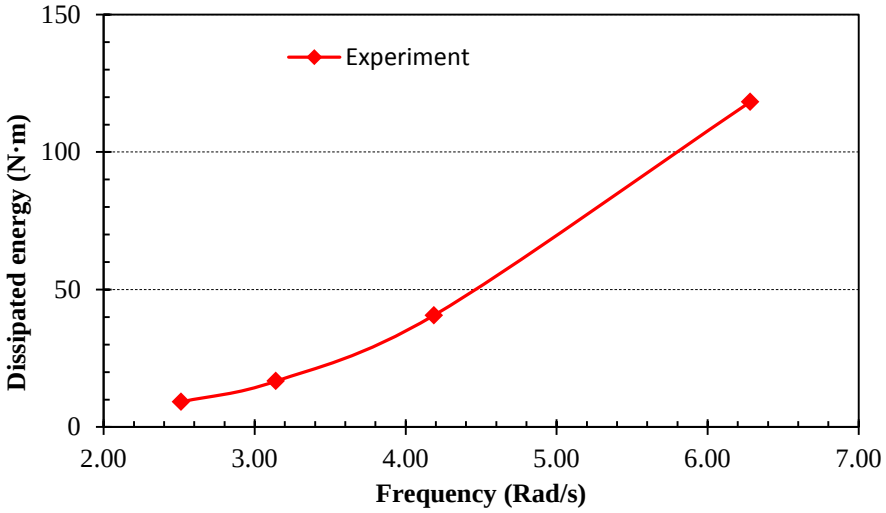

Figure 5-10 Dissipated energy of the mooring line with superimposed harmonic WF motion (varying frequencies)

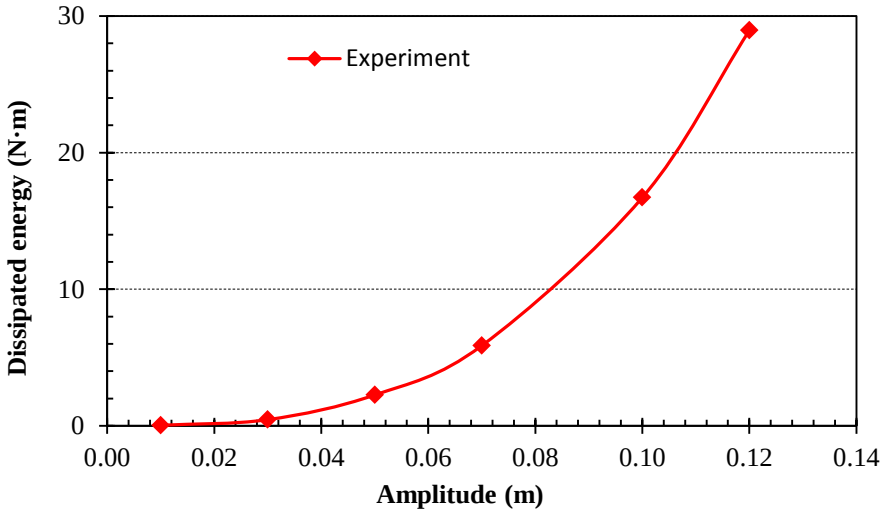

Figure 5-11 Dissipated energy of the mooring line with superimposed harmonic WF motion (varying amplitudes)

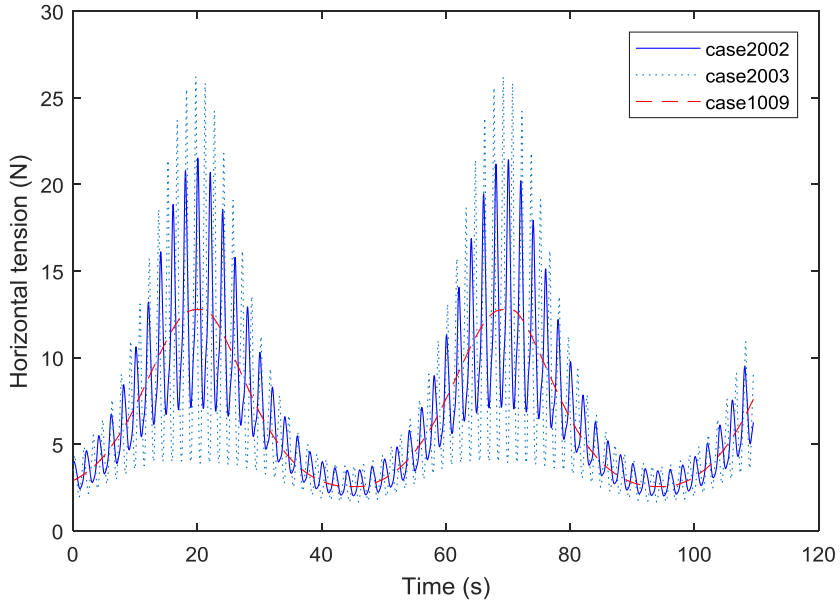

Figure 5-12 Mooring line tension with varying frequencies of harmonic WF motion

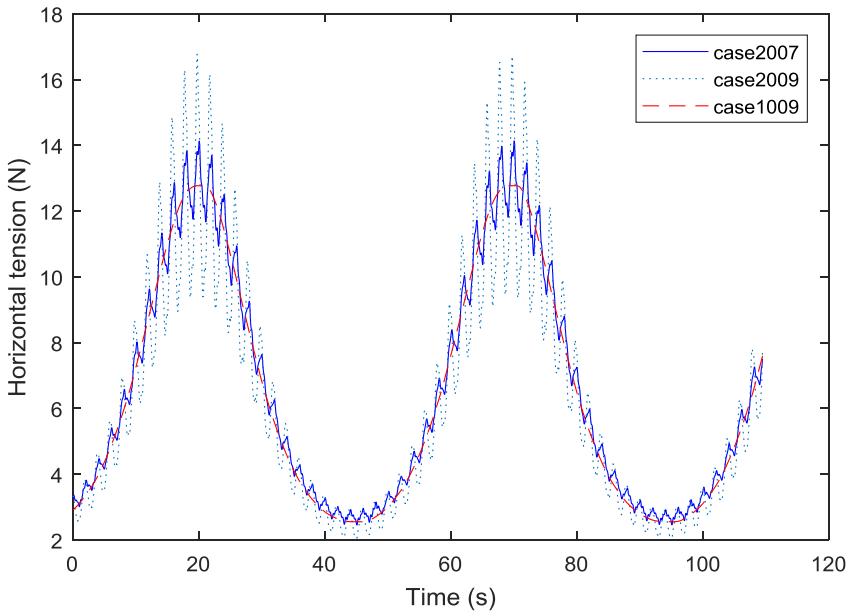

Figure 5-13 Mooring line tension with varying amplitudes of harmonic WF motion

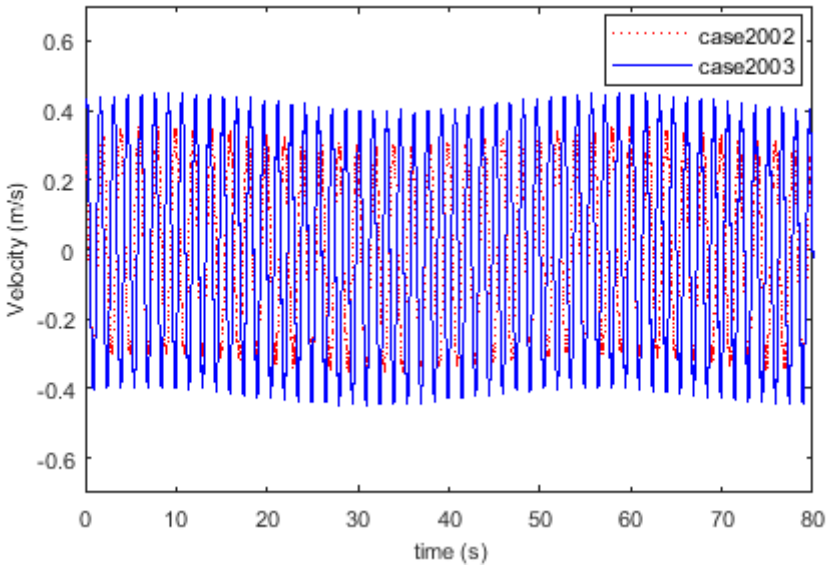

Figure 5-14 Mooring line velocity (fairlead) with frequencies of harmonic WF motion

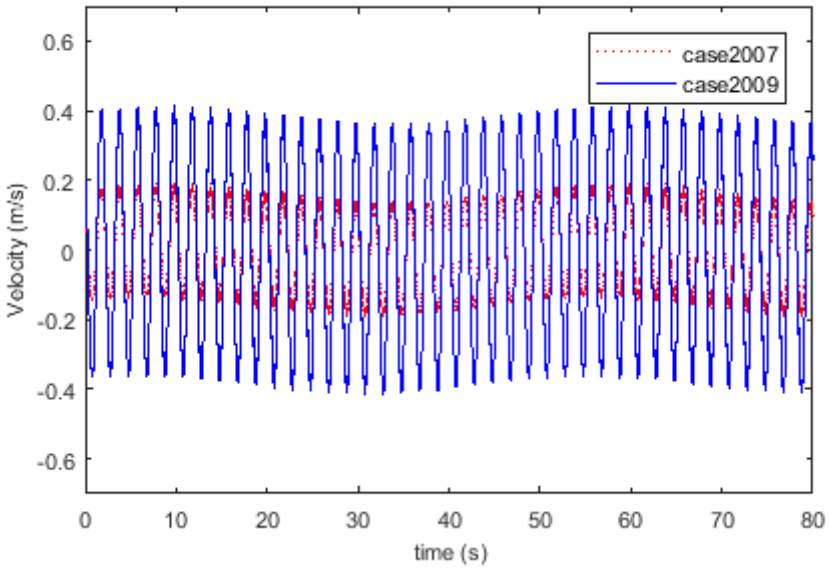

Figure 5-15 Mooring line velocity (fairlead) with varying amplitudes of harmonic WF motion

Table 5-6 Statistics results of the mooring line velocity at the fairlead point for cases with a harmonic WF motions superimposed

Velocity Statistics	Case2002	Case2003	Case2007	Case2009
Maximum Value(m/s)	0.3554	0.4514	0.1948	0.4149
Standard Deviation	0.2258	0.2944	0.1121	0.2689

The reason of the obvious contributions of superimposed WF motions on the increase of LF mooring damping has been explained theoretically by (Huse et al., 1988). Firstly, an arbitrary body moving at constant LF speed V_{lf}, then the drag force acting on the body is

$$F_{D_{lf}} = \frac{1}{2}\rho_w A_p C_D \left|V_{lf}\right| \cdot V_{lf} \tag{5-7}$$

Assuming that the velocity contains a WF component of amplitude V_{wf} superimposed, the velocity is then expressed as

$$V(t) = V_{if} + V_{wf} \cdot \sin\left(\omega_{wf} t\right) \tag{5-8}$$

The drag force with LF motion only and with the superimposed WF motion can be expressed as follow

$$F_{lf}(t) = \frac{1}{2}\rho_w A_p C_D \left|V_{lf}\right| V_{lf} \tag{5-9}$$

$$F_{wf}(t) = \frac{1}{2}\rho_w A_p C_D \left|V_{wf} \cdot \sin\left(\omega_{wf} t\right)\right| \left(V_{wf} \cdot \sin\left(\omega_{wf} t\right)\right) \tag{5-10}$$

Where A_p is the projected area of the body.

The dissipated energy that representing the LF mooring line damping is then expressed by

$$E_m = \int_0^T F_D(t) \cdot V_{lf}(t) \cdot dt \qquad \textbf{5-11}$$

Where $F_D(t)$ is the drag force, which is expressed as $F_D(t) = F_{lf}(t) + F_{wf}(t)$; T is a low-frequency cycle, expressed by $T = 2\pi / \omega_{lf}$, substituting the drag force into Equation 5-11, it is obtained

$$E_m = \frac{1}{2} \rho_w A_p C_D V_{lf}^3 \int_0^T |U_1| \cdot U_1 \cdot \cos(\omega_{lf} t)\, dt \qquad \textbf{5-12}$$

Where

$$U_1 = \cos(\omega_{lf} t) + \frac{V_{wf}}{V_{lf}} \cdot \cos(\omega_{wf} t + \phi_{wf}) \qquad \textbf{5-13}$$

Where ω_{lf} and ω_{wf} are frequency of low- and wave-frequency components respectively, ϕ_{wf} is the phase angle.

For the case of a pure LF motion the energy dissipation E_0 would rewritten by Equation 5-12 when V_{wf} put equal to zero, it would be described as

$$E_0 = \frac{1}{2} \rho_w A_p C_D V_{lf}^3 \int_0^T \left|\cos(\omega_{lf} t)\right| \cdot \cos^2(\omega_{lf} t)\, dt \qquad \textbf{5-14}$$

By numerical integration of Equation 5-12, it can be resulted that the ratio of E_m / E_0 always will be larger than one. That is to say, the superimposed WF motion will always make contributions on the dissipated energy of the mooring line; it is also in complete agreement with the results of the numerical simulations.

5.5.3.2 Effect of two harmonic WF motions

To assess the effect of the superimposed WF motion on the mooring line damping, a single sinusoidal WF motion is commonly considered in previous literature. However, the random WF motions are the most common existing in reality, thus it is more reasonable to take the effect of random WF into consideration. Here, to study the contributions of the random WF motions, quantitatively, two harmonic WF motions are taken into account. One harmonic WF motion remains unchanged, while the other one is defined with varying frequencies and amplitudes. The results of experimental tests with two harmonic WF motions superimposed are listed in Table 5-7. The damping coefficient is linearized by mooring line energy dissipation.

Table 5-7 Experimental results of mooring line damping (two harmonic WF motions)

	LF oscillation		**WF oscillation**				**Experimental Results**	
	A_{lf} **(m)**	ω_{lf} **(rad/s)**	A_{wf_1} **(m)**	A_{wf_2} **(m)**	ω_{wf_1} **(rad/s)**	ω_{wf_2} **(rad/s)**	**Energy dissipation (N·m)**	**Damping coefficient (N·s/m)**
Case3001	0.2	0.1269	0.1	0.05	2.5133	2.5133	28.9523	1814.97
Case3002	0.2	0.1269	0.1	0.05	3.1416	2.5133	23.0282	1443.83
Case3003	0.2	0.1269	0.1	0.05	4.1888	2.5133	42.1067	2640.57
Case3004	0.2	0.1269	0.1	0.05	6.2832	2.5133	118.3078	7416.20
Case3005	0.2	0.1269	0.01	0.05	3.1416	2.5133	1.3564	85.02
Case3006	0.2	0.1269	0.03	0.05	3.1416	2.5133	2.5405	159.23
Case3007	0.2	0.1269	0.05	0.05	3.1416	2.5133	5.2175	327.08
Case3008	0.2	0.1269	0.07	0.05	3.1416	2.5133	10.3142	646.91
Case3009	0.2	0.1269	0.12	0.05	3.1416	2.5133	36.0228	2258.23

It can be found from the results of Table 5-7 that:

Compared to the contributions from one harmonic WF motion, there is a significant increase of mooring line damping with two harmonic WF motions superimposed. With the increase of the frequency for superimposed WF motion, the dissipated energy of mooring line generally rises, however with an exception of Case3001, as presented in Figure 5-16. The dissipated energy for Case3001 ($\omega_{wf_1} = 2.5133\,rad/s$) is higher than that of Case3002 ($\omega_{wf_1} = 3.1416\,rad/s$); the reason is because both frequencies of WF motion we selected were equal to $2.5133 rad/s$ and were superimposed in phase, so always having a constructive effect on the result; however, the two different frequencies of Case3002-Case3004 will cause both constructive and also destructive effects on the oscillation due to the different phases. From the time histories of the velocity displayed in Figure 5-20, it is difficult to compare their values. However, we could further compare their statistical results listed in Table 5-8; it can be found that the standard deviation of Case3001 is bigger than that of Case3002. In this case, when comparing the mooring line tension as displayed in Figure 5-18, the extreme values of that for Case3001 are bigger than those of Case3002.

While for Case3004 ($\omega_{wf_1} = 6.2832\,rad/s$) and Case3003 ($\omega_{wf_1} = 4.1888\,rad/s$), the mooring line dissipation energy showed just a bit larger than the value of Case2004 and Case2003. It is because the maximum line tension in this two cases is higher than 50N but, the measurement range of force transducer is however only 0~±50N, thus the limitation will make some loss for line tension measurement, which will lead to the loss of estimated mooring line dissipated energy. It is regarded that the measured results of Case3003 and Case3004 underestimate the mooring line induced damping.

From Figure 5-17, when superimposed with two harmonic WF motion, the mooring line dissipated energy will increase in comparison with one of WF motion amplitude. Comparing the results of Case3005~Case3010 with that of Case2005~Case2010, it can be found that there will be more energy dissipated when two harmonic WF motions are

superimposed. And also it can be found that the mooring line tension increases significantly, as shown in Figure 5-19, which also suggests the drag force is rising.

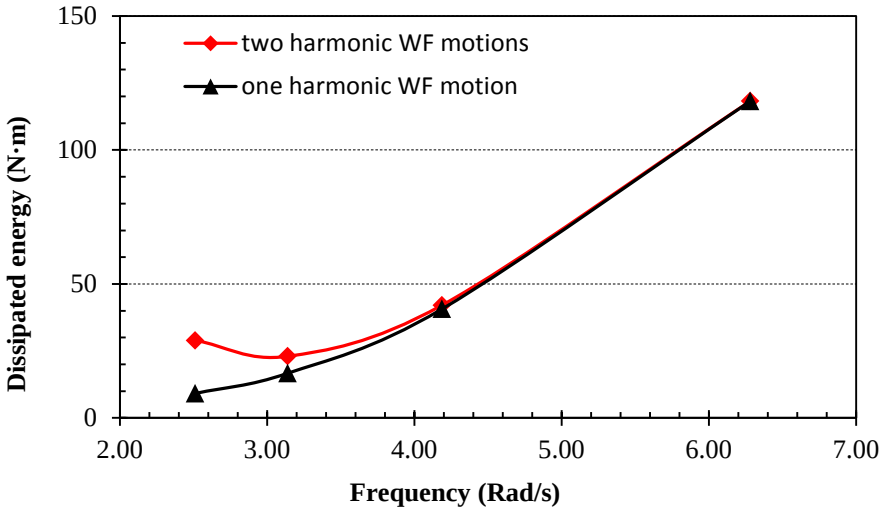

Figure 5-16 Dissipated energy of the mooring line with two harmonic WF motions superimposed (varying frequencies)

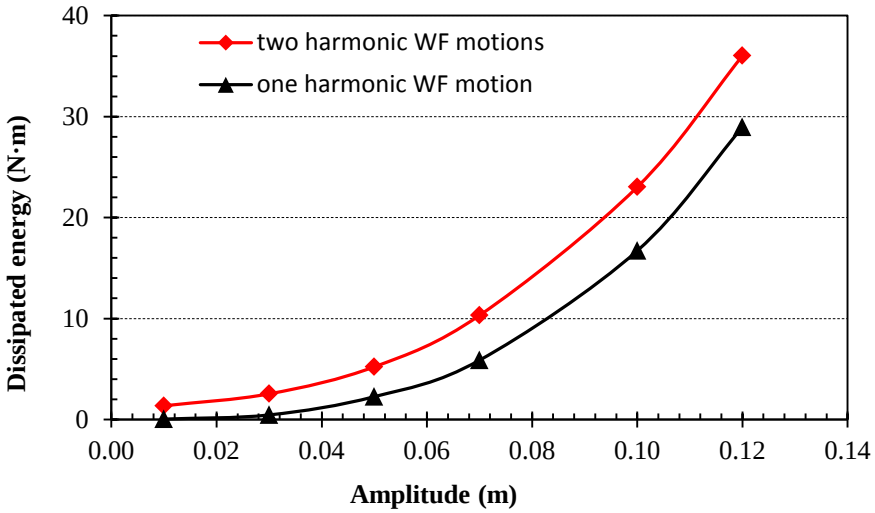

Figure 5-17 Dissipated energy of the mooring line with two harmonic WF motions superimposed (varying amplitudes)

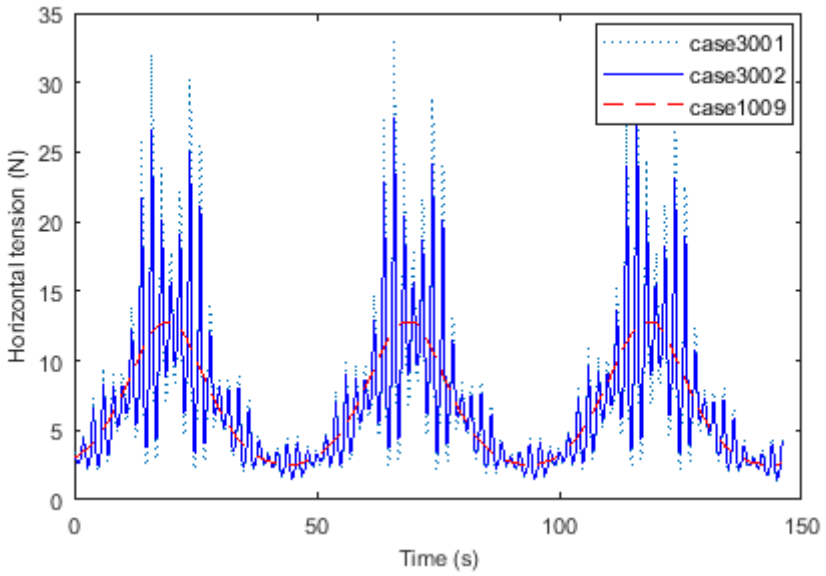

Figure 5-18 Mooring line tension with varying frequencies of two harmonic WF motions

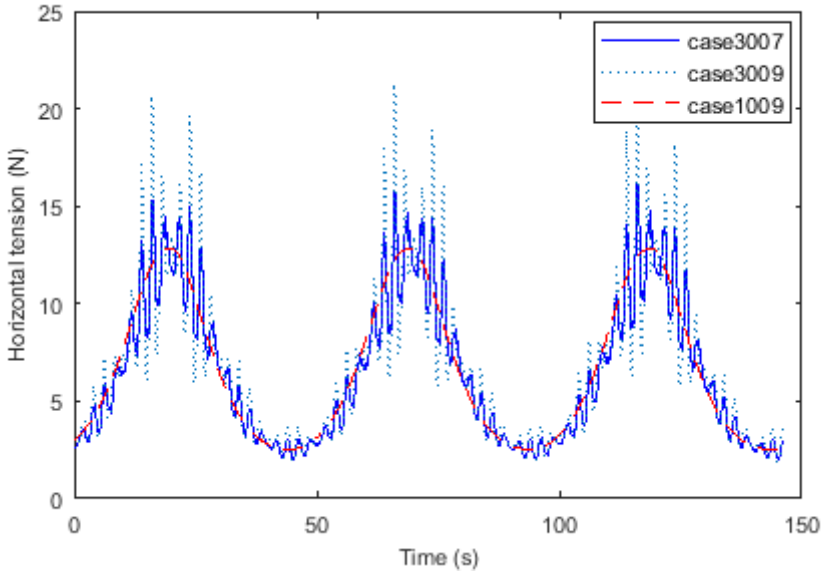

Figure 5-19 Mooring line tension with varying amplitudes of two harmonic WF motions

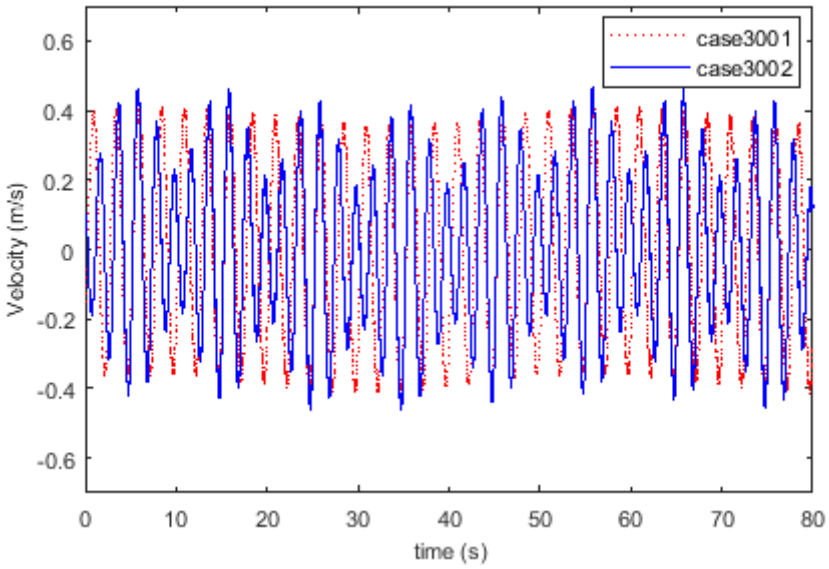

Figure 5-20 Mooring line velocity (fairlead) with varying frequencies of two harmonic WF motions

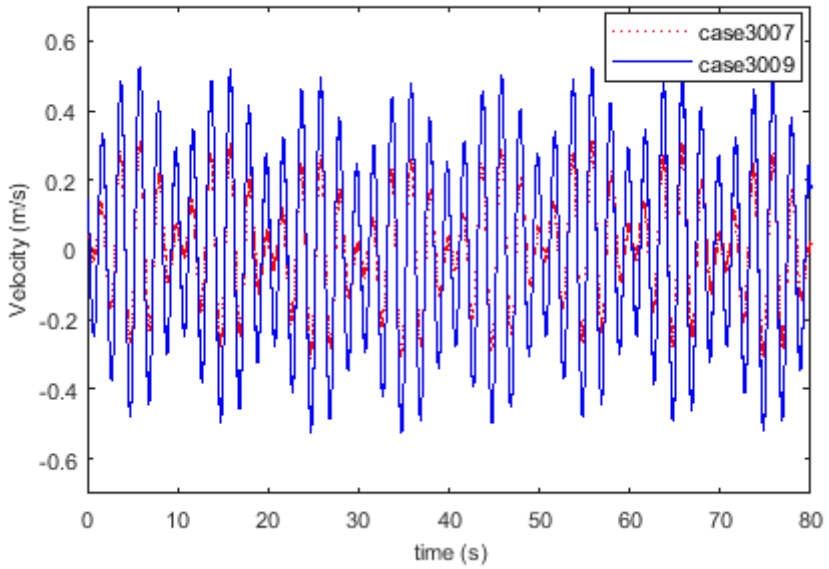

Figure 5-21 Mooring line velocity (fairlead) with varying amplitudes of two harmonic WF motions

Table 5-8 Statistics results of the mooring line velocity at the fairlead point for cases with two harmonic WF motions superimposed

Velocity Statistics	Case3001	Case3002	Case3007	Case3009
Maximum Value(m/s)	0.4157	0.4688	0.3199	0.5312
Standard Deviation	0.2674	0.2399	0.1436	0.2816

5.5.3.3 Effect of a random WF motion

The effect of two harmonic WF motions on mooring line induced damping was analysed previously; a random WF motion is taken into consideration in this part. In practice, the motion of a moored offshore structure cannot be descried by pure sinusoidal motions, as it is determined by the random wave force acting on itself. Wave spectra are widely used to describe regular waves, in order to assess the effect of the random WF motion on mooring line damping, quantitatively. It is reasonable to define a series of random WF motions based on Jonswap spectra. The inverse Fourier transform is used to convert the Jonswap spectra into time histories, which can be superimposed with the LF oscillation and input to the numerical model. Duration of 500s was chosen which can both coincide with the LF oscillation, and generate reasonable results. The Jonswap spectrums used in the case study are shown in Figure 5-22 and Figure 5-23.

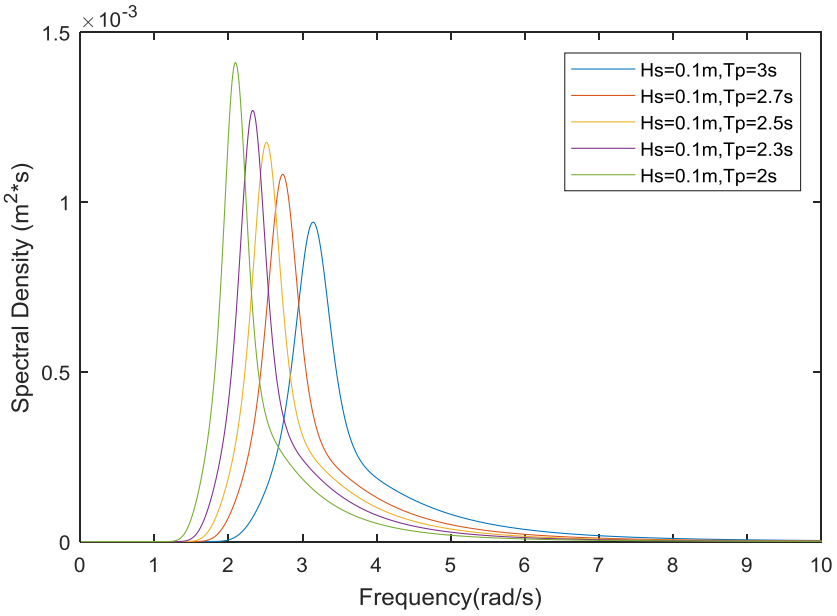

Figure 5-22 Spectrum model for varying peak period

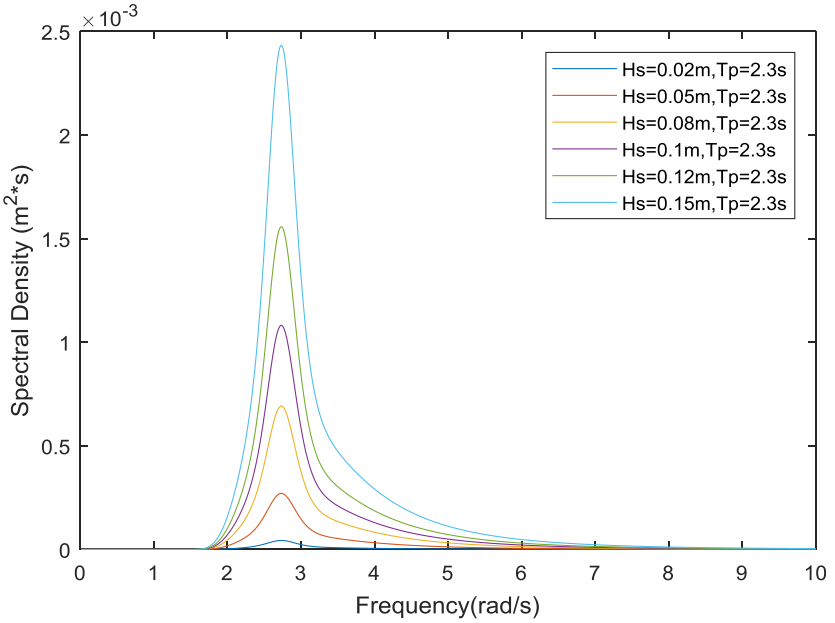

Figure 5-23 Spectrum model for varying significant height

It can be found from the results of random WF motions superimposed that: The mooring line dissipated energy of random WF motion superimposed is bigger than that of pure LF motion oscillation, and this tendency coincides with the results with

harmonic WF motions superimposed. From Figure 5-24, as the peak period of the random WF motion increase, the energy dissipated due to the mooring line damping decreases dramatically. It is hard to compare the velocity shown in Figure 5-26; however, we could find that the extreme value and standard deviation are both reducing with the increase of the peak period, as listed in Table 5-8. It will lead to a decrease of the drag force, and then the mooring line induced damping will be smaller.

With the increase of the significant height of random WF motion, the mooring line dissipation energy demonstrates a rising tendency as shown in Figure 5-25. From the velocity time histories of Case4008 and Case4009 displayed in Figure 5-27, the velocity of bigger significant height (Case4009) is higher than that of Case4008, which means the bigger drag force. Considering the random characteristics of irregular WF motion, the statistical results of the velocity distribution are also compared in Table 5-8, and it is found that the standard deviation is increasing with the significant height increases. As a result, the higher significant height of random WF motion superimposed will lead to more dissipated energy of mooring line.

Table 5-9 Experimental results of mooring line damping (random WF motion)

	LF oscillation		**WF oscillation**		**Experimental Results**	
	A_{lf} **(m)**	ω_{lf} **(rad/s)**	H_s **(m)**	T_p **(s)**	**Energy dissipation (N·m)**	**Damping coefficient (N·s/m)**
Case4001	0.2	0.1269	0.1	2	3.3007	207.82
Case4002	0.2	0.1269	0.1	2.3	2.4225	148.93
Case4003	0.2	0.1269	0.1	2.5	1.8200	115.27
Case4004	0.2	0.1269	0.1	2.7	1.4627	92.06
Case4005	0.2	0.1269	0.1	3	0.9467	60.43
Case4006	0.2	0.1269	0.02	2.3	0.0497	3.08

Case4007	0.2	0.1269	0.05	2.3	0.4507	28.06
Case4008	0.2	0.1269	0.08	2.3	0.5638	34.45
Case4009	0.2	0.1269	0.12	2.3	3.1543	192.22
Case4010	0.2	0.1269	0.15	2.3	6.9839	427.38

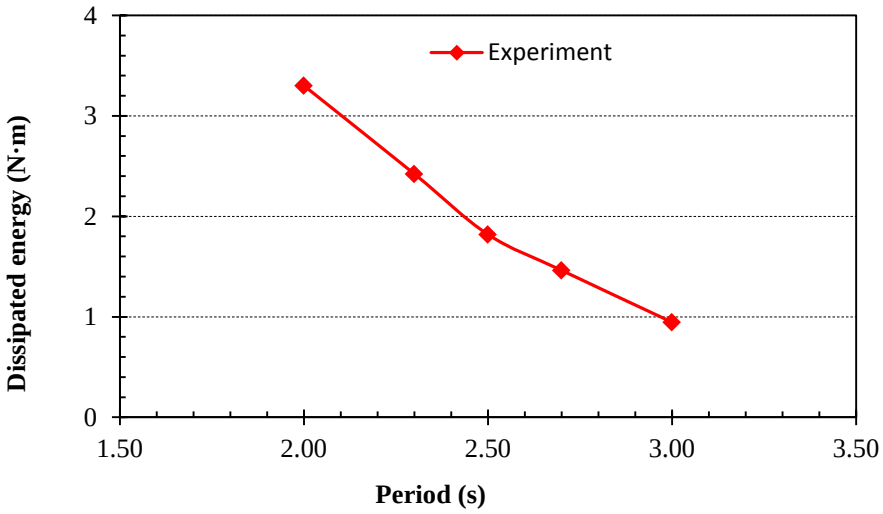

Figure 5-24 Dissipated energy of the mooring line with random WF motion superimposed (varying period)

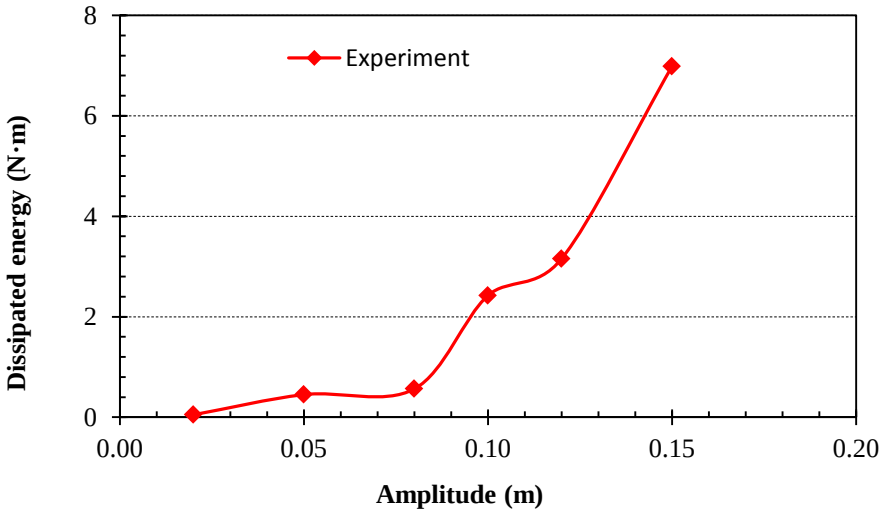

Figure 5-25 Dissipated energy of the mooring line with random WF motion superimposed (varying amplitudes)

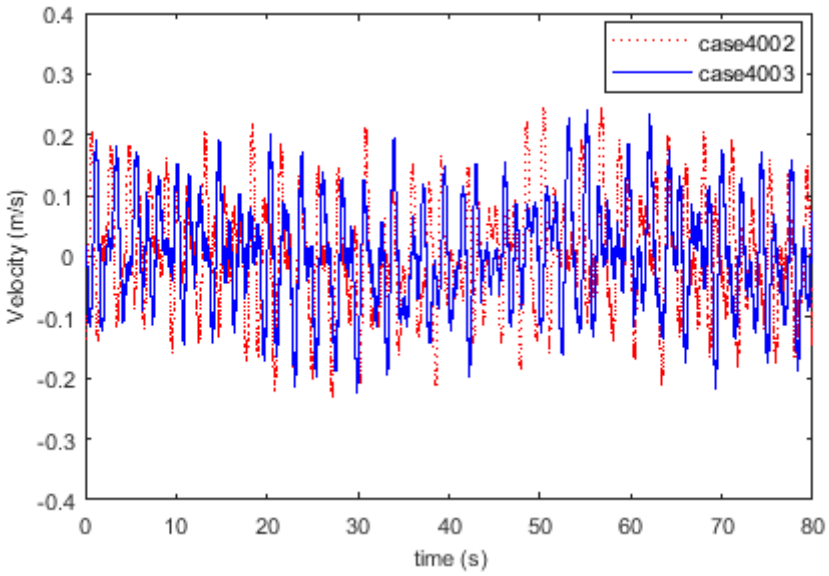

Figure 5-26 Mooring line velocity (fairlead) with varying peak period of random WF motion

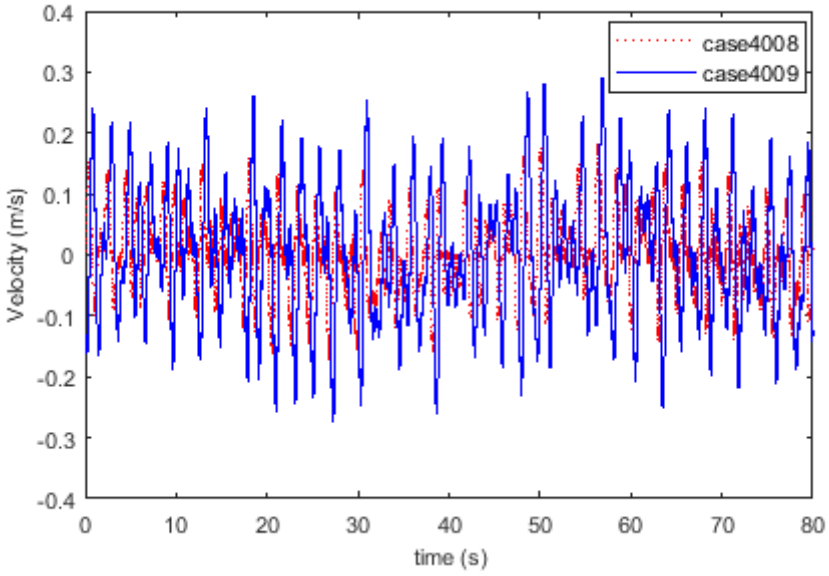

Figure 5-27 Mooring line velocity (fairlead) with varying significant height of random WF motion

Table 5-10 Statistics results of the mooring line velocity at the fairlead point for cases with two harmonic WF motions superimposed

Velocity Statistics	Case4002	Case4003	Case4008	Case4009
Maximum Value(m/s)	0.3039	0.2631	0.2234	0.3509
Standard Deviation	0.0933	0.0862	0.0669	0.1115

5.6 Concluding remarks

In this chapter, mooring induced damping is studied by experimental tests. The parametric analyses include variations of oscillating frequency and amplitude is investigated. The relationship between line velocity and mooring line damping is discussed.

It can be found that the dissipated energy represents 'mooring line damping' is influence by motion velocity. Because of this reason, the mooring line damping is increasing with the increase of oscillation frequency. This trend is also suitable for the oscillations of harmonic WF motion superimposed. Meanwhile, as the amplitude of oscillation increasing, the mooring line induced damping also has an increase. We could also find that the superimposed WF motion makes significant contribution on mooring line damping, comparing to the results of pure LF oscillations.

For the cases of random WF motion superimposed, the results coincide with those of harmonic WF motion superimposed.

In order to estimate the mooring line damping, some formulas are recommended from the results of the cases considered in this chapter. It could model mooring line damping in a simple way, although it is affected by complicated factors, such as LF oscillation, WF motion, and pretension and so on.

The relationship between mooring line tension and mooring line damping is also discussed. For pure LF oscillation, the mooring line tension is mainly determined by static stiffness, the mooring line tension thus did not change for different frequencies. However, the mooring line tension is dominated by mooring line dynamic, so the mooring line tension in increasing as the frequency of WF motion increases.

6 Sensitivity analysis of drag coefficient

6.1 Introduction

In this chapter experimental results on the mooring line tension and mooring line induced damping will be compared with results of computations. In order to validate the feasibility and accuracy of numerical calculation using Orcaflex, the experimental model is simulated and calculated based on oscillations that are the same as those defined in model tests. Chain mooring line can be regarded as a slender cylinder when considering the drag force acting on itself in the water. Thus, Morison Equation is widely applied to calculate the drag force; however, there is an issue of hydrodynamic coefficient determination. It is known that the hydrodynamic coefficients are functions of R_n and KC , in addition to this, they are also functions of the surface roughness that caused by marine growth.

Here, because the mooring line damping is dependent on the drag force acting on itself, thus the effect of drag coefficient will be taken into account in this part. As we known, the drag coefficient is commonly defined as having a constant value in numerical calculations, because of the limitation about the knowledge of its value. It is usually defined in very coarse ranges recommended in related rules. However, most of these values are determined by experiments in steady flow and the effect of KC and R_n are not included. The methods to determine the hydrodynamic coefficients based on the experimental tests will be presented in Appendix B. As indicated in (Huse, 1989), it was concluded that the damping of moorings estimated by numerical calculation has significant discrepancy with experimental results because of neglecting the effect of drag coefficient variations. Moreover, the drag coefficient is also critical to the mooring line dynamic response and fatigue performance. Thus, the sensitivity of the value of drag coefficient will also be investigated in this chapter.

6.2 The determination of the drag coefficient (C_D)

The mooring line induced damping is mainly due to the drag force acting on the mooring line. A sufficiently exact determination of the drag forces is essential for predicting the mooring line damping and for selecting the appropriate mooring configuration. The drag force can be written as:

$$F_D = \frac{1}{2} C_D \rho A (v - u)^2 \qquad \textbf{6-1}$$

The drag coefficient is a characteristic dimensionless number for a mooring line in the flow field, depending on the Reynolds number and KC number:

$$C_D = \frac{2F_D}{\rho A (v - u)^2} = f(Rn, KC) \qquad \textbf{6-2}$$

Where F_D represents drag force, C_D drag coefficient, ρ mass density of the fluid, A cross-sectional area, based with nominal diameter for chain line, $(v - u)$ relative velocity. In this study, the effect of the roughness on drag coefficient is not taken into account.

From equation 6-2, the valuation of the drag coefficient depends on factors of R_n and KC. According to the comparison between experimental and numerical results of the mooring line response presented in section 6.3, it is found that a constant value of drag coefficient does not apply to all cases. In order to investigate the relationship between the drag coefficient and these factors, a fitted drag coefficient for each case is determined by experimental result. Meanwhile, the fitted drag coefficient will also be applied in numerical calculation for validation.

6.2.1 Drag coefficient with R_n and KC

The drag coefficients for cases of pure LF oscillation, with a harmonic WF motion, two harmonic WF motions and random WF motion superimposed with different KC numbers are illustrated in Figure 6-1 to Figure 6-4. In general, it is found that the drag coefficient changes on a case-by-case basis; that is to say, the drag coefficient should not be assigned with a fixed constant, because its value is dependent to complicated factors.

From Figure 6-1 to Figure 6-4, there is a generally decreasing trend with KC number. This is not so apparent with some results of lower KC cases for pure LF oscillation, and with a harmonic WF motion superimposed. The results for KC values of 124, 249 and 287 seem occur anomalous. This may due to the effects of R_n number.

From the drag coefficient data derived by experimental results shown in Figure 6-2 and Figure 6-3, the non-linear fitting method is executed to the all cases and the uniform fitting formula is obtained from the results which showed as:

$$C_D = 7E-06KC^2 - 0.0074KC + 3.7318 \qquad \textbf{6-3}$$

Where the KC range 200~500, and the Reynolds number with the value range 0~3000. The formula is derived by the experimental results which are low-Reynold cases.

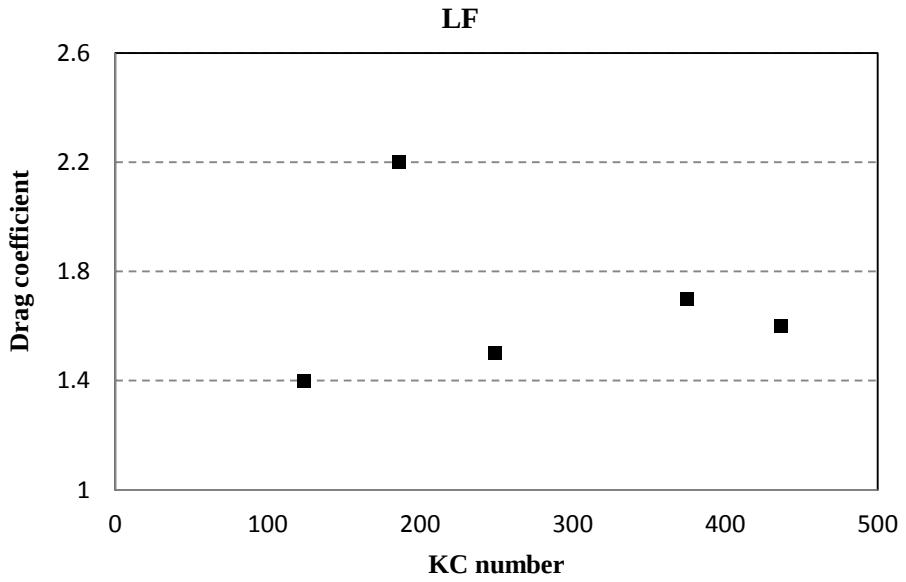

Figure 6-1 Drag coefficients for pure LF oscillations

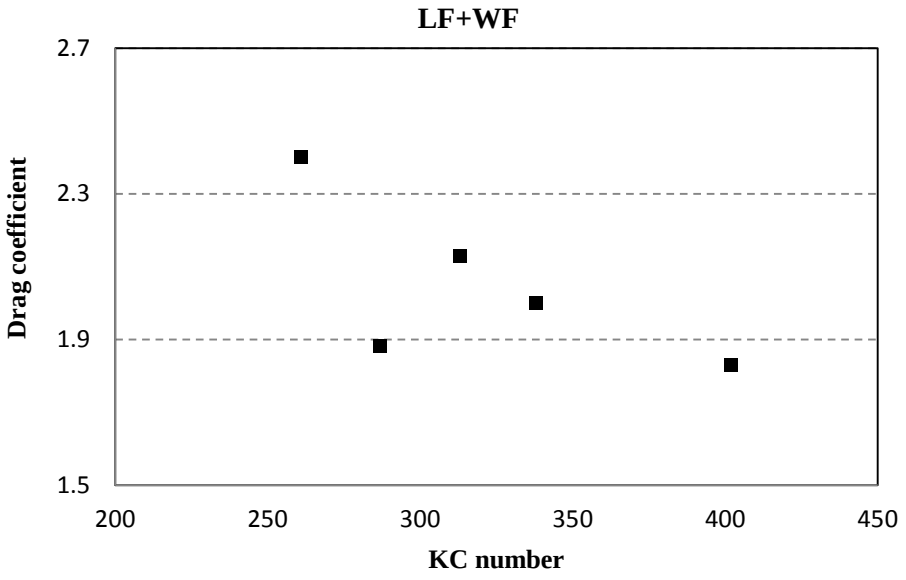

Figure 6-2 Drag coefficients for LF oscillation superimposed with a harmonic WF motion

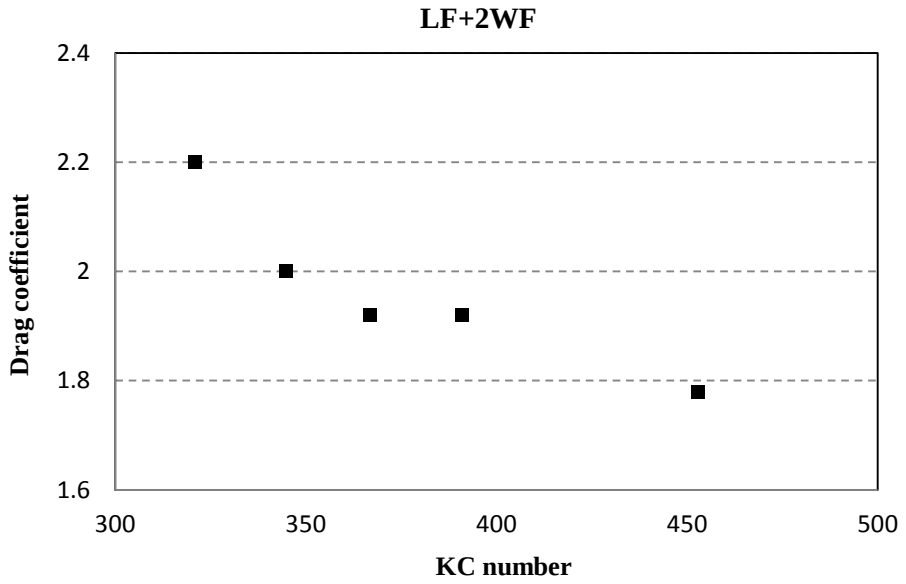

Figure 6-3 Drag coefficients for LF oscillation superimposed with two harmonic WF motion

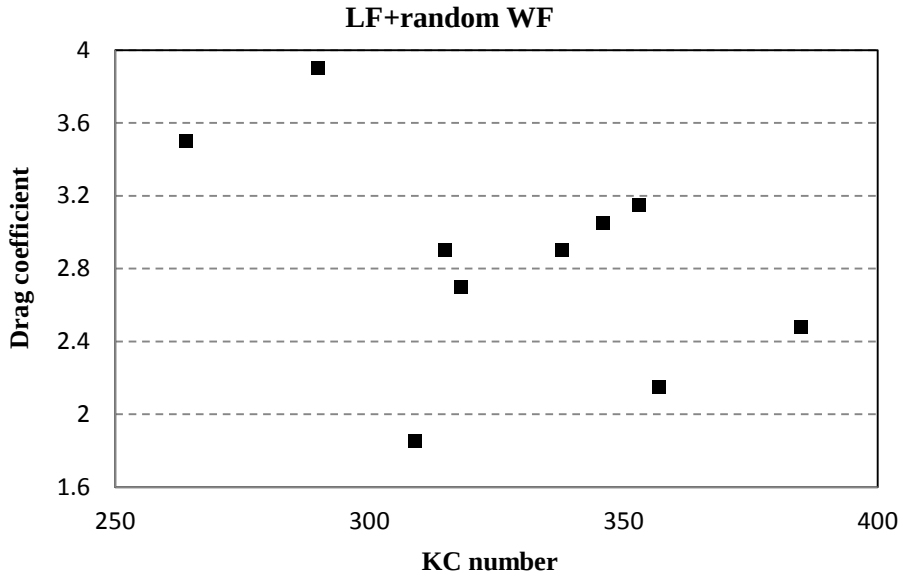

Figure 6-4 Drag coefficients for LF oscillation superimposed with a random WF motion

In order to investigate the effect of the R_n number to drag coefficient, fixed KC number of 311 and 376 are considered separately with pure LF oscillation, and with a harmonic WF motion superimposed. Figure 6-5 presents the results of drag coefficients with

different R_n number of pure LF oscillations. It is shown that a decrease in drag coefficient with increasing R_n number when lower than 200, but an increase occur with R_n number increases above 200.

Considering cases with superimposed WF motions, the drag coefficients with different R_n number are shown in Figure 6-6. As anticipated an increase in drag coefficient will result in each case, comparing to the value for the state when no WF motion was applied. The drag coefficients for these higher R_n number are seen to be decreasing when R_n increase.

The non-linear fitting method is executed to the all cases in Figure 6-5 and Figure 6-6, and the uniform fitting formula are obtained from the results which showed as:

$$C_D = 5E-05R_n^2 - 0.0193R_n + 3.5132 \quad \textbf{6-4}$$

$$C_D = 9E-08R_n^2 - 0.0005R_n + 2.5578 \quad \textbf{6-5}$$

These two formulas show the relationship between drag coefficient and Reynolds number for LF oscillation and LF superimposed with WF motions cases, where KC number equal to 311 and 376 separately.

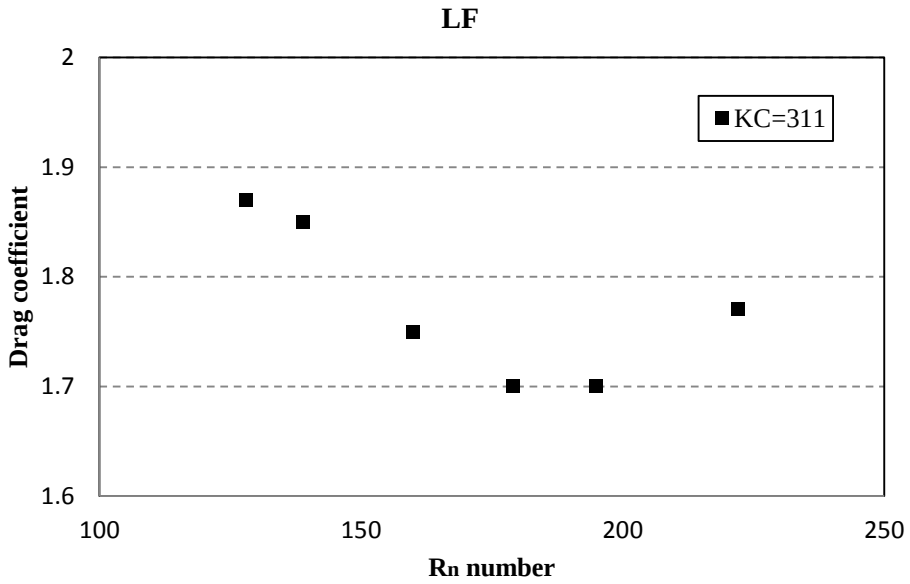

Figure 6-5 Drag coefficients with various R_n number (pure LF oscillation)

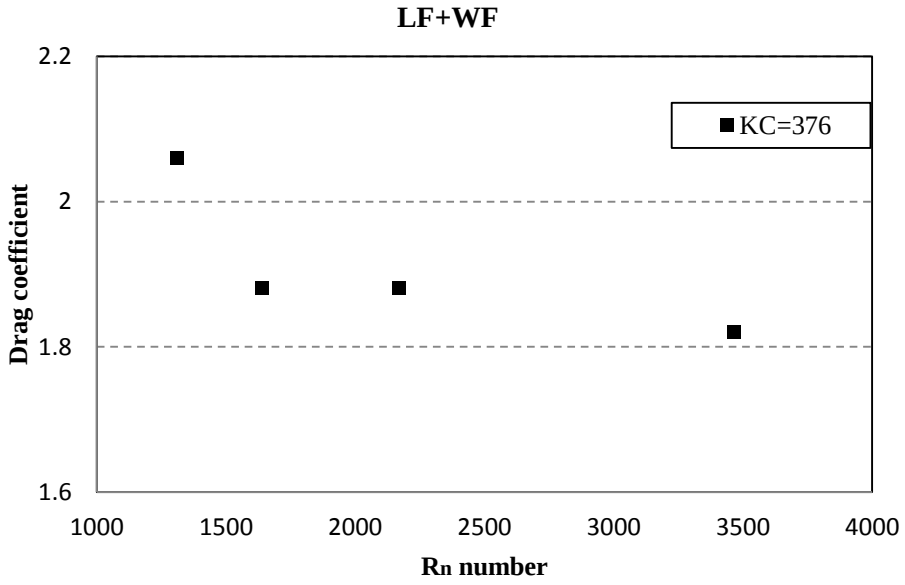

Figure 6-6 Drag coefficients with various R_n number (LF superimposed with a harmonic WF motion)

Mooring chain is linked by a lot of chain rings, so it is difficult to determine the hydrodynamic coefficient with experimental discovery path. According to the mooring line response from the experimental data in chapter 5, the drag coefficient ranges from

1.4-2.4 for cases of LF oscillation, LF & WF oscillations and LF & 2WF oscillations. Combined with the empirical value recommended by DNV GL(2010), the drag coefficient is valued with 1.8 to assess the mooring line energy dissipation. Meanwhile, the inertia coefficient of 1.0 as a constant is selected to compute the mooring line response. In order to estimate the sensitivity of the mooring line damping and dynamic tension to the value of drag coefficient, value of 1.6 and 2.0 are selected to apply to the cases of pure LF oscillation and with WF motion superimposed, separately.

6.2.2 Mooring line tension

To investigate the accuracy of the drag coefficient, the mooring line responses computed with assumed hydrodynamic coefficients are compared with those from model tests. In general, it can be found that the mooring line tension calculated with selected drag coefficient is in good agreement with the experimental data, as shown in Figure 6-7 to Figure 6-10. This illustrates that the assumed values for drag coefficient are reasonable to assess the mooring line response for cases in this thesis. In addition, it is feasible to adopt Orcaflex in estimating the mooring line response.

In Figure 6-7, Case1006 and Case1007 are selected as representations, their time histories of mooring line tension in horizontal direction are displayed. It can be found that the mooring line tension from experimental measurement agrees well with that from numerical calculation predicted. For these cases of LF oscillations, the mooring line tension is not sensitive to the value of drag coefficient, because the tension is dominated by its own stiffness. The drag force acting on the mooring line is very small due to the small velocity. It can be found that a unit increase of drag coefficient only make a small percentage ($< 0.001\%$) contributions on the mooring line tension. It is regarded that the value of drag coefficient has a small effect on the mooring line tension based on the LF oscillation cases.

For cases of low-frequency superimposed with wave-frequency oscillations, the mooring line tension histories calculated by Orcaflex are compared with the

experimental measured data. The mooring tension histories for case2001 and case2009, case3002 and case3008, and case4001 and case4010 are presented in Figure 6-8 to Figure 6-10. It can be found that the mooring line tension is increasing as the drag coefficient increased. It is different from the result of cases of LF oscillations; because the drag force becomes dominant in these cases of superimposed WF motion, and the drag force is increasing with the increase of the drag coefficient.

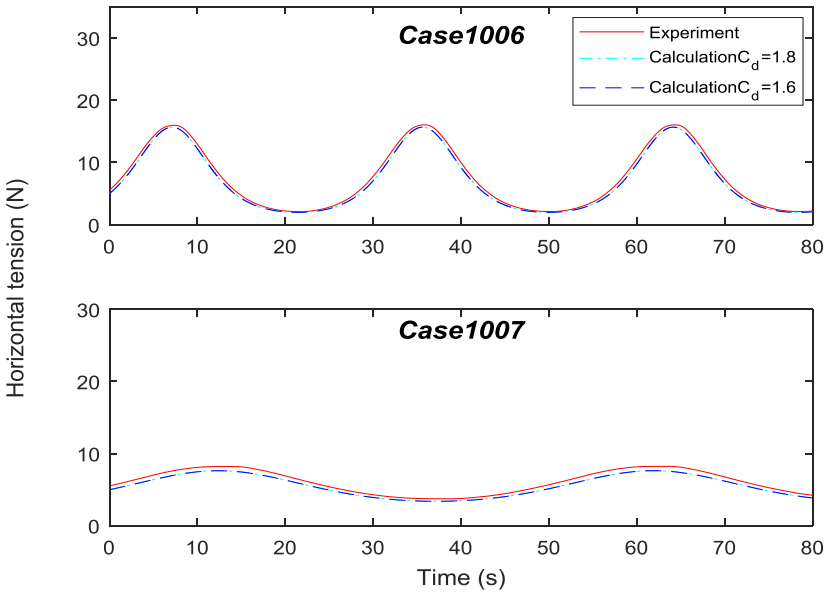

Figure 6-7 The horizontal tension histories for LF oscillation (Experiment Vs. Calculation)

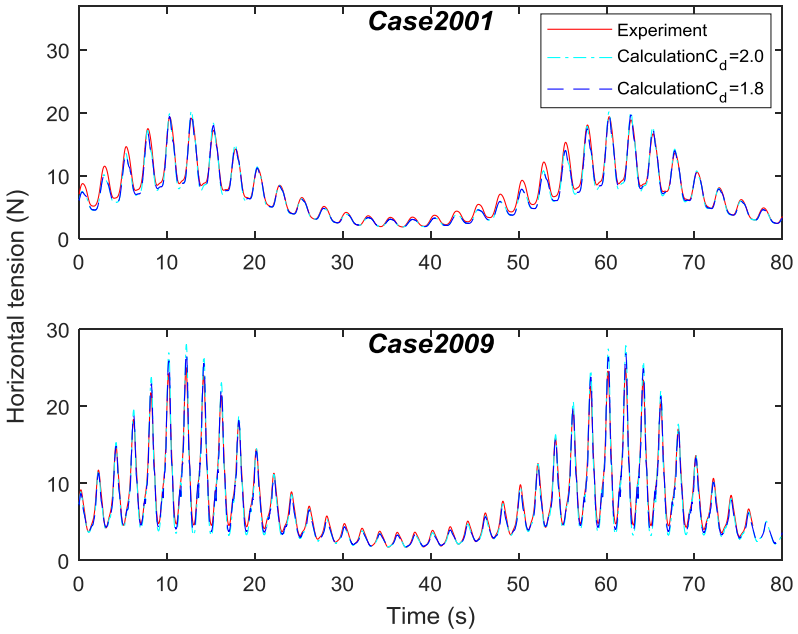

Figure 6-8 The horizontal tension histories for cases of a harmonic WF motion superimposed (Experiment Vs. Calculation)

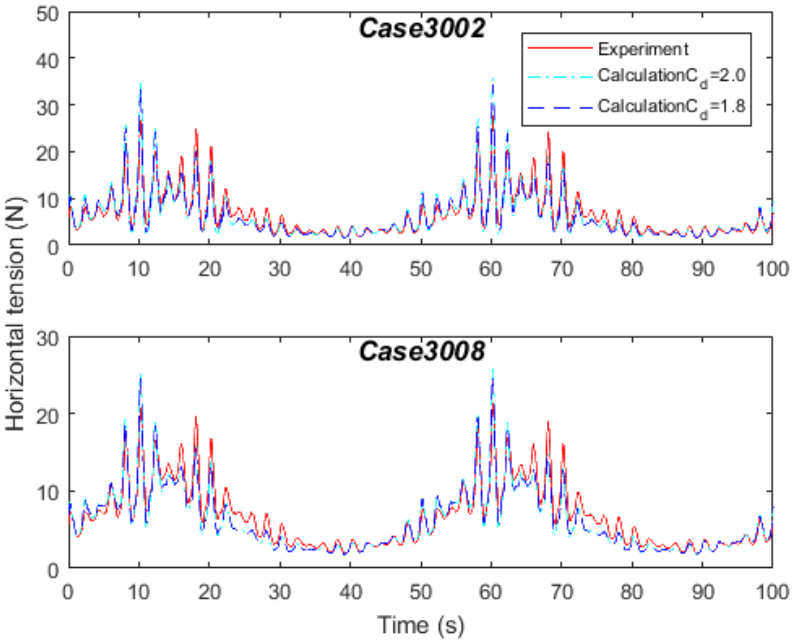

Figure 6-9 The horizontal tension histories for cases of two harmonic WF motions superimposed (Experiment Vs. Calculation)

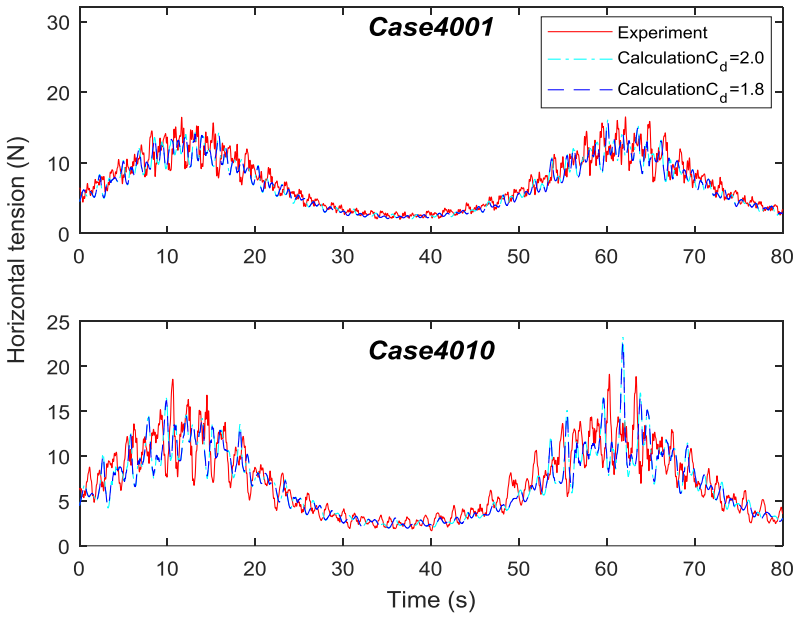

Figure 6-10 The horizontal tension histories for cases of random WF motion superimposed (Experiment Vs. Calculation)

6.3 Sensitivity of the mooring line damping on the drag coefficient

According to the relationship of drag coefficient to R_n and KC number, the drag coefficient is determined as 1.8. Meanwhile, for the pure LF oscillation cases, the slow velocity would lead to low level of R_n, drag coefficient (C_D) of 1.6 is thus chose to investigate the effect of drag coefficient variation. For cases oscillated by pure LF motion superimposed with WF motions, drag coefficient of 2.0 is applied. Here, the numerical calculations are based on the prototype mooring line of the experimental model. The oscillation for the prototype is also scaled-up by the cases of experimental tests; the results are listed from Table 6-1 though Table 6-4.

Table 6-1 Dissipated energy for different value of drag coefficient (pure LF oscillation)

	Experimental Measured (N · m)	**Numerical Calculation (N · m)**				**Increase By (N · m)**	R_n
		C_D **=1.8**	**Error (%)**	C_D **=1.6**	**Error (%)**		
Case1001	4.90E5	4.74E5	-3.42%	4.24E5	-13.68%	5.00E4	8.35E4
Case1002	5.73E5	5.63E5	-2.19%	5.00E5	-13.14%	6.30E4	9.09E4
Case1003	7.24E5	7.47E5	3.49%	6.63E5	-8.14%	6.30E4	1.05E5
Case1004	8.59E5	9.24E5	7.32%	8.23E5	-4.39%	1.01E5	1.16E5
Case1005	1.04E6	1.10E6	5.65%	9.82E5	-5.65%	8.40E4	1.27E5
Case1006	1.41E6	1.43E6	1.49%	1.28E6	-9.52%	1.55E5	1.45E5
Case1007	1.63E4	2.52E4	50.00%	2.10E4	25.00%	1.01E5	3.29E4
Case1008	9.65E4	7.98E4	-17.39%	7.14E4	-26.09%	8.40E3	4.95E4
Case1009	1.77E5	2.10E5	19.05%	1.89E5	7.14%	2.10E4	6.64E4
Case1010	9.25E5	9.82E5	6.36%	8.73E5	-5.45%	1.09E5	8.35E4
Case1011	1.72E6	1.94E6	12.44%	1.72E6	0.00%	2.20E5	1.01E5

Table 6-2 Dissipated energy of different value of drag coefficient (a harmonic WF oscillation superimposed)

	Experimental Measured (N · m)	**Numerical Calculation (N · m)**				**Increase By (N · m)**	R_n
		C_D **=1.8**	**Error (%)**	C_D **=2.0**	**Error (%)**		
Case2001	3.84E8	3.37E8	-12.37%	3.73E8	-2.96%	3.60E7	8.32E5
Case2002	7.02E8	6.76E8	-3.66%	7.45E8	6.20%	6.90E7	1.04E6
Case2003	1.71E9	1.64E9	-3.82%	1.77E9	3.77%	1.30E8	1.40E6
Case2004	4.84E9	4.82E9	-0.60%	5.02E9	3.61%	2.00E8	2.91E6
Case2005	1.65E6	1.27E6	-23.10%	1.41E6	-14.72%	1.40E5	1.51E5
Case2006	1.90E7	1.83E7	-3.43%	2.03E7	7.03%	2.00E6	3.29E5
Case2007	9.49E7	8.02E7	-15.47%	8.89E7	-6.35%	8.70E6	5.20E5
Case2008	2.46E8	2.22E8	-10.07%	2.45E8	-0.43%	2.30E7	7.22E5
Case2009	1.22E9	1.20E9	-1.11%	1.31E9	8.06%	1.10E8	1.25E6

Table 6-3 Dissipated energy of different value of drag coefficient (two harmonic WF oscillation superimposed)

	Experimental Measured	**Numerical Calculation (N · m)**				**Increase By**	R_n
	(N · m)	C_D **=1.8**	**Error (%)**	C_D **=2.0**	**Error (%)**	**(N · m)**	
Case3001	1.22E9	1.26E9	3.26%	1.37E9	12.94%	1.10E8	1.34E6
Case3002	9.67E8	9.56E8	-1.13%	1.04E9	7.73%	8.40E7	1.49E6
Case3003	1.77E9	1.95E9	10.36%	2.08E9	17.72%	1.30E8	1.96E6
Case3004	4.97E9	5.19E9	4.43%	5.41E9	8.85%	2.20E8	2.85E6
Case3005	5.69E7	4.67E7	-17.97%	5.18E7	-9.02%	5.10E6	5.17E5
Case3006	1.07E8	9.54E7	-10.59%	1.06E8	-0.95%	1.06E7	7.24E5
Case3007	2.19E8	2.06E8	-5.95%	2.28E8	4.05%	2.20E7	9.37E5
Case3008	4.33E8	4.08E8	-5.73%	4.50E8	3.90%	4.20E7	1.15E6
Case3009	1.51E9	1.52E9	0.75%	1.64E9	8.69%	1.20E8	1.76E6

Table 6-4 Dissipated energy of different value of drag coefficient (random WF oscillation superimposed)

	Experimental Measured (N · m)	Numerical Calculation (N · m)				Increase By (N · m)	R_n
		C_D =1.8	Error (%)	C_D =2.0	Error (%)		
Case4001	1.39E8	9.88E7	-28.71%	1.08E8	-21.73%	9.20E6	1.81E6
Case4002	1.02E8	6.54E7	-35.70%	7.21E7	-29.07%	6.70E6	1.61E6
Case4003	7.64E7	4.54E7	-40.60%	5.02E7	-34.30%	4.80E6	1.54E6
Case4004	6.14E7	3.69E7	-39.97%	4.08E7	-33.51%	3.90E6	1.47E6
Case4005	3.97E7	2.48E7	-37.65%	2.75E7	-30.84%	2.70E6	1.12E6
Case4006	2.09E6	1.05E6	-49.70%	1.16E6	-44.27%	1.10E5	3.91E5
Case4007	1.89E7	9.12E6	-51.79%	1.01E7	-46.71%	9.80E5	8.11E5
Case4008	2.37E7	2.32E7	-1.92%	2.56E7	8.35%	2.40E6	1.28E6
Case4009	1.32E8	1.13E8	-14.96%	1.24E8	-6.34%	1.10E7	1.95E6
Case4010	2.93E8	2.21E8	-24.57%	2.43E8	-17.23%	2.20E7	2.48E6

6.3.1 With pure LF oscillation

In Table 6-1, the results of dissipated energy of mooring line through numerical computation are listed, and the results are also presented in Figure 6-11 and Figure 6-12. It is shown that in general the dissipated energy from simulation predicted is reasonably well agreed with them of the experimental tests. For Case1001- Case1011, it can be found that the dissipated energy based on the drag coefficient of 1.8 and 1.6, both have the potential to rise with the increase of LF oscillation frequency. With the amplitude of LF motion rising, they also show an increasing trend. This is consistence with the trend of experimental results.

The discrepancies between the dissipated energy from experimental tests and numerical calculations are less than 15%, except for case1007, case1008 and case1009. Compared to other cases, the damping level of the mentioned three cases is very low, which is less than $2.00E5N \cdot m$. This is to say, a tiny error will make considerable impact on the result of mooring line energy dissipation, and it would thus lead to a considerable discrepancy. Meanwhile, it is shown that the cases with higher damping level will have less percentage of errors. And also, it is found that most of the R_n for the mentioned cases are at low level ($< 5.0E5$), except for some cases of WF motion superimposed. It is reasonable that the R_n should be taken into account when considering the hydrodynamic coefficient applied in calculation.

When considering the effect of proportional change of drag coefficient to the proportional change of energy dissipation, it can be found that the energy dissipation can increase by over than 95% due to a unit increase of drag coefficient. In this case, it is regarded that the value of drag coefficient (C_D) would make significant contribution on the energy dissipation, because its increasing will lead to the increase of drag force.

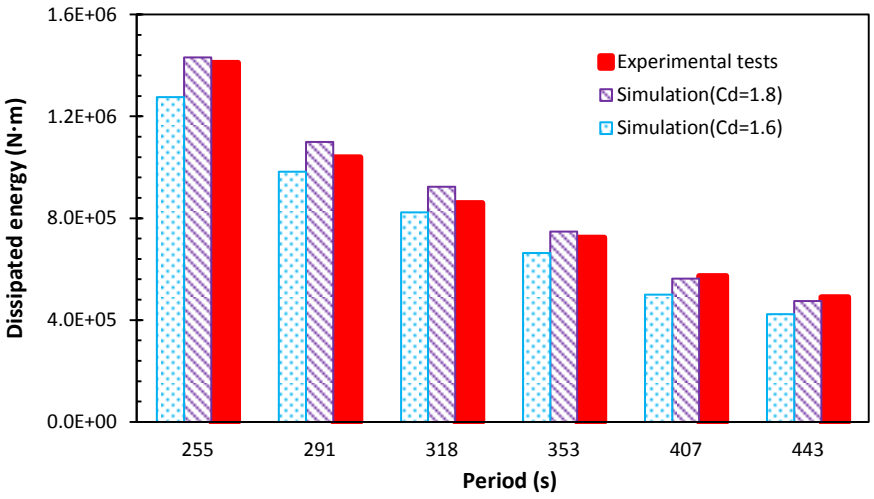

Figure 6-11 Dissipated energy of different drag coefficient (varying periods)

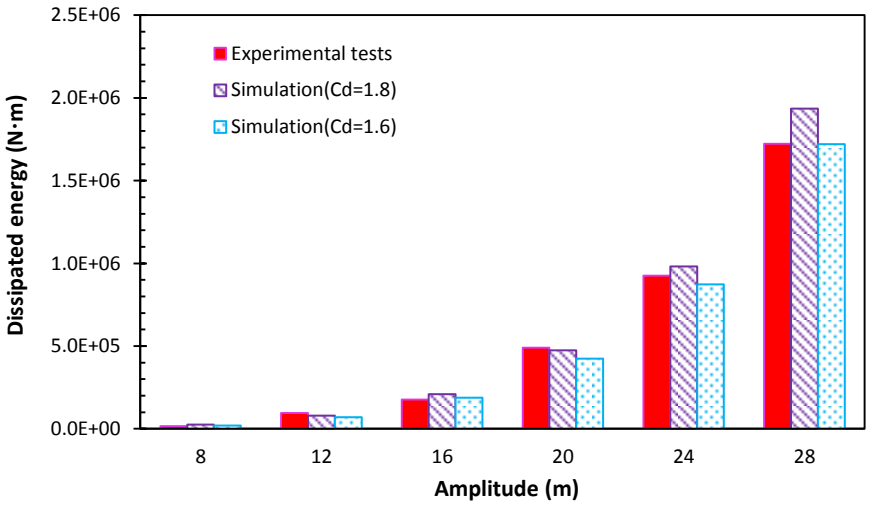

Figure 6-12 Dissipated energy of different drag coefficient (varying amplitudes)

6.3.2 LF oscillation superimposed with a harmonic WF motion

The results of computations and measurements with respect to the dissipated energy on different drag coefficient are presented in Table 6-2. It is shown that the energy dissipation of experiments and computations are in good agreement. From Figure 6-13, the results predicted show the potential of the dissipated energy increasing as the frequency of WF motion gets bigger, from drag coefficient of 1.8 to 2.0. With the increase of amplitude of WF motion superimposed, the dissipated energy increases, and it presents a non-linear relationship, as shown in Figure 6-14. According to the results predicted, it is considered that Orcaflex can be used to reasonable assess the mooring line damping in for the cases of LF oscillation superimposed with a harmonic WF motion.

The discrepancy between the results of experimental test and numerical calculation for Case2005 is big. It is because the damping level is very low, thus a small error will lead to a considerable discrepancy. Meanwhile, it is found that the valuation of drag coefficient plays an important role on mooring line damping. We could find that a unit increase of the drag coefficient (C_D) will lead to 40%-98% increase of the energy

dissipation. As a result, in order to assess the mooring line damping precisely, it is crucial to determine the drag coefficient in a more accurate way.

Meanwhile, as the value of drag coefficient increasing from 1.8 to 2.0, the energy dissipation increases by 1.40E5 N · m to 2.00E8 N · m. It is found that the amount of the increase is related to the level of the velocity. When the velocity is higher, the change of the drag coefficient will make more contributions on the drag force acting on the mooring line, and then cause bigger energy dissipation.

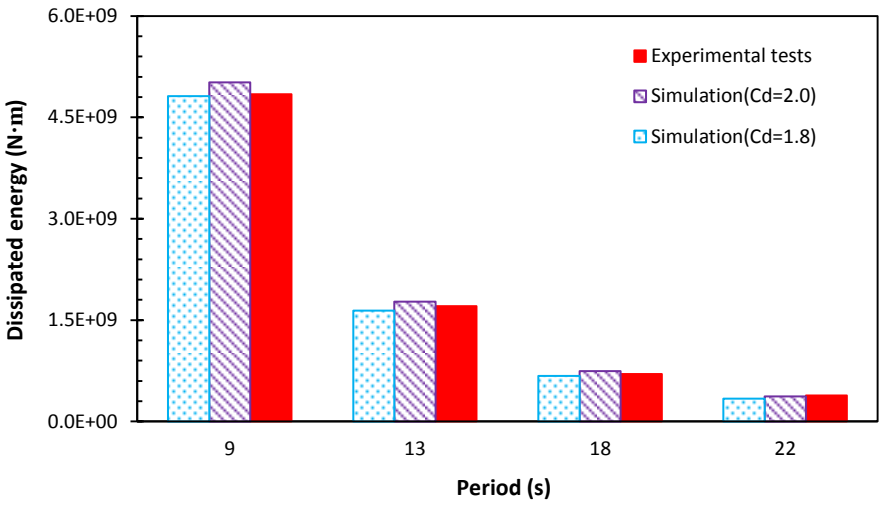

Figure 6-13 Dissipated energy of different drag coefficient (varying periods)

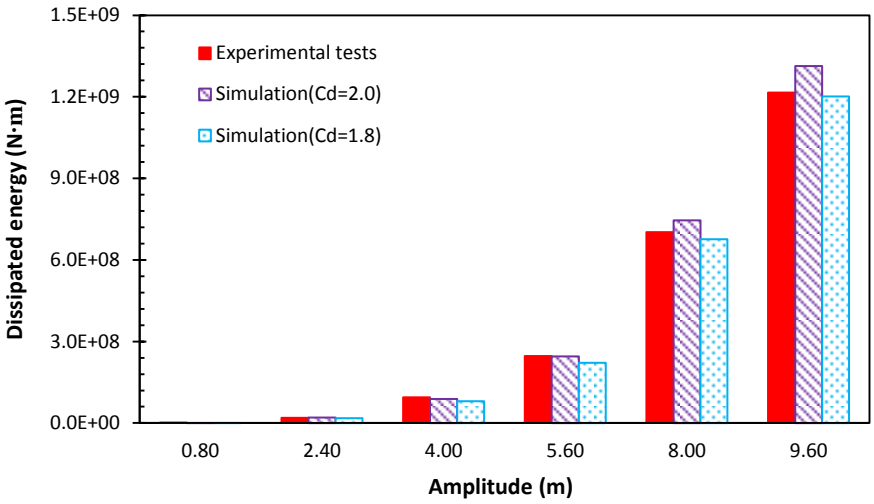

Figure 6-14 Dissipated energy of different drag coefficient (varying amplitude)

6.3.3 LF oscillation superimposed with two harmonic WF motions

For cases of two harmonic WF motions superimposed, the results of numerical computations and experimental measurements with respect of the mooring line energy dissipation are given in Table 6-3, and the comparisons are displayed in Figure 6-15 and Figure 6-16. In general, the results of computations are in accordance with the experimental tests. As the amplitude of superimposed WF motion increases, the dissipated energy will rise. The dissipated energy calculated based on the drag coefficient values from 1.8 to 2.0 is rising as the frequency of WF motion increases, with an exception of Case3001. The results indicate that reasonable results of mooring line damping can be predicted with the numerical computation we applied.

Same as analysed in last section, the valuation of drag coefficient makes significant contributions to mooring line damping, because its value would affect the predicted drag force directly, and consequently change the mooring line dynamic tension and damping. It can be found that the mooring line damping are both getting higher as the drag coefficient rises from 1.8 to 2.0, as shown from Figure 6-15 and Figure 6-16. The percentage of rise in energy dissipation due to a unit increase of drag coefficient can reach 40% to 98%, depends on cases. As a result, it is regarded that the determination of

the drag coefficient is an important issue for predicting the mooring line damping precisely.

Here, although the predicted results of mooring line energy dissipation are roughly in the reasonable range of measurements, we also find that it is difficult to define a constant drag coefficient that suits all different cases.

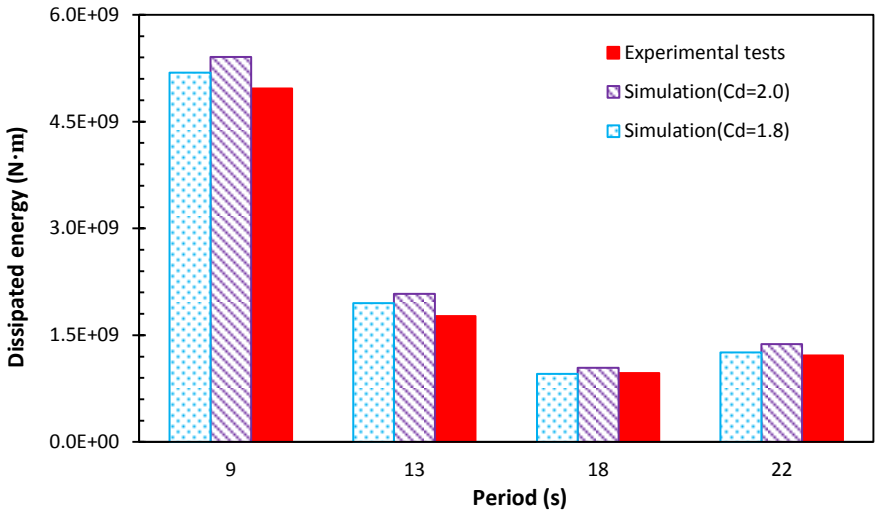

Figure 6-15 Dissipated energy of different drag coefficient (varying periods)

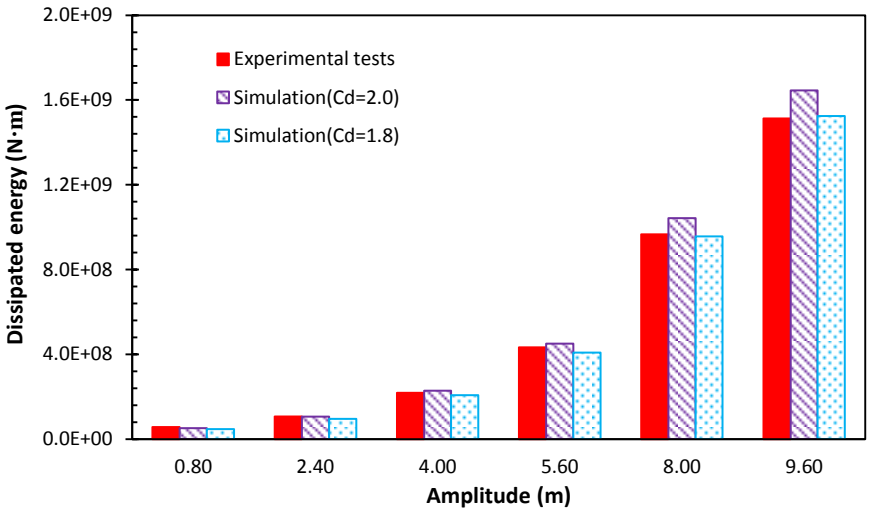

Figure 6-16 Dissipated energy of different drag coefficient (varying amplitude)

6.3.4 LF oscillation superimposed with random WF motion

Here, the mooring line is oscillated by a pure LF motion superimposed with a random WF motion; the random WF motion is produced by Jonswap spectrum, same as that defined for model tests. The results of numerical computations and experimental measurements based on random WF motion superimposed are given in Table 6-4, and the comparisons are displayed in Figure 6-17 and Figure 6-18. Compared to the measurement results, the numerical computations underestimated the energy dissipation of the mooring line except the Case4008. This discrepancy is mainly due to the difference of the mooring tension measured and predicted. With the random WF motion superimposed, the time histories of the oscillations are characterized with the stochastic nature, and it will lead to the discrepancy of the mooring line tension. On the other hand, some high frequency components within the mooring line tension may hide behind the random error that is produced in the experiment, and this part would be filtered by the low-pass filter. These errors would bring the considerable differences of energy dissipation between measurement and computation, because the energy dissipation is obtained by the integration of the multiplication of the horizontal tension and the velocity.

However, the results calculated are at the consistent level with that measured. Meanwhile, when the peak period of the random WF motion increases, the energy dissipation shows a decline. On the contrary, the energy dissipation increases as the amplitude of the superimposed WF motion rises. It is regarded that the method applied to calculate the mooring line damping is reasonable.

Meanwhile, as shown in Figure 6-17 and Figure 6-18, an increase of the drag coefficient would make significant contribution to mooring line damping. The reason is that the drag force acting on the mooring line getting larger due to the increase of the drag coefficient, and it will lead to more damping force induced by mooring line. The percentage of the rise in energy dissipation due to a unit change of drag coefficient can

reach up to 98%, depends on the level of velocity. In this case, the valuation of drag coefficient is very important to mooring line damping assessment.

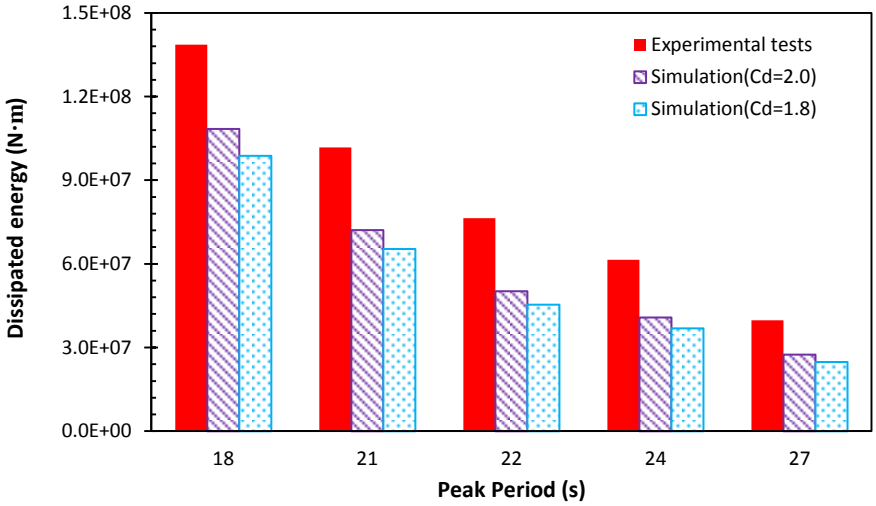

Figure 6-17 Dissipated energy of different drag coefficient (varying periods)

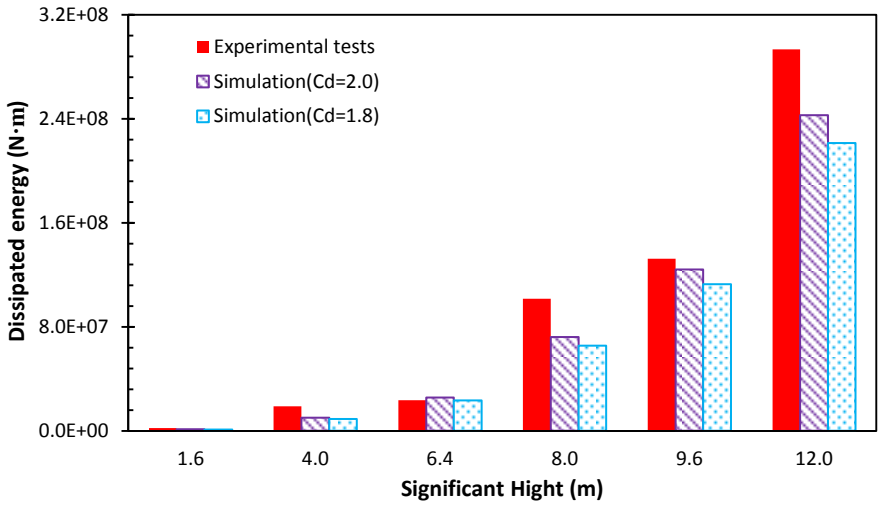

Figure 6-18 Dissipated energy of different drag coefficient (varying amplitude)

6.4 The sensitivity of the drag coefficient variation along the mooring line

From the discussion in last section, it is shown that the mooring line tension and damping are sensitive to the valuation of the drag coefficient, and it is reasonable to define the drag coefficient with different value case by case. That is to say, the drag coefficient is a case-dependent factor, because it is dependent on the level of R_n and KC. In addition, the velocity is a nonlinear distribution along the mooring line, which means the value of drag coefficient should be specially defined along the mooring line.

In order to investigate the sensitivity of the mooring line tension and damping to the drag coefficient (C_D) variation, the mooring line is divided by several sections with a fixed length. Defining Case2008 with a constant drag coefficient of 1.8 as the base case, calculations are repeated based on each section of the mooring line are applied with an increase of drag coefficient (C_D=2.0). Then which part of the mooring line is more sensitive to the mooring line damping and dynamic tension will be determined. Compared to the energy dissipation of the base case, the dissipated energy variation by the drag coefficient variation of the corresponding section are obtained and presented in Figure 6-19. Meanwhile, the normal relative velocity along the arc length of the mooring line is displayed in Figure 6-20.

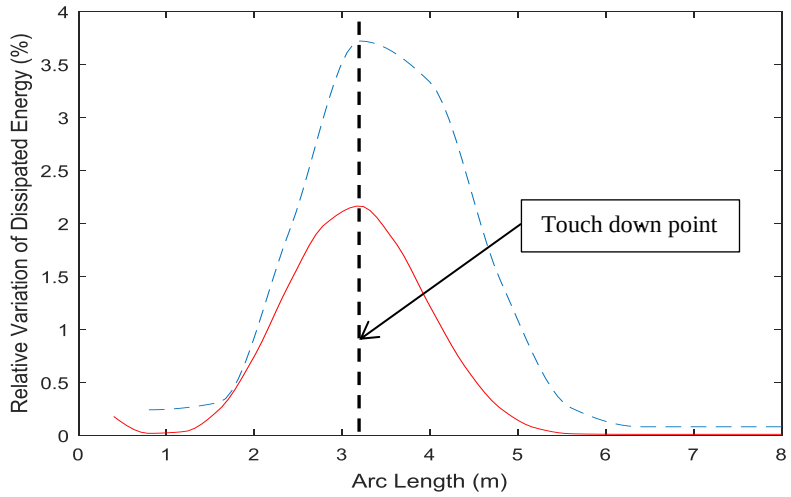

Figure 6-19 The variation of energy dissipation by the drag coefficient variation (red line represents 20 sections divided, blue line represents 10 sections divided)

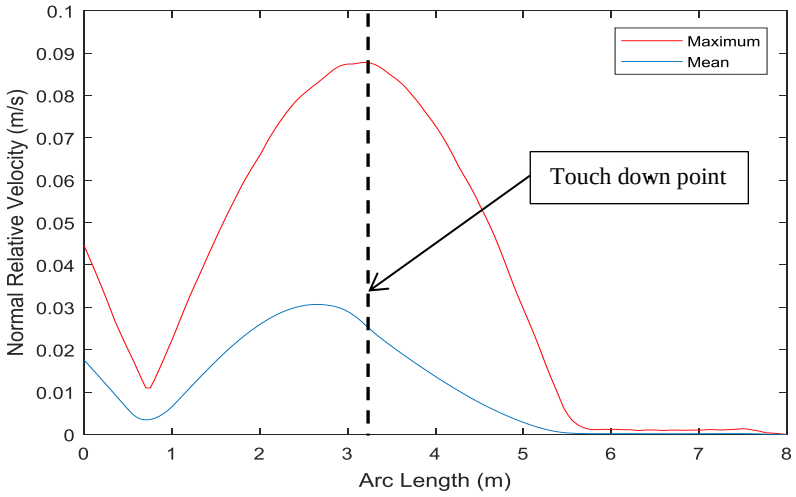

Figure 6-20 Normal relative velocity along the arc length of the line

From Figure 6-19, it can be seen that the component near touch down area is the most sensitive part to the drag coefficient variation. It is coincides with the distribution of normal relative velocity along the arc length, as shown in Figure 6-20. From the two lines illustrated in Figure 6-19, it is also found that the section length for the drag coefficient (C_D) variation has impact on the energy dissipation variation.

6.5 Concluding remarks

In this chapter, the comparison between the results of experimental tests and numerical calculations is studied. Different values of drag coefficient are applied in numerical computation with Orcaflex, the effect of drag coefficient variation to mooring line damping is then studied. And also, the relationships between the drag coefficient (C_D) and Reynolds (R_n) and KC number are investigated. Through the study, it can be seen that:

The trend of the mooring line induced damping resulted from numerical simulation is correspondent to that from model tests. In this case, it is regarded that the method using numerical simulation with Orcaflex is feasible to estimate the mooring line induced damping.

In order to ensure the accuracy of the estimation, the proper valuation of drag coefficient is of much importance. Because this factor is crucial to the drag force acting on the mooring line, and the drag force is the source of mooring line induced damping. Through the study, it is found the drag coefficient ranges from 1.5 to 4.0, depends on cases with different oscillations. With the increase of KC number, the drag coefficient shows decrease except some anomalies occurred in some low KC cases. It is attributed to the effect of R_n number. It is regarded that the drag coefficient should not be a fixed constant when considering the mooring line damping, because it is affected by complicated factors, such as R_n and KC number.

Considering the dissipated energy variations due to C_D variations, the most sensitive parts are at areas of fairlead and touch down point. It is in accordance with the results of velocity variations due to C_D variations.

7 Conclusion and recommendation

7.1 Introduction

The previous chapters have documented the theoretical and experimental and numerical techniques employed for this study of the mooring-induced damping. In this chapter, a conclusive discussion regarding the estimation of the mooring line is presented, based on the results of force oscillation model tests and numerical calculation. Finally, further research work is recommended.

7.2 Conclusion

Mooring line integrity is of most importance for the floating structures in deep water. With the water depth increasing, the coupling between the large volume floater and the mooring system becomes crucial for the estimation of the floater's LF motions and mean offset. And also, its motion in reverse would affect the dynamic responses of the mooring system. In coupled analysis, the mooring line damping will be included by calculating the drag force on the dynamically analysed mooring system, and the assessment of the mooring line damping will clarify its contribution to the total damping and its effect on the global response.

The mooring damping is of much complexity, as it is influenced by floater motions, line configurations, and environmental conditions: the excitation amplitude and frequency, line material, pretension, current velocity and drag coefficient. Thus there is no uniform agreement concerning the estimation of mooring-induced damping in offshore engineering. The relationships between these parameters and mooring line damping are investigated in this thesis:

Firstly, the methods based on quasi-static analysis and time domain (TD) dynamic analyses are compared for assessing the mooring line damping. A typical chain

mooring line in shallow water and a wire mooring line in deep water are used to verify the mooring line damping, with the oscillations of LF and HF at the fairlead point. The 'indicator diagram' method based on the time domain (TD) dynamic analysis of the mooring line using Orcaflex, is applied for damping assessment. In order to validate the efficiency and accuracy of the method, the results are compared with those of previous references. Meanwhile, a non-dimensional analysis for more factors that would affect the mooring line damping is studied in this chapter. The mooring induced damping is clearly a complex phenomenon and appears to be influenced by many variates. The strong variation of mooring line damping with parameters indicates that:

- For the chain line in shallow water, the increase of the oscillation amplitude leads to an increase in mooring line linearized damping. It is because the mooring line movement velocity is higher and the drag forces are proportional to velocity squared. And also due to this reason, it is found that the increase of the oscillation period reduces the velocity and decreases the dissipated energy and linearized damping.
- The present calculation in the time domain using Orcaflex, can produce results of good agreement with the quasi-static method of the previous references, except for an anomaly in the case of 5.4m*10s for wire line in deep water. The mooring line in this case is light weight and it is likely to break the quasi-static condition in deep water. It results in the discrepancy in computing mooring line dynamic response with the two approaches.
- Comparing the results of HF oscillation for the chain in shallow water and the wire in deep water, it can be found that the line response and mooring line damping contribution of the former one show a significant high-frequency component, while none with the latter one. It is difficult to conclude the influence of the water depth and mooring line material to the mooring line damping. In other words, the factors make important and complicate effect on the mooring line damping, as a result, a parametric study in the following section is investigated.

- The effects from stiffness and seabed friction are very limited; that is to say, these effects are negligible in the investigation of mooring line damping.
- The behaviour of the response to surge motion is quite different from that due to heave motions. Dramatic changes for the effect of the mooring damping in horizontal, however without many traces of longitudinal contributions of the mooring line. This is because the cross-flow drags of the mooring line compound for the surge motions of the fairlead, but the effects of heave motion compete in longitudinal direction. From the results of surge motion, heave motion and combined surge & heave motions, significant contributions to the horizontal damping due to the heave motion superimposed. On the contrary, the superimposed surge motion hardly effect on the mooring line vertical damping.
- The effects from pretension and scope to the mooring line damping are mainly due to the geometries of the mooring line, including the total length and suspension length. The shorter scope line picks up off the bottom all the way to the anchor, while the larger scope line still has mooring line resting on the bottom. The shorter scope line has larger damping when the frequency or amplitude increases. The variation in damping with pretension presents a peak at non-dimensional pretension around 20. The mooring line behaviour changes from catenary to taut when the pretension getting bigger. The stretch response of the taut mooring will decrease the mooring line damping because the relative velocity of the line and the water reduces in comparison with the catenary case.
- The influence of current velocity is related to the mooring velocity. When the current velocity is big enough to change the line movement, it will have a considerable influence on mooring line damping.

Secondly experimental tests were carried out to investigate the variation in mooring induced damping with different excitations. The parametric analyses include variations of frequency and amplitude, for pure LF, and LF superimposed with a harmonic WF, with two harmonic WF, and with random WF motions. The relationship between line velocity and mooring line damping was discussed. It was found that:

- The dissipated energy that causes 'mooring line damping' is mainly due to the quadratic drag force acting on the line; it is thus influenced by its movement velocity. Because of this reason, the mooring line damping increases with the increase of oscillation frequency. For the same reason, as the amplitude of oscillation increases, the mooring line induced linearized damping also increases. I also find that the superimposed WF motion makes a significant contribution to mooring line linearized damping, comparing to the results of pure LF oscillations and this is also consistent with the effect of quadratic damping.
- Some damping estimation formulas are recommended from the results of the pure LF oscillation, and with a single harmonic WF motion and two harmonic WF motions superimposed. In this way, the mooring line damping can be estimated in a simple way. It is an efficient method to assess the mooring damping for an initial check.
- For the cases of random WF motion superimposed on the LF motion, the mooring line damping decreases with the increase of the oscillation peak period. It is because of the reduction in both the extreme value and standard deviation of the velocity. When the significant height of random WF motion is increasing, the dissipated energy generally increases. But there was an unusual occurred with varying amplitude of random WF motion superimposed; a slight drop to the energy dissipation for amplitude of 0.08m. This trend can be seen from the velocity statistics accordingly.
- For pure LF oscillation, the mooring line tension did not always change as the frequency increased. For the mooring line move in very slow speed, the mooring line tension is mainly determined by static stiffness, which is only related to its position. However, when the WF motion is superimposed, the mooring line tension is dominated by mooring line dynamics, so the mooring line tension increases as the frequency of the WF motion increases.

Thirdly the comparison between the results from experimental tests and numerical calculations is studied. For numerical simulation, the value of drag coefficient should be given, and its value is important to calculate the force on the mooring line.

Thus the effect of drag coefficient is investigated. And also, the relationships between the drag coefficient (C_D) and Reynolds (R_n) and KC number are investigated. Through the study, it can be seen that:

- The assessment of the mooring line induced damping from numerical simulation agrees well with that from model tests. In this case, the method of numerical calculation using Orcaflex is suitable to model and estimate the mooring line damping.
- Morison equation is applied on the slender structures and it is crucial to apply a carefully selected drag coefficient in the numerical simulation because this factor is crucial to the drag force acting on the mooring line. For the cases in this study, the drag coefficient derived from the experimental results ranges from 1.5 to 4.0. When the KC number is increasing, the drag coefficient decreases, except for some anomalies occurring in low KC cases. It is attributed to the effect from R_n number. It is recommended that the drag coefficient should not be a fixed constant when considering the mooring line damping, because its value is affected by complicated factors, such as R_n and KC number. With the non-linear fitting method executed to the all experimental results for cases of pure LF oscillation, LF superimposed with one WF motion and LF oscillation superimposed with two WF motions, the uniform fitting formulas are obtained as:

$$C_D = 7E-06KC^2 - 0.0074KC + 3.7318;$$

$$C_D = 5E-05R_n^2 - 0.0193R_n + 3.5132, \quad \text{For } KC = 311;$$

$$C_D = 9E-08R_n^2 - 0.0005R_n + 2.5578, \quad \text{For } KC = 376;$$

The formulas are fitted to the results of model tests for oscillating a single mooring line, where the typical model Reynold's number and Keulegan-Carpenter number KC are as:

LF: R_n = ~200, KC = 100~450;

LF and WF motion: R_n = 200~4000, KC = 250~450.

- It is indicated that the drag coefficient should be different for cases of LF oscillation and those of WF motion superimposed.
- Due to the velocity distribution along the mooring line, those parts with high relative velocities are also the most sensitive to the drag coefficient. The parts most sensitive to the effect of C_D variations on the dissipated energy are in the vicinity of the fairlead and touch down point.

7.3 Recommended future work

The present study has contributed to the oscillation parameters, drag coefficient and other factors that have an effect on mooring line induced damping. The following investigations are worthy of further effort:

7.3.1 Model tests with excitations both in the horizontal and vertical directions, and assessing the effects on damping

Experimental tests were conducted for oscillations in the surge direction in the present work. In reality, the six degrees of freedom of the floating structure movement interact with the mooring. It is indicated that the WF motion in heave direction makes contributions to mooring line damping in surge direction, from the numerical results of non-dimensional analysis;

7.3.2 Enhanced experiments under different flows for chain link, wire rope and fibre rope, to recommend the C_D values for mooring lines

Drag coefficient C_D value is an important issue in numerical calculation of the force on the mooring line and more work to help guide its selection would be helpful;

7.3.3 Damping model for taut mooring line

Mooring line of catenary type is applied to assess its damping force in this study. As is found, the predominant configuration presents differences between catenary and taut mooring systems, more work on taught mooring damping is needed;

7.3.4 Mooring line damping for different water depths

The water depth is remained fixed during the experimental studies because of the dimension of the laboratory tank. More work of in different water depths is worthy of investigation;

7.3.5 The effect of small scale and the use of truncated mooring systems in tank testing

In order to investigate the coupled effects between the mooring system and floating structures in deep-water, small scale and hybrid model testing technique are commonly applied. The effect of the small scale and truncated mooring system on the mooring line damping needs to be investigated.

References

2013. Rules and Regulations for the Classification of a Floating Offshore Installation at a Fixed Location. *In:* REGISTER, L. S. (ed.). Lloyd's Register.

2015. *Deep offshore reserves, a strategic resource for future energy solutions* [Online]. Available: https://**www.total.com/en/news/deep-offshore-reserves-strategic-resource-future-energy-solutions?folder=7737**.

A.M.A. HASSAN, M. J. D. A. E. A. 2010. Wave drift forces and responses in deep water and extreme environmental conditions. *Proceeding of the HYDRALAB III Joint User Meeting*.

AAMO, O. M. & FOSSEN, T. I. 2000. Finite element modelling of mooring lines. *Mathematics and Computers in Simulation,* 53, 415-422.

ABS 1993. Recommended practice for design, analysis and maintenance of mooring for floating production system. Washington D.C.

ANTONUTTI, R., PEYRARD, C., INCECIK, A., INGRAM, D. & JOHANNING, L. 2018. Dynamic mooring simulation with Code_Aster with application to a floating wind turbine. *Ocean Engineering,* 151, 366-377.

API-RP2RD 1998. Design of risers for Floating Production Systems (FPSs) and Tension-Leg Platforms (TLPs) American Petroleum Institute.

API-RP2SK 2005. Design and analysis of stationkeeping systems for floating structures. American Petroleum Institute.

AZCONA, J., MUNDUATE, X., GONZÁLEZ, L. & NYGAARD, T. A. 2017a. Experimental validation of a dynamic mooring lines code with tension and motion measurements of a submerged chain. *Ocean Engineering,* 129, 415-427.

AZCONA, J., MUNDUATE, X., GONZÁLEZ, L. & NYGAARD, T. A. 2017b. Experimental validation of a dynamic mooring lines code with tension and motion measurements of a submerged chain. *Ocean Engineering,* 129, 415-427.

BARLTROP, N. D. P. 1998. *Floating structures: a guide for design and analysis,* Oilfield Publications Limited.

BARTON, C. M. 2017. FPSO market still faces challenges. Available: https://**www.offshore-mag.com/articles/print/volume-77/issue-8/productions-operations/fpso-market-still-faces-challenges.html**.

BAUDUIN, C. & NACIRI, M. 1999. A Contribution on Quasi-Static Mooring Line Damping. *Journal of Offshore Mechanics and Arctic Engineering,* 122, 125-133.

BERGDAHL, L., PALM, J., ESKILSSON, C. & LINDAHL, J. 2016. Dynamically Scaled Model Experiment of a Mooring Cable. *Journal of Marine Science and Engineering,* 4, 5.

BOOM, H. J. J. V. D. 1985. Dynamic behaviour of mooring lines. *Behaviour of offshore structures*.

BROWN, D. T. & FANG, J. 1996. Hydrodynamic damping contributions for an advanced floating production system design. *Marine Structures,* 9, 649-670.

BROWN, D. T. & MAVRAKOS, S. 1999. Comparative study on mooring line dynamic loading. *Marine Structures,* 12, 131-151.

BUCKHAM, B. J. 2003. *Dynamics modelling of low-tension tethers for submerged remotely operated vehicles.* PhD, University of Victoria, Canada.

C. WEBSTER, W. 1995. Mooring-induced damping. *Ocean Engineering,* 22, 571-591.

CHAKHMAKHCHEV, A. & RUSHWORTH, P. 2010. Global Overview of Recent Exploration Investment in Deepwater-New Discoveries, Plays and Exploration Potential.

Available: http://www.searchanddiscovery.com/pdfz/documents/2010/40656chakhmakhchev/ndx_chakhmakhchev.pdf.html.

CHEN, X., DING, Y., ZHANG, J., LIAGRE, P., NIEDZWECKI, J. & TEIGEN, P. 2006. Coupled dynamic analysis of a mini TLP: Comparison with measurements. *Ocean Engineering,* 33, 93-117.

DENTON, N. 2006. Floating production system.

DERCKSEN, A., HUIJSMANS, R.H.M. AND WICHERS, J.E.W. 1992. An improved method for calculating the contribution of hydrodynamic chain damping on low-frequency vessel motions. *OTC 6967, Houston,* 209-218.

DESSI, D. & MINNA, S. S. 2014. Experimental Investigation vs Numerical Simulation of the Dynamic Response of a Moored Floating Structure to Waves. V08BT06A027.

DNV-OS-E301 2010. Position Mooring. *In:* STANDARD, D. O. (ed.).

DNV-RP-C205 2010. Environmental Conditions and Environmental Loads. *In:* PRACTICE, D. R. (ed.).

DRORI, G. 2015. Underlying Causes of Mooring Lines Failures Across the Industry.

DUPRE, R. 2015. Floating production industry pause in 2015, likely rebound in 2016. Available: https://www.offshore-mag.com/articles/print/volume-75/issue-3/departments/vessels-rigs-surface-systems/floating-production-industry-pause-in-2015-likely-rebound-in-2016.html.

FAN, T., QIAO, D. & OU, J. 2014. Innovative approach to design truncated mooring system based on static and damping equivalent. *Ships and Offshore Structures,* 9, 557-568.

FAN, T., QIAO, D., YAN, J., CHEN, C. & OU, J. 2017a. Experimental verification of a semi-submersible platform with truncated mooring system based on static and damping equivalence. *Ships and Offshore Structures,* 12, 1145-1153.

FAN, T., QIAO, D., YAN, J., CHEN, C. & OU, J. 2017b. An improved quasi-static model for mooring-induced damping estimation using in the truncation design of mooring system. *Ocean Engineering,* 136, 322-329.

FAN, T., REN, N., CHENG, Y., CHEN, C. & OU, J. 2018. Applicability analysis of truncated mooring system based on static and damping equivalence. *Ocean Engineering,* 147, 458-475.

FITZGERALD, J. & BERGDAHL, L. 2008. Including moorings in the assessment of a generic offshore wave energy converter: A frequency domain approach. *Marine Structures,* 21, 23-46.

GARRETT, D. L. 1982. Dynamic Analysis of Slender Rods. *Journal of Energy Resources Technology,* 104, 302-306.

GARRETT, D. L. 2005. Coupled analysis of floating production systems. *Ocean Engineering,* 32, 802-816.

HALL, M. & GOUPEE, A. 2015. Validation of a lumped-mass mooring line model with DeepCwind semisubmersible model test data. *Ocean Engineering,* 104, 590-603.

HE, X. T. T. C., TANG, Y., LIU, L. & ZHANG, R. 2018. Design of the Mooring System for a Floating Wave Energy Converter. *Journal of Coastal Research,* 85, 1351-1355.

HUANG, S. 1994. Dynamic analysis of three-dimensional marine cables. *Ocean Engineering,* 21, 587-605.

HUIJSMANS, J. E. W. W. A. R. H. M. 1984. On the low-frequency hydrodynamic damping forces acting on offshore moored vessels. *Offshore Technology Conference*, OTC 4813.

HUSE, E. 1986a. Influence of mooring line damping upon rig motion. *OTC paper 5204, Houston, TX*, 433-438.

HUSE, E. 1986b. Influence Of Mooring Line Damping Upon Rig Motions. Offshore Technology Conference.

HUSE, E. 1991. New Developments in Prediction of Mooring System Damping. *Offshore Technology Conference*. Houston, Texas: Offshore Technology Conference.

HUSE, E., A/S, M., MATSUMOTO, K. & NIPPON, K. K. K. 1988. Practical estimation of mooring line damping. *OTC 1988-5676*, 543-552.

HUSE, E. A. M., K 1989. Mooring line damping due to first- and second-order vessel motion. *OTC6137, Houston*, 135-148.

JING, F., ZHANG, L. & YANG, Z. 2012. Fatigue life prediction of mooring chains for a floating tidal current power station. *Journal of Marine Science and Application*, 11, 216-221.

JOHANNING, L., SMITH, G. H. & WOLFRAM, J. 2007. Measurements of static and dynamic mooring line damping and their importance for floating WEC devices. *Ocean Engineering*, 34, 1918-1934.

JONKMAN, J. M., BUTTERFIELD, S., MUSIAL, W. & SCOTT, G. 2009. Definition of a 5-MW Reference Wind Turbine for Offshore Development. Golden, Colorado, USA: National Renewable Energy Laboratory.

JOURNÉE, J. M. J. & MASSIE, W. W. 2001. *Offshore Hydrodynamics*, Delft University of Technology.

K. MA, A. D., P.SMEDLEY, 2013. A historical review on integrity issues of permanent mooring system. *OTC 2013-24025*.

KARIMIRAD, M. 2013. Modeling aspects of a floating wind turbine for coupled wave–wind-induced dynamic analyses. *Renewable Energy*, 53, 299-305.

KHAN, N. U. & ANSARI, K. A. 1986. On the dynamics of a multicomponent mooring line. *Computers & Structures,* 22, 311-334.

KOCH, W. 2015. Is Deepwater Drilling Safer, 5 Years After Worst Oil Spill? *National Geographic.*

KREUZER, E. & WILKE, U. 2003. Dynamics of mooring systems in ocean engineering. *Archive of Applied Mechanics,* 73, 270-281.

KWAN, C. T. & BRUEN, F. J. 1991. Mooring Line Dynamics: Comparison of Time Domain, Frequency Domain, and Quasi-Static Analyses. Offshore Technology Conference.

LIU, Y. & BERGDAHL, L. 1997. Influence of current and seabed friction on mooring cable response: comparison between time-domain and frequency-domain analysis. *Engineering Structures,* 19, 945-953.

LIU, Y. & BERGDAHL, L. 1998. Improvement on Huse's Model for Estimating Mooring Cable Induced Damping. *Proc., 17th OMAE Conference.*

LIU, Y. & BERGDAHL, L. 1999. On combination formulae for the extremes of wave-frequency and low-frequency responses. *Applied Ocean Research,* 21, 41-46.

LOW, Y. M. & LANGLEY, R. S. 2006. Time and frequency domain coupled analysis of deepwater floating production systems. *Applied Ocean Research,* 28, 371-385.

LOW, Y. M. & LANGLEY, R. S. 2008. A hybrid time/frequency domain approach for efficient coupled analysis of vessel/mooring/riser dynamics. *Ocean Engineering,* 35, 433-446.

LYONS, G. J., BROWN, D. T. & LIN, H. M. 1997. Drag Coefficients For Mooring Line Hydrodynamic Damping. *The Seventh International Offshore and Polar Engineering Conference.* Honolulu, Hawaii, USA: International Society of Offshore and Polar Engineers.

MATSUMOTO, K. 1991a. The Influence of Mooring Line Damping on the Prediction of Low-Frequency Vessel Motions at Sea. Offshore Technology Conference.

MATSUMOTO, K. 1991b. The influence of mooring line damping on the prediction of low-frequency vessel motions at sea. *OTC 6660, Houston*, 119-128.

MAVRAKOS, S. A., PAPAZOGLOU, V. J., TRIANTAFYLLOU, M. S. & HATJIGEORGIOU, J. 1996. Deep water mooring dynamics. *Marine Structures,* 9, 181-209.

NAKAJIMA, T., MOTORA, S. & FUJINO, M. 1982. On the Dynamic Analysis of Multi-Component Mooring Lines. *Offshore Technology Conference.* Houston, Texas: Offshore Technology Conference.

NAKAMURA, M., KOTERAYAMA, W. & KYOZUKA, Y. 1991. Slow drift damping due to drag forces acting on mooring lines. *Ocean Engineering,* 18, 283-296.

NIELSEN, F. G. & BINDINGBØ, A. U. 2000. Extreme loads in taut mooring lines and mooring line induced damping: an asymptotic approach. *Applied Ocean Research,* 22, 103-118.

NOBELDENTON 2005. FPS Mooring Intrgrity JIP Report. *A4163.* Aberdeen.

O'DONOGHUE, T. & LINFOOT, B. T. 1992. An experimental study of turret-moored floating production systems. *Applied Ocean Research,* 14, 127-139.

ORCAFLEX Orcarflex User Manual Version 9.7a. *In:* LTD, O. (ed.). Ulverston Cumbria, Uk.

ORMBERG, H. & LARSEN, K. 1998. Coupled analysis of floater motion and mooring dynamics for a turret-moored ship. *Applied Ocean Research,* 20, 55-67.

PALM, J., MOURA PAREDES, G., ESKILSSON, C., TAVEIRA PINO, F. & BERGDAHL, L. Simulation of mooring cable dynamics using a discontinuous galerkin method. *In:* ENGINEERING, P. O. V. I. C. O. C. M. I. M., ed., 2013 Hamburg, Germany.

PAPAZOGLOU, V. J., MAVRAKOS, S. A. & TRIANTAFYLLOU, M. S. 1990. Non-linear cable response and model testing in water. *Journal of Sound and Vibration,* 140, 103-115.

PAULLING, J. R. W., W.C. A consistent, large-amplitude analysis of the coupled response of a TLP and tendon system. Proceedings of the fifth international offshore mechanics and arctic engineering, 1986.

QIAO, D. & OU, J. 2010. Time domain simulation of the mooring induced damping in low frequency excitaion. *2010 International Conference on computer Application and System Modeling.*

QIAO, D. & OU, J. 2014. Mooring Line Damping Estimation for a Floating Wind Turbine. *The Scientific World Journal,* 2014, 10.

RAAIJMAKERS, R. M. B., J.A. An experimental verification of Huse's model on calculation of mooring line damping. Proceeding of the Eighth BOSS Conference 1997. 439-452.

SARKAR, A. & EATOCK TAYLOR, R. 2000. Effects of mooring line drag damping on response statistics of vessels excited by first- and second-order wave forces. *Ocean Engineering,* 27, 667-686.

SCHELLIN, T. E. & KIRSCH, A. 1989. Low-frequency damping of a moored semisubmersible obtained from simulated extinction tests and mean wave drift forces. *Applied Ocean Research,* 11, 202-211.

SETHURAMAN, L. & VENUGOPAL, V. 2013. Hydrodynamic response of a stepped-spar floating wind turbine: Numerical modelling and tank testing. *Renewable Energy,* 52, 160-174.

SMITH, N. 2011. Gryphon Alpha Loss of Heading, Mooring System Failure and Subsequent Loss of Position. MAERSK.

TAHAR, A. & KIM, M. H. 2003. Hull/mooring/riser coupled dynamic analysis and sensitivity study of a tanker-based FPSO. *Applied Ocean Research,* 25, 367-382.

TAHAR, A. & KIM, M. H. 2008. Coupled-dynamic analysis of floating structures with polyester mooring lines. *Ocean Engineering,* 35, 1676-1685.

THOMAS, D. O. & HEARN, G. E. 1994. Deepwater mooring line dynamics with emphasis on seabed interference effects. *OTC-7488, 26th Offshore Technology Conference.* Houston, USA.

THOMSEN, J. B. F., F.; KOFOED, J.P. 2017. Screening of Available Tools for Dynamic Mooring Analysis of Wave Energy Converters. *Energies,* 10(7), 853.

TRIANTAFYLLOU, M. S., YUE, D.K.P. AND TEIN, D.Y.S. 1994. Damping of moored floating structures. *OTC 7489, Houston,* 215-224.

VENDHAN, C. P. 2019. Coupled dynamics of deepwater structures - issues and challenges. *Ships and Offshore Structures,* 14(4), 343-353.

WALTON, T. S. & POLACHEK, H. 1959. Calculation of nonlinear transient motion of cables. Washington, D. C., USA: David Taylor Model Basin.

WICHERS, J. E. W. & HUIJSMANS, R. H. M. 1990. The Contribution of Hydrodynamic Damping Induced by Mooring Chains on Low-Frequency Vessel Motions. Offshore Technology Conference.

WICHERS, J. E. W. & HUIJSMANS, R. M. H. 1984. On the Low-Frequency Hydrodynamic Damping Forces Acting on Offshore Moored Vessels. Offshore Technology Conference.

XIONG, L.-Z., YANG, J.-M., LV, H.-N., ZHAO, W.-H. & KOU, Y.-F. 2016. Study on global performances and mooring-induced damping of a semi-submersible. *China Ocean Engineering,* 30, 671-686.

XU, S. & JI, C.-Y. 2014. Dynamics of large-truncated mooring systems coupled with a catenary moored semi-submersible. *China Ocean Engineering,* 28, 149-162.

XU, S., JI, C. & GUEDES SOARES, C. 2018. Experimental study on taut and hybrid moorings damping and their relation with system dynamics. *Ocean Engineering,* 154, 322-340.

XU, Z. & HUANG, S. 2014. Numerical investigation of mooring line damping and the drag coefficients of studless chain links. *Journal of Marine Science and Application,* 13, 76-84.

YANG, W. S. 2007. *Hydrodynamic analysis of mooring lines based on optical tracking experiments.* Doctoral dissertation, Texas A&M University.

YANG, Y., CHEN, J.-X. & HUANG, S. 2016. Mooring line damping due to low-frequency superimposed with wave-frequency random line top end motion. *Ocean Engineering,* 112, 243-252.

YUAN, Z.-M., JI, C.-Y., CHEN, M.-L. & ZHANG, Y. 2011. Coupled Analysis of Floating Structures With a New Mooring System. *30th International Conference on Ocean, Offshore and Arctic Engineering.* Rotterdam, The Netherlands.

ZHANG, S.-X., TANG, Y.-G. & LIU, X.-J. 2012. Experimental investigation of nonlinear dynamic tension in mooring lines. *Journal of Marine Science and Technology,* 17, 181-186.

Appendix A Mooring line statics

The general static solutions of mooring line are described by the catenary equation, as shown in Figure A- 1; an element of a mooring line lying in the $x-y$ plane is selected as the objective. Let T be the tension in the line, w is the submerged weight of the mooring line, ds is the length of the infinitesimal mooring element and ϕ is the angle to horizontal made by the element. Then, the two equilibrium equations obtained by resolving forces tangentially and normally to the element become:

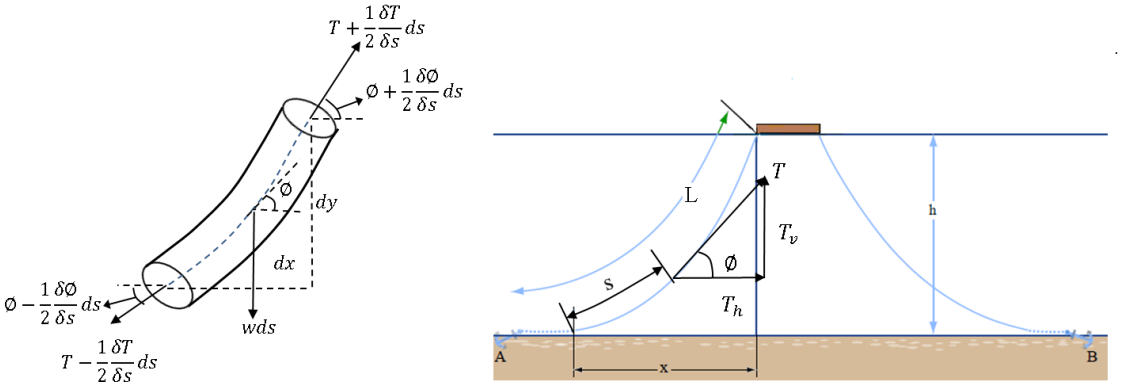

Figure A- 1 Mooring line element

$$\frac{dT}{ds} = w\sin\phi \qquad \textbf{A- 1}$$

$$\frac{d\phi}{ds} = \frac{w}{T}\cos\phi \qquad \textbf{A- 2}$$

Dividing equation(A- 1) by equation(A- 2) provides an equation for T in terms of T and ϕ alone:

$$\frac{dT}{d\phi} = T\tan\phi \quad \text{or} \quad \frac{dT}{T} = \tan\phi\, d\phi \qquad \textbf{A- 3}$$

Integrating equation(A- 3) and imposing the boundary conditions, $\phi = 0; T = T_H$,where T_H is the horizontal force in the mooring line, results in the following relationship:

$$\ln(T) = \ln(\sec\phi) + c \;\rightarrow\; T = \frac{T_H}{\cos\phi} \qquad \textbf{A- 4}$$

This also follows directly from horizontal equilibrium.

Substituting equation(A- 4) into equation(A- 2) and integrating the resulting equation linking s and ϕ , and imposing the boundary condition that $s = 0$ when $\phi = 0$ implying that the mooring line length is measured from the point of tangential touchdown at a horizontal seabed, provides the following:

$$\int \frac{d\phi}{\cos^2\phi} = \int \frac{w\,ds}{T_H} \qquad \textbf{A- 5}$$

$$\therefore \tan\phi = \frac{ws}{T_H} \quad \therefore \quad T_H = \frac{ws}{\tan\phi}$$

Equation (A- 4) and (A- 5) thus provide methods for the calculation of the tension and the horizontal force at any point in the mooring line defined by s and ϕ . The vertical force at any point can then be simply derived from vector algebra:

$$T_V = \sqrt{T^2 - T_H^2} = ws \qquad \textbf{A- 6}$$

This also follows directly from vertical equilibrium of the cable between 0 and s .

Appendix B Morison Equation Coefficient Determination

In this part, a vertical cylinder is assumed to be fixed in a horizontal sinusoidal oscillatory flow. The force per unit length acting on the cylinder can be predicted using the Morison equation with two empirical coefficients:

$$F(t) = \frac{\pi}{4}\rho C_m D^2 \cdot \dot{u}(t) + \frac{1}{2}\rho C_D D \cdot u(t)\left|u(t)\right| \qquad \textbf{B- 1}$$

The value of the dimensionless force coefficient C_D and C_m can be determined experimentally in a variety of ways. The first step, however, is always to get a recording of the force, F , as a function of time, t . A characteristic of the flow – usually the velocity–will form the second time function.

The measurement can be made in a variety of test set-ups.

1. Oscillating flows can be generated in a large U-tube. Unfortunately the flow can only oscillate with a limited frequency range – the natural oscillation frequency for the installation - unless an expensive driving system is installed. An advantage of a U-tube, on the other hand, is that its oscillating flow is relatively 'pure' and turbulence-free. A discussion continues about the applicability of results from such idealized tests in field situations, however.

2. A second method is to impose forced oscillations to a cylinder in still water. The flow – when seen from the perspective of the cylinder – appears similar to that in a U-tube but the inertia force is not the same.

3. A third possibility is to place a vertical cylinder in regular waves. The waves are generated by a wave maker located at one end of the experimental tank; they are

absorbed on an artificial beach at the other end. In this case it is often the wave height (actually the water surface elevation) which is measured as a function of time. The horizontal water velocity and acceleration at the location of the cylinder are in this latter case determined using linear wave theory.

$$u(z,t) = \frac{w\eta}{2} \cdot \frac{\cosh\left[k(z+h)\right]}{\sinh(k \cdot h)} \cdot \cos(\omega t) = u_a(z) \cdot \cos(\omega t) \qquad \textbf{B- 2}$$

$$\dot{u}(z,t) = -\frac{\omega^2 \eta}{2} \cdot \frac{\cosh\left[k(z+h)\right]}{\sinh(k \cdot h)} \cdot \sin(\omega t) = -\omega \cdot u_a(z) \cdot \sin(\omega t) \qquad \textbf{B- 3}$$

in which:

$\omega = 2\pi/T =$ wave frequency (rad/s)

$k = 2\pi/\lambda =$ wave number (rad/m)

$z =$ elevation from the still water level (m)

$H =$ wave height (m)

$h =$ water depth (m)

$T =$ wave period (s)

$\lambda =$ wave length (m)

$u_a(z) =$ amplitude of horizontal water velocity component (m/s)

Note that even though u_a is now a function of z , this will not really complicate matters when studying the forces on a short segment of a cylinder. The change in u_a over such a short distance can be neglected.

With any of these methods, the resultant force on a section of the cylinder is often measured by mounting that section on a set of leaf springs which are equipped with strain gauges. These- via a Wheatstone bridge circuit and a proper calibration – provide the force record, $F(t)$ to use in conjunction with the measured or computed $u(t)$ and $\dot{u}(t)$.

Data processing

Once the necessary data time series have been obtained, one is still faced with the problem of determining the appropriate C_D and C_m values. Here, again, one has several options dependent upon the computer facilities available.

1. Morison's method

Morison, himself, suggested a simple method to determine the two unknown coefficients. His method was elegant in that it was possible to determine the coefficients without the use of computers. His approach was suitable for hand processing and depended upon the realization that when:

u is maximum, $\dot{u}$ is zero so that at that instant, t_1, $F(t_1) = F_D$ and

$\dot{u}$ is maximum, u is zero so that at that instant, t_2, $F(t_2) = F_I$.

Figure B- 1 shows a sample of an idealized measurement record. Under each of the above specific conditions, equation (B- 1) can be re-arranged to yield:

$$C_D = \frac{2F}{\rho D \cdot u_a |u_a|} \text{ at an instant } t_1 \text{ when } \dot{u} = 0 \qquad \textbf{B- 4}$$

$$C_m = \frac{4F}{\pi \rho D^2 \cdot \omega u_a} \text{ at an instant } t_2 \text{ when } u = 0$$

The method is simple, but it lacks accuracy because:

A small error in the velocity record can cause a significant phase error. Since the curve of $F(t)$ can be steep (especially when determining C_D in Figure B- 1), this can cause quite some error in this coefficient. The effect on C_m is usually smaller.

Information from only two instances in the time record is used to determine the coefficients; the rest is thrown away.

Morison reduced errors by averaging the coefficients over a large number of measurements (wave periods).

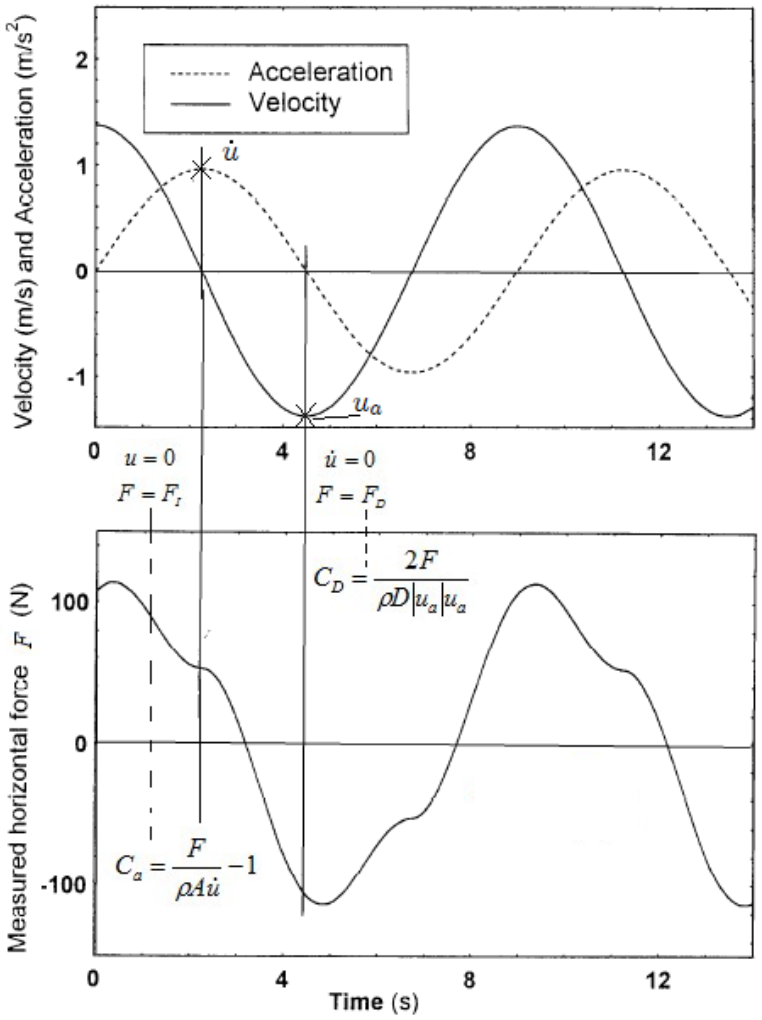

Figure B- 1 Hydrodynamic coefficients determination by Morison (Journée and Massie, 2001)

One might try to use this same approach at other time instants in the record. The only difficulty, however, is that one is then confronted with a single equation (for F at that instant) but with two unknown coefficients. This cannot be solved uniquely. A second equation could be created by examining the situation at a second, independent time instant. A generalization of this would be to use the data pairs at every instant with a least squares fitting technique. This is discussed below, but only after another approach using Fourier series has been presented.

2. Fourier Series Approach

An entirely different method for determining the drag and inertia coefficients is based upon the comparison of similar terms in each of two Fourier series: One for the water motion and one for the force.

Since modern laboratory data records are stored at discrete time steps (instead if as continuous signals), the integrals needed to evaluate the Fourier coefficients are replaced by equivalent sums.

Looking at this in a bit more detail, the water velocity and acceleration is already in a nice form as given in equation (B- 2). A single Fourier series term is sufficient to schematize this quite exactly. Since the inertia force, F_I, is also well behaved, it can be 'captured' with a single Fourier series term as well.

The only remaining problem is the series development of the drag term; this requires the development of a function of form:

$$f(t) = A\cos(\omega t)\cdot\left|\cos(\omega t)\right| \qquad \textbf{B- 5}$$

The drag force, dependent upon $u|u|$, develops into a series of odd-numbered harmonics in a Fourier series; only the first harmonic terms are used here. Since this has amplitude of $\frac{8}{3\pi}$ times the original signal, one must multiply the first order harmonic of the force in phase with the velocity by a factor $\frac{8}{3\pi}$ to get the amplitude of the quadratic drag force.

Once this has been done, then the determination of C_D and C_m from the analysis of the compete force signal, $F(t)$ is completely straightforward. Since the inertia force component shows up now in the b_1 term of the series development, the results are:

$$C_D = \frac{3\pi}{4\rho D}\cdot a_1 \qquad and \qquad C_m = \frac{4}{\pi D^2 \rho}\cdot \frac{b_1}{\omega u_a} \tag{B- 6}$$

in which the following amplitudes are found:

a_1 = velocity-dependent Fourier amplitude (kg/m^2)

b_1 = acceleration-dependent Fourier amplitude (N m)

Notice that with this method one has used data from the entire time record in the determination of the Fourier series components and thus for the determination of C_D and C_m. This should be an improvement over the method used originally by Morison, but on the other hand, it is still only as accurate as the linearization can be.

3. Least Squares Method

A third approach treats the basic Morison equation (B- 1), as a computational approximation, $F(t, C_D, C_m)_{computed}$, for the measured force record, $F(t)_{measured}$. One is now faced with only the problem of determining the (linear) unknown coefficients, C_D and C_m. This is done by minimizing some residual difference (or fit criterion) function. The method of least squares uses a residual function of the form:

$$R(C_D, C_m) = \int_0^T \left[F(t)_{measured} - F(t, C_D, C_m)_{computed} \right]^2 dt \tag{B- 7}$$

in which T is now the length of the measurement record.

Now one only need to iteratively evaluate equation (B- 7) for various values of C_D and C_m until the residual function, $R(C_D, C_m)$ is minimized. If one were to plot this function in three dimensions – with C_D and C_m on the two orthogonal horizontal axes and $R(C_D, C_m)$ on the vertical axis, then one would find a sort of 'bowl-shaped' function. It doesn't take too much thought to realize that if the shape of the bottom of this 'bowl' is rather flat, then there are many combination of C_D and C_m which give about the same $R(C_D, C_m)$ function value. The consequence of this is that it is quite difficult to determine the 'best' C_D and C_m values exactly in a numerical way. In the other hand, it is theoretically possible to determine the minimum of the function. $R(C_D, C_m)$ by setting both of its partial derivatives, $\frac{\partial R}{\partial C_D}$ and $\frac{\partial R}{\partial C_m}$ equal to zero analytically.